Photophysics and Photovoltaic Application of Direct Heteroarylation Derived Isoindigo Based Copolymers

by

Newayemedhin Tegegne

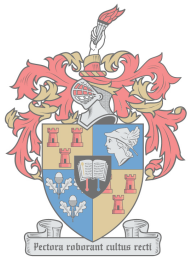

Thesis presented in partial fulfilment of the requirements for the degree of

Doctor of Philosophy

at the Stellenbosch University

Supervisors:

Prof. Heinrich Schwoerer
Dr. Christine Steenkamp

March 2018

Declaration

By submitting this dissertation electronically, I declare that the entirety of the work contained therein is my own, original work, that I am the sole author thereof (save to the extent explicitly otherwise stated), that reproduction and publication thereof by Stellenbosch University will not infringe any third party rights and that I have not previously in its entirety or in part submitted it for obtaining any qualification.

Date: March 2018

Abstract

Environmental friendliness, ease of fabrication, low cost and mechanical flexibility make organic solar cells a potential future of renewable energy sources. The structure of organic materials such as conjugated polymers play an important role in their optoelectronic properties that are relevant to power conversion efficiency of organic solar cells. Copolymers have an internal donor-acceptor coupling that will reduce the band gap from the respective donor or acceptor units. Fundamental photophysical properties of such copolymers is crucial to understand efficiency limiting factors. The dynamics associated with charge transfer in the molecules, in the solid films and bulk hetrojunction composites were studied using fs-transient absorption spectroscopy in three copolymers. The result on a bithiophene-isoindigo copolymer in dilute solution showed an intramolecular charge transfer state generation rate of 2 ps. The bulk heterojunction film of a blend of **P2TI**:PCBM71, showed a fast charge generation (<250 fs). But only 40 % of the charge carriers could stay longer than 2 ns. This is due to a poor charge percolation pathways in the active layer morphology. The low power conversion efficiency in **P2TI**:PCBM71 based solar cells is due to poor percolation pathway to charge carriers. Moreover, we studied effect of side chains on photophysics of two terthiophene-isoindigo copolymers. The result showed when the length of the alkyl side chains at position 3 and 4 of the first and the last terthiophene unit increases from (C_8H_{17}) by four methyl units to ($C_{12}H_{25}$), the intramolecular charge transfer rate slows down from 4.5 ps to 13 ps. The longer side chains also lowers exciton life time by creating a barrier for interchain interaction. Exciton diffusion is less efficient when the side chains are longer.

Opsomming

Organiese sonselle is moontlik die gesig van toekomstige hernubare energiebronne weens die omgewingsvriendelikheid, lae vervaardigingskoste en meganiese buigsaamheid daarvan. Die struktuur van organiese materiale, soos gekonjugeerde polimere, speel n belanrike rol in hul opto-elektriese eienskappe wat tersaaklik is tot die drywing omskakelingsdoeltreffendheid van organiese sonselle. Ko-polimere het interne skenker-ontvanger koppelings wat die bandgaping van die onderskeie donor of ontvanger eenhede verklein. Om die faktore wat die doeltreffendheid beperk te verstaan is dit belangrik om die fundamentele fotofisiese eienskappe van sulke ko-polimere te verstaan. Die dinamika geassosier met ladingsoordrag in die molekule (in die soliede films en in heterogene massa-aansluiting materiaal) is bestudeer deur middel van fs-oorgangsabsorbsie spektroskopie in drie ko-polimere. Die resultaat vann bitiofeen-isoindigo (bithiophene-isoindigo) ko-polimeer in verdunde oplossing, het n intramolekulłre tempo van ladingsoordrag van 2 ps getoon. Die heterogene massa-aansluiting film met n mengsel van P2TI:PCBM71, het n vinnige ladingsopwekking van $<$250 fs getoon. Slegs 40% van die lading draers kon egter langer as 2 ns bestaan, weens swak deursype-llingskanale vir ladings in die aktiewe lae se morfologie. Die lae drywing omskakelingsdoeltreffendheid in P2TI:PCBM71 gebaseerde sonselle is ook weens die swak lading deursypell-ingskanale. Die effek wat syketting op die fotofisika van twee tritiofeen-isoindigo (terthiophene-isoindigo) ko-polimere is verder ondersoek. Die resultate wys dat wanner die lengte van die alkiel syketting by posisie 3 en 4 van die eerste en laaste tritiofeen eenheid vergroot van (C_8H_{17}) met vier metiel eenhede tot ($C_{12}H_{25}$), raak die intramolekulłre ladingsoordrag tempo stadiger van 4.5 ps na 13 ps. Die langer syketting verlaag ook die leeftyd van die elektron-holte paar (exciton) deur interketting wisselwerking te verhinder. Diffusie van elektron-holte pare is minder effektief wanneer die syketting langer is.

Acknowledgment

All the glory be to God who has encouraged and helped me all the way through my study.

I want to say thank you to my supervisor Prof. Heinrich Schwoerer for his guidance through this work. I am grateful to him for helping me understand the complex experimental set up with patience. His love for science was an encouragement to always go deeper in the work. The team spirit he created in our group is amazing. I want to say thank you to Essra, Iulia and Xavier for their contribution in taking measurements and discussions on the data analysis. Thank you Dr. Olay Ollufiemi and Mr. Ahmed Mohammed for helping me with the density functional calculation.

I am also grateful to my co-supervisor Dr. Steenkamp who is also the head of the laser research institute (LRI). The LRI group has created a conducive environment for anyone to work. I would like to say thanks to all LRI members.

This work would not be true without the help of Dr. Zelalem, Prof. Wendimagegn and Prof. Andersson. Thank you for synthesizing the copolymers I studied. The discussions we had in several times helped me understand the materials and interpret the measurements.

I am also grateful to Prof. Schlettwein and his group. I fabricated solar cell devices and characterized their performance in their lab. I am also thankful for their hospitality during my two months stay in Germany.

Finally, I would like to say thank you to my friends and family. Your help in these three years was immeasurable. I am always grateful to my little boy Eyobed for putting smile on my face even in times I was frustrating. I am blessed to have you.

Contents

1. Introduction

The sun power that reaches the earth surface is 120,000 terawatts. This power is six thoudand times the present rate of the energy consumption [1]. The energy consumption rate of our world in 2001 was 13.5 TW. In 2050, the energy consumption rate is expected to be 27.6 TW which is double the value on 2001 [2]. Currently, fossil fuels are the main source of our energy consumption. Besides the ever increasing cost, the amount of crude oil is depleting fast. This calls for immediate renewable energy sources. Solar cells are solar harvesting devices that are used to convert solar energy to electricity. The first solar cell was fabricated using monocrystalline Si at Bell Telephone Laboratories in 1954 with a power conversion efficiency of 6% [2]. During the following decade, a power conversion efficiency of 25% using monocrystalline Si was reported, which is close to the theoretically predicted value by Shockley and Queisser [3]. Shockley and Queisser calculated power conversion efficiency of a Si solar cell and predicted a maximum attainable power conversion efficiency to be 32% [3]. In their calculation, spectrum losses of a Si (band gap = 1.1 eV) based single p-n junction solar cell alone accounts for 33% loss. The challenge in Si based photovoltaic technology is the high cost of production. After 5 to 6 decades of research the cost of production has reduced to 1.42 dollars per watt [4]. However, electricity generated using these solar cells could contribute $\approx$ 1.5% of the total electricity generated globally in 2016 [5].

In 1970's a new era of cheap alternative organic semiconductor came after the discovery of electrical conductivity in polyacetylene when it is partially oxidized. Alan J. Heeger, Alan G. MacDiarmid and Hideki Shirakawa received the "Nobel Prize in chemistry 2010" for their discovery of conducting polymers[6]. Tang *et. al.*demonstrated the use of these organic semicondutors in light emitting diodes for the first time in 1980's[7].

Organic semiconductors are extracted from abundant materials like plants. This makes them less expensive and easier in terms of synthesis than inorganic semiconductors. Their structure can easily be tailored to a desired electrical and optical property. Structurally, diverse conjugated polymers have been utilized for organic solar cells (OSCs). The power conversion efficiency of OSCs has exceeded 10% in a single junction small area devices [8, 9]. The performance of these solar cells is determined by many factors that include the active layer materials, device morphology and interfacial energetics. In addition, the stability of OSCs has been a bottleneck for commercialization. OSCs can be solution processed unlike the inorganic ones. Besides being inexpensive to produce, organic semiconductors can easily be printed on flexible substrates. Thus, OSCs can be mass produced with inexpensive techniques like roll-to-roll or ink-jet printing.

In this work, three low band gap copolymers based on isoindigo as an acceptor were studied for solar cell applications in Indium Tin Oxide (ITO)- free geometry. Their performance was studied using the standard current-voltage characterization.

The photovoltaic performance of these OSCs indicated a farther study on the fundamental charge generation and recombination processes is important to understand the difference among the solar cells. This is important to further understand performance-structure relation of the solar cell devices. Thus, with this motivation we farther studied the fundamental photophysics. We started the photophysics study with steady state spectroscopy. We then proceed to fs-Transient absorption spectroscopy to get a better temporal resolution to the underlying charge generation and recombination mechanism. We started the photo-physics study of the copolymers in dilute solution to avoid any interchain interaction, then to pristine copolymer films. Finally, we performed photo-physics measurements on the actual active layer of the solar cells which is copolymer:PCBM71 bulk heterojunction composite films.

The work is organized as follows: in chapter 2 OSCs and their basic working principles are introduced. In chapter 3, I will focus on the entire photophysics, charge generation and recombination dynamics in an OSC. In chapter 4, the experimental techniques and sample preparation will be discussed briefly. Chapter 5 and 6 deal with results. In chapter 5, the result of a photophysics study on a bithiophene-isoindigo, **P2TI**, copolymer and its application in ITO free solar cells will be discussed. In chapter 6, I will discuss the effect of length of side chains on the photophysics and macroscopic solar cell parameters using two similar terthiophene-isoindigo copolymers. The length of side chains on the terthiophene unit was the only difference between the two copolymers. In the study, it was possible to conclude that the length of side chains on the terthiophene unit has a significant effect from the intra-molecular interaction within the copolymer to the solar cell performance when blended in bulk heterojunction composite with PCBM71. Finally, I will conclude this work with a short summary and some recommendations for future work.

2. Organic solar cells

Solar energy is the most abundant clean source of renewable energy that can be used for electricity generation using photovoltaic (PV) cells. Semiconductors, mainly inorganic ones, are used in the fabrication of these PV cells. In the past three to four decades, organic semiconductors, mainly conjugated polymers, came to the picture as conductive material for PV application. Organic semiconductors have a unique property that combines semiconducting property with a chemical composition of plastics. This creates an endless opportunity of tailoring their electrical, optical and mechanical property. It also opens a wide variety of applications of organic semiconductors in light emitting diodes, organic field effect transistors, displays and OSCs. Organic semiconductors have a high extinction coefficient which enables efficient absorption of photons in a layer of only few hundred nanometres. Thus, OSCs have light weight and are flexible. OSCs are usually fabricated with inexpensive solution processable techniques like spin coating or evaporation processing. The recent development in fabrication of OSCs in the view of mass production is going towards roll-to-roll printing technique. This technique is similar to a simple ink-jet printing. A flexible substrate is used in roll-to-roll printing of OSCs. Besides their mechanical flexibility, their diverse colours opens a unique opportunity for engineers to design specific application. A recent work from German researchers showed the possibility of exploiting their mechanical flexibility and diverse colors for use in self-powered devices like electronic eyeglasses with integrated solar cells[10].

2.1 Organic semiconductors

Organic semiconductors are mainly made of carbon and hydrogen atoms with few hetero-atoms like sulphur, oxygen and nitrogen included. The backbone of these materials is formed by a chain of carbon atoms with alternating single and double bonds. This is crucial to their semiconducting property. The semiconducting nature of organic semiconductors is different from inorganic ones like silicon, germanium, and GaAs. In inorganic semiconductors, free charge carriers can be created by thermal excitation of electrons from a valence band to a conduction band. An intrinsic conductivity between 10^{-8} S/cm to 10^{-2} S/cm is common in inorganic semiconductors. Conductivity in organic semiconductors is extrinsic which is result of charge injection by electrodes, doping or from the dissociation of electron-hole pairs. The dielectric constant of inorganic semiconductors is enough to effectively screen the coulomb effects between electrons and holes (see section 3.2.2). As a result, excitation of an electron from the valence band to conduction band in this class of materials creates free charge carriers. In contrast, the dielectric constant (ϵ_r) of inorganic semiconductors is low (ϵ_r = 3 - 4) compared to Si (ϵ_r = 11). Thus, photo-excitation of electrons from the valence band to

the conduction band creates tightly bound electron-hole pairs. The Coulomb energy of this electron-hole pair is about 0.5 - 1.0 eV which is much higher than thermal energy at room temperature (kT $\approx$ 0.025 eV). This precludes creating any significant amount of charge carriers by thermal excitation at room temperature.

Origin of electrical conductivity and band gap of organic semiconductors

The main categories of organic semiconductors include conjugated small molecules and conjugated polymers. Polymers are made of repeating units called monomers. Based on the number of monomers, polymers are classified as oligomers (short polymers) or polymer. Polymers with 20 to 100 monomers are called oligomers; polymers with more than 100 monomers are called polymers. This work will focus on conjugated polymers. Conjugated polymers are mainly made of carbon. Understanding the electronic configuration of carbon atoms is important to understand the semiconducting property of this class of materials. Atomic carbon has six electrons arranged in $1s^2$, $2s^2$, $2p^2$ configuration. Carbon can hybridize its four valence electrons in three ways : sp, sp^2 and sp^3 . When a carbon atom with sp^3 hybridized orbitals forms a bond with other atoms, the four sp^3 hybridized orbitals form a tight covalent bond forming a σ bond. These σ orbitals are oriented at 109.5^0 between them. This is the case with ethane (C_2H_6). In a similar way, one 's' orbital and two 'p' orbitals can hybridize and form three sp^2 hybridized orbitals. The three sp^2 hybridized orbitals will be at 120^0 to each other. The remaining p_z orbital lies orthogonal to that plane. Polyacetylene $(C_2H_2)_n$ (PA), the simplest polymer, is a good example for sp^2 hybridization. In PA, a carbon atom forms bonds with two other carbon atoms and a hydrogen atom. The three sp^2 hybridized orbitals form the covalent bonding in the molecule: C-C, C-C and C-H. The remaining p_z orbital overlaps with the other p_z orbitals of each carbon atoms in the polymer chain and form a quasi-free electron cloud.

The sp^2 hybridized orbitals overlap along the internuclear axis of the atoms, consequently their split into bonding-σ and anti-boning-σ^* orbitals is high (see Figure 1). But the p_z orbitals overlap further away from the internuclear distance, which makes the splitting of bonding-π and anti-boning-π^* orbitals lower. The energy of the σ or π bonding orbital are lower than the hybridized sp^2 or overlapped p_z orbitals respectively. Similarly, the energy of the σ^* or π^* bonding orbitals are higher than the hybridized sp^2 or overlapped p_z orbitals respectively. As more and more sp^2 hybridized carbon atoms are covalently bonded and the p_z orbitals overlap sufficiently, the π electrons become de-localized in the extended π system. The atomic orbitals will evolve into molecular orbitals. The highest unoccupied molecular orbital (HOMO) is the π orbital and the next lowest unoccupied molecular orbital (LUMO) is π^* orbital (Figure 2.1). The band gap of the polymer will be the difference between the HOMO and the LUMO levels.

PA can be taken as an example to discuss origin of band gap in organic semiconductors (see Figure 2.2). PA would be metallic if the double bond is delocalized along the chain as shown in the Figure 2.2b but such structures are unstable. This structure will be distorted into alternating single and double bonds. In doing so, the periodicity of the lattice will change from 'a' to '2a' as shown in Figure 2.2b and c. A finite band gap will open as a result of this distortion. This alternation of bond length is due to the gain in electronic energy that compensates the elastic energy and is called Peirels effect

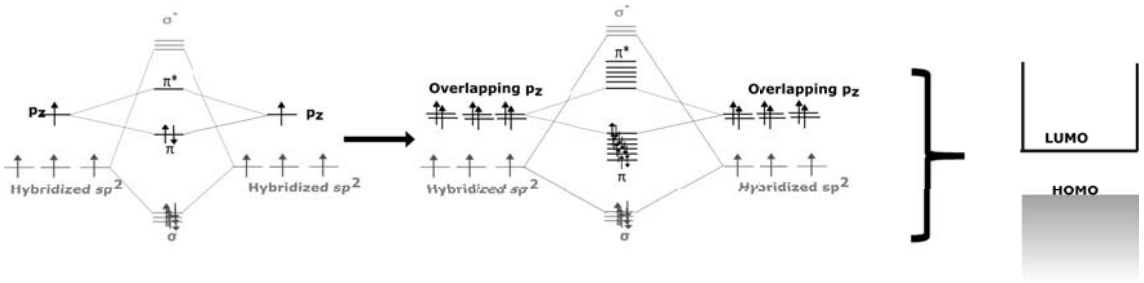

Figure 2.1: In C_2H_2 molecule, the hybridized sp^2 and the p_z orbitals split into (σ or π) bonding and (σ^* or π^*) anti-bonding orbitals respectively (left). Addition of more molecules into the conjugated system will increase the number of the hybridized sp^2 and the overlapping p_z orbitals (center) and the full conjugated system will have molecular orbitals, HOMO and LUMO.

[11].

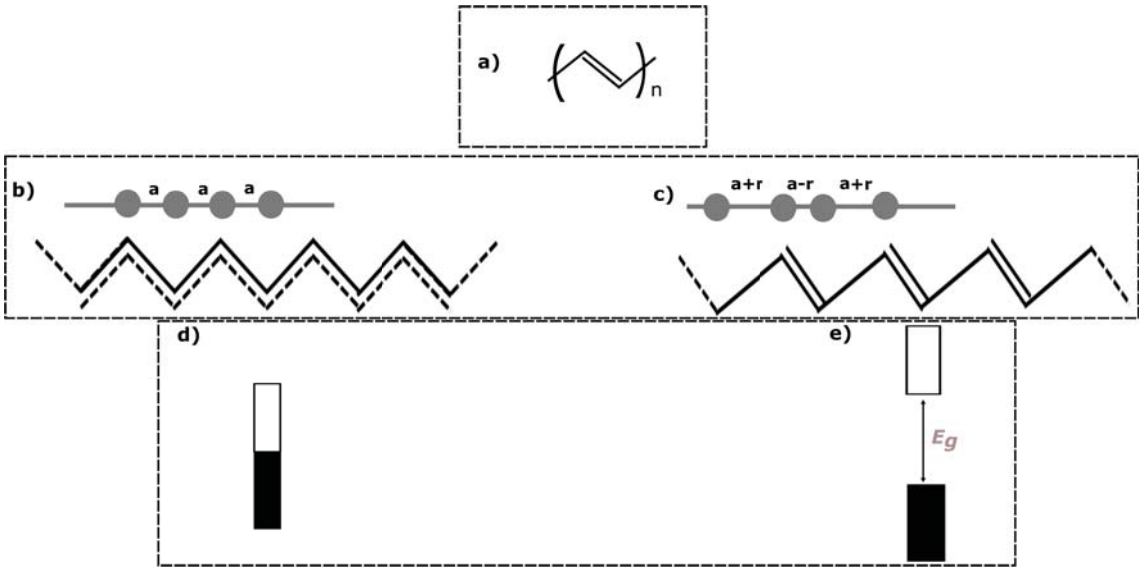

Figure 2.2: a) Structure of PA b) Equidistant bonds create delocalized π electrons along the backbone. The periodicity of the lattice will be 'a' c) an alternating longer single and shorter double bonds with a periodicity of '2a' d) PA is in a metallic state when the bonds are equal e) the alternating single and double bonds disrupts the periodicity and opens a finite band gap.

2.2 Low band gap polymers

The band gap of a polymer determines its application in electronics. This section discusses why we need low band gap polymers for OSC application. Some synthesise techniques to produce low band gap polymer will also be discussed

2.2.1 Why low band gap polymers?

The solar irradiance that reaches the earth is Air Mass (AM) 1.5. Most of the intensity in this AM 1.5 spectrum is concentrated below 2000 nm. The number of photons in the spectrum determines the photocurrent density that can be generated using photovoltaic cells. The maximum current spectrum (Figure 2.3b) that can be generated with

a solar cell under an illumination of AM 1.5 sun at a global tilt is calculated and is shown in Figure 2.3a (black line). It was assumed each photon generates an electron. The integrated photon flux over wavelength multiplied by the charge of an electron gives us the maximum current density that can be generated in an ideal case.

As shown in Figure 2.3b, a material that has a broad abosoption that can extend to higher wavelength region between 1000 nm and $\approx$ 2000 nm can generate the maximum . Hence, extracting this part of the solar spectrum can boost the photo-current density of organic solar cells. Low band gap polymers with broad absorption that extends to longer wavelength region of the solar spectrum have a better photon harvest. Therefore, the spectral coverage of these low band gap polymers is essential for higher photo-current generation.

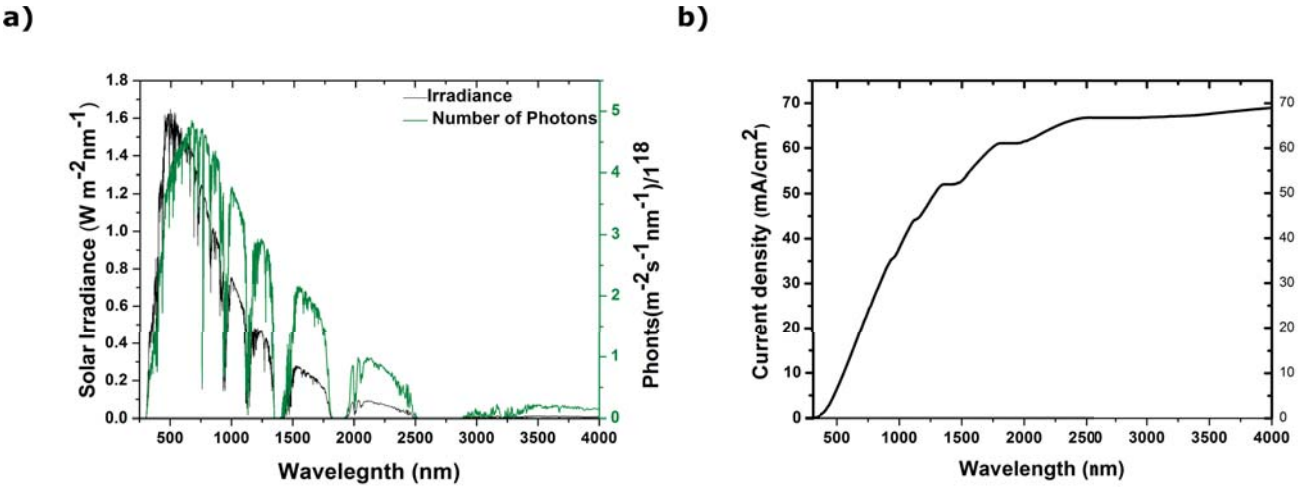

Figure 2.3: a) Spectral irradiance of AM 1.5 sun at a global tilt (black line) and number of photons (green line). b) the maximum current density is calculated assuming each photon generates an electron.

The above discussion focused only on current density relation with band gap without including other photovoltaic efficiency determining factors. However, low band gap polymer based OSCs suffer with low open circuit voltage. Open circuit voltage is determined by the energy difference between the HOMO of the donor polymer and the LUMO of the acceptor. The HOMO level of low band gap polymers can get closer to the LUMO level of the acceptor material which will consequently lower the open circuit voltage. An ideal low band gap polymer for highly preforming solar cells would thus be a polymer that can harvest the longer wavelength region of solar spectrum, with deep HOMO level to ensure high open circuit voltage and appropriate LUMO level for exciton dissociation with the acceptor material (see Section 2.4).

2.2.2 How to produce low band gap polymers?

Synthetic chemists can tune the band gap of polymers in a number of ways. Few of them will be discussed in this section.

Increasing conjugation length. Increasing the conjugation length of a polymer will increase the number of overlapping p_z orbitals. Consequently, the higher de-localized electron cloud in the backbone of the polymer will result in lower band gap. But when such polymers are used in OSCs, the power conversion efficiency is limited. The long conjugation length might exceed the exciton diffusion length. Exciton in such materials

will relax before leaving the polymer chain for charge photogeneration (see Section 2.4).

Bond length alternation: The band gap of a conjugated polymer is also determined by the degree of variation between the single and double bond lengths. Conjugated polymers in their ground state are found in two mesomeric structures: aromatic and quinoid form. In the aromatic structure, the π electrons are more confined while in quinoid structure they get de-localized in the backbone of the polymer. This de-localization in quinoid structure will lower band gap of the polymer. Therefore, by varying the ratio of aromatic and quinoid structures in the backbone of a polymer, the band gap can be tuned. A good example for this is a fused ring system in poly(isothianaphtane), PITN. PITN strongly favours a quinoid structure to preserves the aromaticity of benzene rings (see Figure 2.4 bottom) because benzene has a more stable aromatic structure. The gap of this polymer is 1 eV [12]. A polythiophene (PT) (see Figure 2.4 top) on the other hand has a stable aromatic structure consequently its band gap is twice the band gap of PITN.

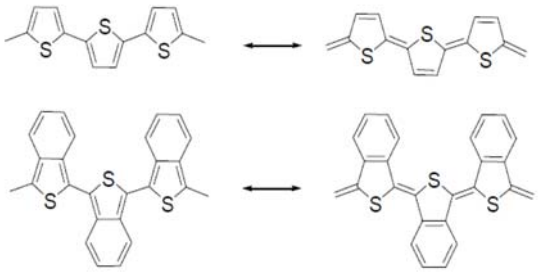

Figure 2.4: Aromatic (left) and quinoid (right) structure of PT (top) and PITN(bottom). The attached benzene rings in PITN favours quinoid structure which resulted in half the band gap of PT.

Polymers with alternating donor and acceptor units: Copolymers: Polymers can be classified as electron donating and electron accepting based on their electron affinity. This is analogues to p and n type inorganic semiconductors respectively. An electron rich donor (D) polymer and an electron deficient acceptor (A) polymer can be coupled in a D - A copolymer. Let us take one of the copolymers characterized in this work as an example (see Figure 2.9). A bithiophene donor unit and an acceptor isoindigo unit are coupled to synthesize **P2TI** (see Figure 2.9). The alternation of D and A units in D-A copolymers results in two mesomeric structures: D - A and $D^{+} = A^{-}$ [13]. The alternation of D and A units in the backbone of a copolymer favours double bond character due to de-localization of electrons. This double bond character leads to the formation of a stable quinoid structure which makes the copolymers have lower band gap than the D or A polymer units.

From molecular orbital point of view, the lowering of band gap in copolymer is due to the following reason: when a D polymer and an A polymer units are chemically bonded, a new energy level arises in the D-A copolymer. The HOMO level of the D-A copolymer will be the hybridized energy level of the HOMOs of the D and A polymer units. The same is true with the LUMO level of the D-A copolymer. The new HOMO and LUMO levels of the D-A copolymer are higher than the two HOMOs and lower than the two LUMOs of the D and A polymer units. Consequently, the D-A copolymer will have a lower band gap (see Figure 2.5). It is important that the HOMO and LUMO of the D-A copolymer is closer to the HOMO and LUMO of the D and A polymer

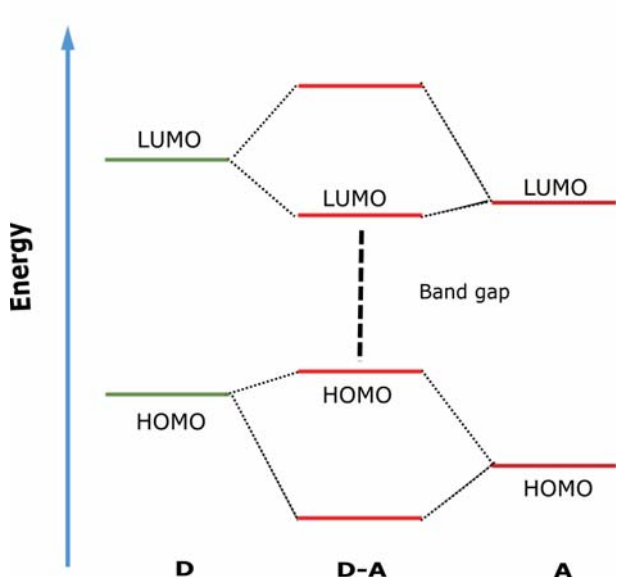

Figure 2.5: Band gap of D-A copolymers: the HOMO and LUMO levels of the D-A copolymers are the hybridized HOMOs and LUMOs of the D and A units respectively. The HOMO of the D-A copolymer is close to the HOMO of the D. Similarly, the LUMO of the copolymer is close to LUMO of the A unit.

units respectively. A facile way to tune the band gap of the D-A copolymers is thus by raising the HOMO and lowering the LUMO of the D and A polymer units respectively. Chemists attach electron rich units like aloxy on the D polymer to raise the HOMO level by increasing its electron donating property. Electron deficient units like NO_2 are attached to A polymer units to enhance its electron withdrawing property which consequently will lower the LUMO level of the polymer.

There is a charge transfer between the D and A units within a D-A copolymer molecules. This intramolecular charge transfer creates a new energy levels in the D-A copolymer different from the D or A polymer units (see Figure 2.5). The new energy level has a HOMO closer to the D polymer unit and LUMO closer to the A polymer unit. Therefore, D-A copolymers have a lower band gap than the constituent polymer units due to this intramolecular charge transfer.

2.3 Copolymer studied in this work

In this work, three D-A copolymers were studied (see Figure 2.9). The three copolymers have a similar A polymer unit called isoindigo. The D polymer units in the three polymers have a slight difference as will be discussed latter. Let us start discussing each of the D and A units separately and will come back to the D-A copolymers studied in this work.

Thiophenes as donor units: Sulphur atom in a thiophene ring has high polarizability that gives it a prominent electron donating property. Thiophenes can also be readily modified at different positions of the ring. Attaching different side chains to increase its solubility in common solvents is possible. Polythiophenes (PT) are one of the most widely used conjugated polymers for OSC application. The band gap of PT is 2 eV [14]. This high band gap is due to its aromatic structure as discussed above. The absorption spectra of these class of polymers is narrow which makes their solar harvest poor. A

number of PT donor polymers were synthesized by coupling the thiophene units in different ways. Among them Poly 3-hexyl thiophene (P3HT) (see Figure 2.7a) is one of the most studied polymers. As shown in Figure 2.6, P3HT can harvest the solar spectrum below 600 nm and its photon absorption from AM 1.5 solar irradiance is $<$ 20%. This narrow absorption is detrimental to the photocurrent generation which in turn will affect the power conversion efficiency of P3HT based OSCs.

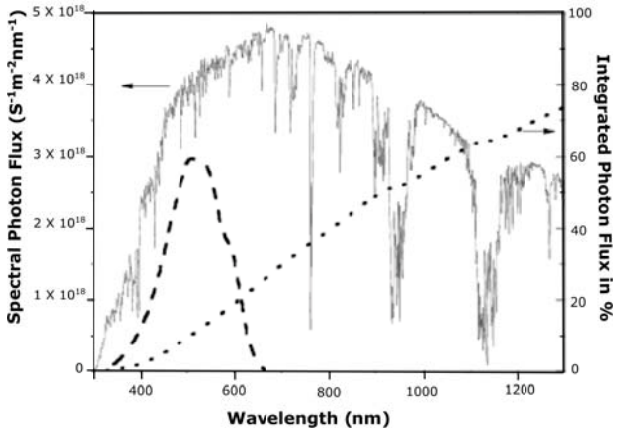

Figure 2.6: Spectral coverage of absorption of P3HT (dashed line) with AM 1.5 solar irradiance. The integrated photon below each wavelength is shown with dotted line.

PT are used as donor units in D-A copolymers due to their excellent electron donating property. The electron donating property of these class of polymers can be improved by fusing two thiophene units as in thieno[2,3-b]thiophene or coupling them with benzene as in benozodithiophene (BDT) etc.. (see Figure 2.7c and d)

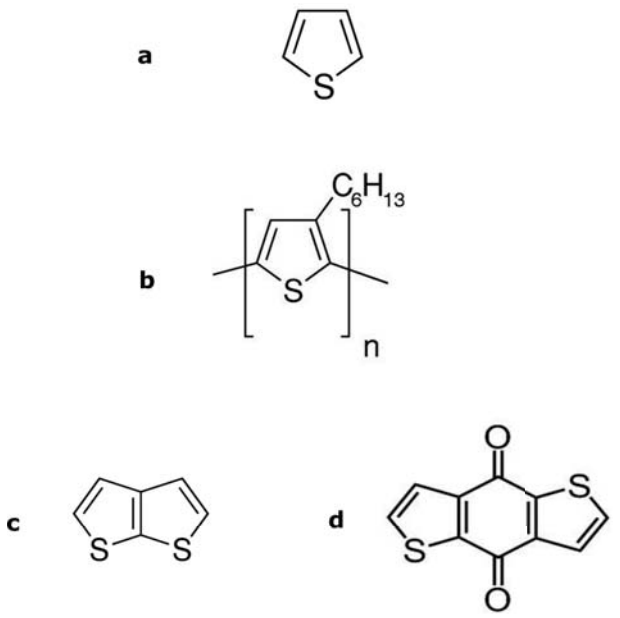

Figure 2.7: Chemical structure of a) Thiophene b) P3HT c) Thieno[2,3-b]thiophene d) Benzo[1,2-b:4,5-b']dithiophene-4,8-dione

Isoindigo as acceptor unit: As compared to the electron rich polymers, electron deficient units are few in numbers due to the challenge in synthesis. Few of them include quinoxaline, diketopyrrolo [3,4-c]-pyrrole-1-4-dione (DPP), theino[3,4-c-pyrrole-4-6-dione (TPD) and isoindigo. Isoindigo is a structural isomer of the famous indigo dye, which is widely used in dye industry (see Figure 2.8). It has a symmetrical lactam ring structure that gives it a strong electron withdrawing character [15]. It is brown coloured with absorption maxima at 365 nm and 490 nm [16]. Raynold *et. al.* [17] used isoindigo for the first time as an acceptor unit to build small molecules for OSC application in 2010. Besides its outstanding electron withdrawing character, isoindigo shifts the LUMO level of the resulting copolymer to a desired value for OSC application [16]. The power conversion efficiency of the first OSC reported on 2010 by Reynold using isoindigo containing small molecules was only 1.76% [17]. A power conversion efficiency exceeding 7% was reported by Zaifei *et. al.* [18] in 2013. Latter, Lei *et. al.* reported an OSC based on isoindigo containing copolymers with a power conversion efficiency of 8.05% [19]. This is the maximum power conversion efficiency of isoindigo based OSCs reported to our knowledge.

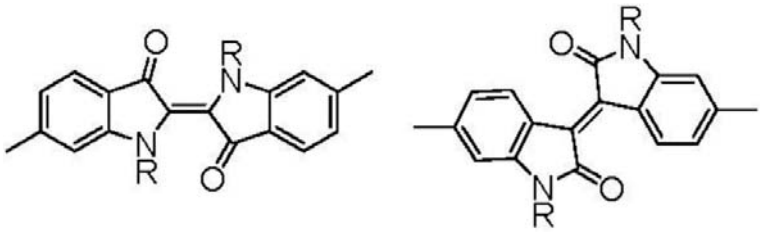

Figure 2.8: Chemical structure of indigo (left) and isoindigo (right). Isoindigo is a structural isomer of indigo dye

Thiophene-isoindigo copolymers: Materials characterized in this work: Three copolymers based on isoindigo as acceptor unit were designed and synthesized. The detail of the synthesis scheme and structural characterization is well documented in Dr. Zelalem's PhD thesis [20]. The motivation for the synthesis of the copolymers is to increase the spectral overlap with solar irradiance thereby reducing the band gap. Three of the copolymers have a slight structural change in the D polymer unit. A structure-property relation that can help improve the performance of such copolymers based OSCs can be drawn with these slight structural changes. The isoindigo unit in these copolymers has 2-octyldodecyl side chains as shown in Figure 2.9.

The first copolymer was synthesized using a bi-thiophene as a D polymer unit. The second and the third polymers have terthiophene D polymer unit. The first copolymer is named **P2TI** the second and the third copolymers are **P3TI-1** and **P3TI-2** respectively. All the three copolymers are soluble in common solvents. They have a similar dark blue color. **P2TI** has lower molecular weight than the other two probably due to the absence of solublizing alkyl side chains (see Table 2.1). Long alkyl side chains were attached chemically in **P3TI-1** and **P3TI-2** to increase their solubility. Their molecular weight was also improved by more than 2 fold from **P2TI**. The alkyl side chain attached to **P3TI-1** (C_8H_{17}) was 4 methyl units lower than the side chain in **P3TI-2** ($C_{12}H_{25}$).

A density functional theory (DFT) calculation was done on one representative monomer unit of a terthiophene-isoindigo copolymer using Gaussian 09 package. A B3LYP func-

Table 2.1: Characterization of copolymers: M_n is number weight, M_w is molecular weight and PDI is the ratio of M_w to M_n

Copolymer	M_n	M_w	PDI
P2TI	6,677	21,557	3.1
P3TI-1	27,405	67,519	2.4
P3TI-2	19,159	45,673	2.3

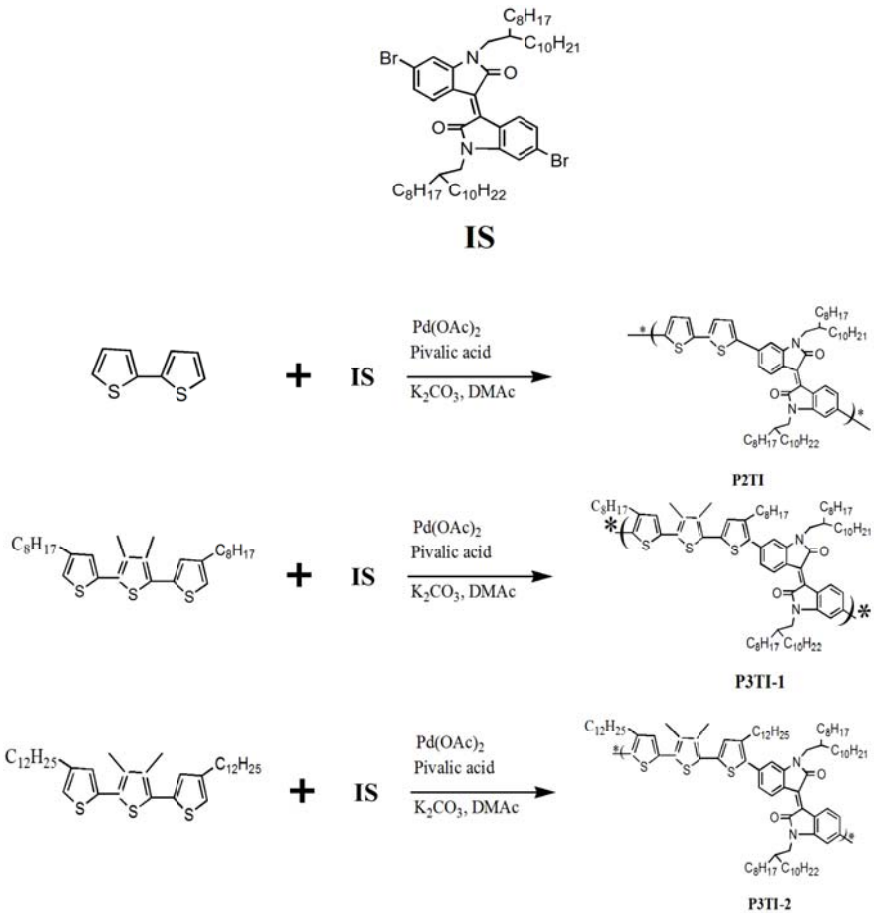

Figure 2.9: Synthesis scheme and structure of copolymers: IS(isoindigo)with 2-octyldodecyl side chains is the acceptor unit in all the three copolymers. The donor units are shown on the left.

tional with basis set CEP-31G was used to calculate the HOMO and LUMO levels of the aforementioned copolymer. The result is shown in Figure 2.10. The electron density in the HOMO is delocalized along the backbone but in the LUMO it is mainly localized on the isoindigo unit. Similar results are expected for all the three polymers because the structure change is very small. Therefore, the HOMO-LUMO transition in the above three copolymers have an intramolecular charge transfer character.

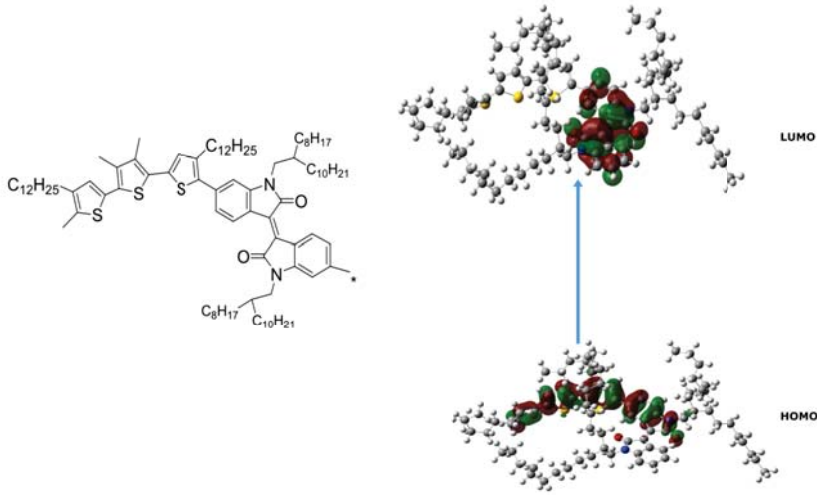

Figure 2.10: DFT calculation on **P3TI-2** monomer. The electron cloud in the HOMO level is delocalized. Due to intramolecular charge transfer between the D and A units, the electron density in the LUMO is mainly concentrated on the A unit.

2.4 Working principle of organic solar cells

The conversion of solar light into electric power using OSCs is a multi step electronic process as opposed to thermal. The steps are sketched in Figure 2.11 and can be summarized as follows:

- **Step-1 Absorption of photons and exciton generation**: Absorption coefficient of conjugated polymers is relatively high as compared to inorganic semiconductors like Si. For example, absorption coefficent of P3HT is $\approx$ 10 times higher than a crystalline Si [21]. Generally, a thin polymer film of thickness $\approx 1\ \mu$m can absorb most of the solar irradiance within its absorption bandwidth. Absorption of photons promotes an electron from the HOMO of a polymer to the LUMO leaving behind a hole. The hole in the HOMO and the electron in the LUMO are tightly bound by Coulomb force. This electron-hole pairs are called exciton.

- **Step-2 Exciton diffusion**: The tightly bound exciton then diffuses to the nearest donor/acceptor (D/A) interface. Exciton diffusion is mainly determined by its diffusion length. A typical exciton diffusion length in conjugated polymers is 5 - 20 nm.

- **Step-3 Exciton dissociation**: The electron will be transferred to LUMO of the acceptor leaving behind the hole in the donor HOMO. The dissociated electron and hole are still bound by a Coulomb force at the D/A interface. The bound electron and hole pairs are called charge transfer (CT) exciton.

- **Step-4 CT exciton dissociation**: Free charge carrier will be generated by the dissociation of CT exciton. The hole on the donor polymer and the electron on the acceptor material are now free and can move within the respective materials.

- **Step-5 Charge transport and collection**: The free electrons and holes will be moving through their electron and hole transporting materials respectively to their respective electrodes. The charge mobility and the percolation paths within the active layer are the main determining factors at this step.

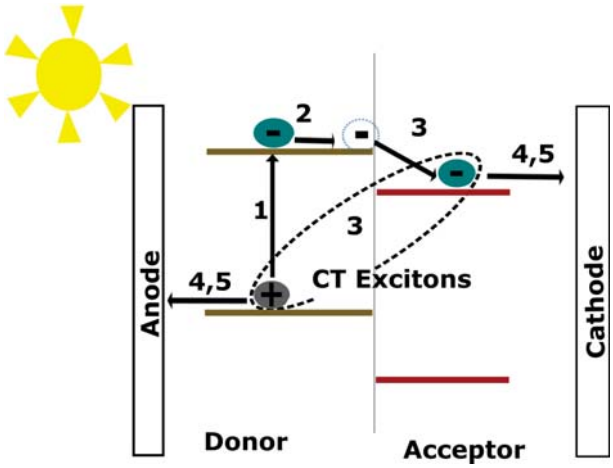

Figure 2.11: Sketch of working principle of organic solar cells. An incident photon generates exciton. The exciton will diffuse to the nearest D/A interface and dissociate into a CT exciton. The CT exciton will finally dissociate into free charges that can be collected in an external circuit.

2.5 Current-voltage characteristics

An OSC is simply a Schottky diode in which a semiconductor is sandwiched between two asymmetric electrodes. The current density (current per unit area) of such devices is given by the following equation:

$$J_D = J_0[exp(\frac{-qV}{nk_BT}) - 1], \tag{2.1}$$

where J_D is the total current density in dark, J_0 is the reverse saturation current density, q is the elementary charge, k_B is Boltzmans constant, T is temperature in Kelvin and n is diode ideality factor. The diode ideality factor is a measure of recombination in the cell has a value between 1 and 3 for OSCs. As shown in Figure 2.12a, a solar cell under illumination generates photocurrent (J_{Ph}). The current density of a solar cell under illumination will then be

$$J = J_0[exp(\frac{-qV}{nk_bT}) - 1] - J_{Ph}. \tag{2.2}$$

The power a solar cell dissipates in an external load is a product of current and voltage. Hence, the performance of a solar cell is determined not only by the illumination but also by the load. Therefore, a standard J-V characterization method was needed. In this method, J-V measurement is taken under simulated AM 1.5 sun with applied voltage to simulate different resistors. The photovoltaic parameters that determine the efficiency of the solar cell can be extracted from the J-V curves as shown in Figure 2.12a. These photovoltaic parameters are summarized below.

- **Short circuit current density (J_{SC})**: A short circuit current is the current that flows through a solar cell when the applied voltage is zero. Since the actual measured current of a solar cell is linearly dependent on the area, it is customary to use the term current density than current. As shown in Figure 2.12a, the J-V curve under illumination is displaced by J_{SC} from the dark J-V curve. This current density is due to part of the photo-generated charge carrier that are collected in the external circuit.

- **Open circuit voltage (V_{OC})**: This is the value of the voltage when there is no current flowing through a solar cell under illumination. Therefore, the photogenerated charge carrier at this condition are cancelled out due to some loss mechanisms.

- **Maximum power (P_{Max})**: The maximum power a solar cell generates is given by the largest area of a rectangle under the J-V curves in the fourth quadrant (see Figure 2.12a). The voltage and the current at P_{Max} point are termed V_{Max} and I_{Max} respectively.

- **Fill factor (FF)**: In an ideal condition P_{Max} corresponds to the product of $V_{OC} \times I_{SC}$ (the blue rectangle in Figure 2.12a). But due to many loss mechanisms in the device, the $P_{Max} < V_{OC} \times I_{SC}$. The squareness of the J-V curve determines the P_{Max}. FF is the measure of this squareness and is given by:

$$FF = \frac{V_{Max} \times I_{Max}}{V_{OC} \times I_{SC}}. \tag{2.3}$$

  Power conversion efficiency (η) of a solar cell is the ratio of the output power to the incident power on the cell. The above four parameters are used to determine the η of a solar cell under an incident illumination of power $P_{incident}$ as follows:

$$\eta = \frac{P_{Max}}{P_{incident}} = FF \times \frac{I_{SC} \times V_{OC}}{P_{incident}}. \tag{2.4}$$

Besides the photovoltaic parameters, the serial (R_s) and the shunt (R_{sh}) resistances can also be calculated from the J-V curves. As shown in the equivalent circuit of a solar cell in Figure 2.12b, the R_s and R_{sh} account for all the resistances in the solar cell device. The R_s is determined by the resistances in the bulk and at both interfaces inside the bulk and the bulk with the electrodes. The R_{sh} accounts for any leakage current. This leakage can be due to some defects in the preparation of the device. These macroscopic parameters can be used to determine charge loss mechanism in the solar cell. A diode under low applied voltage does not start conducting, therefore all the photogenerated current passes through R_{sh}. At intermediate voltages, the diode is conducting and the J-V curve is determined by the diode parameter J_0 and n. At high voltages, the current flow is predominantly determined by R_s. The three regions provide a thumb rule to determine the R_{sh} and R_s from J-V curves. The inverse slope of the J-V curve around J_{SC} gives the value R_{sh} per unit area. Similarly, the inverse slope of the J-V curve around V_{OC} will be R_s per unit area. The value of the R_{sh} and R_s determine the FF which is one of the parameters that determine power conversion efficiency. An ideal solar cell has a very high R_{sh} to block any leakage current and very low R_s.

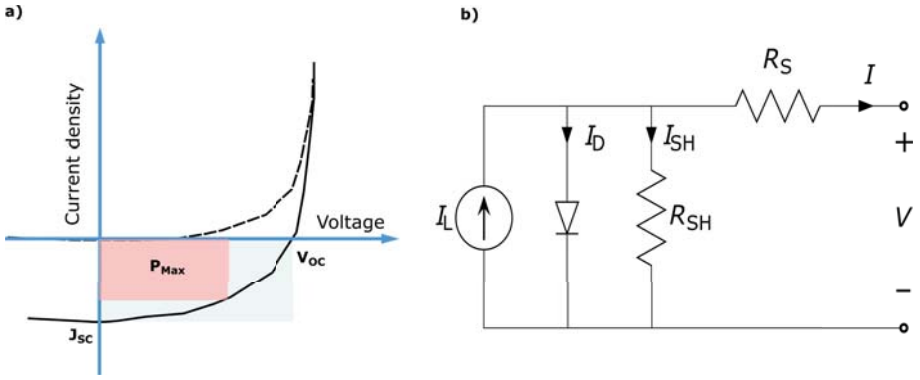

Figure 2.12: a) Current density - Voltage Characteristics of a solar cell in dark (dashed line) and under illumination b) Equivalent circuit of a solar cell. The R_{sh} resistance accounts for leakage current and R_S is due to any hindrance to the current flow in the solar cell.

2.6 The bulk heterojunction concept

The development of OSCs' architecture started with the simplest **single layer OSC** by Weinberger *et. al.* in 1982 [22]. In such devices, the organic semiconductor is sandwiched between two asymmetric electrodes, usually indium tin oxide (ITO) and Al. An incident light promotes an electron from the polymer HOMO to the LUMO leaving behind a hole in the HOMO. This tightly bound exciton can be dissociated by the electric field created due to the the work function difference between the two asymmetric electrodes. Exciton dissociation in such devices is inefficient. Consequently, the power conversion efficiency of a single layer OSC is poor, usually $< 0.1\%$ [23].

The second generation is a **bilayer OSC**. In this architecture, two layers of organic semiconductors with different electron affinity and ionization potential are deposited on top of each other as an active layer of the OSC device. Tang *et. al.* reported the first bilayer OSC using a vacuum deposited CuPc/perlene derivative as donor/acceptor (D/A) materials respectively [24]. The exciton generated in donor organic material after photo-excitation can be dissociated at the D/A interface. Exciton should diffuse to the D/A interface for dissociation. Exciton diffusion length which is typically 5 - 20 nm is a determining factor for dissociation. Therefore, excitons generated further from the diffusion length will have a very low probability of dissociation. The exciton dissociation efficiency in this case can be increased by decreasing the thickness of the donor material but that will limit the photon absorption. The power conversion efficiency of bi-layer OSC never exceeded 1% [25].

The third generation and the most efficient architecture is **bulk heterojunction (BHJ) OSC**. The motivation for this generation of solar cells was to increase the D/A interface in the bi-layer geometry. The active layer is composed of donor and acceptor materials which are intermixed in such a way that the interface between the D/A is ideally in the entire active layer. The exciton generated in the donor material can diffuse to the nearest D/A interface for dissociation. The dissociated electron and hole will then find their way to the electrodes. The first BHJ was fabricated using MEH-PPV and a methano-functionalized C_{60} derivative composite sandwiched between ITO and Ca electrodes [26]. The power conversion efficiency of the first BHJ OSC was 2.9%. The efficiency of BHJ solar cells has now increased to a power conversion efficiency exceeding 10% in single junction[8, 9]and 11% in multi-junction solar cells [27].

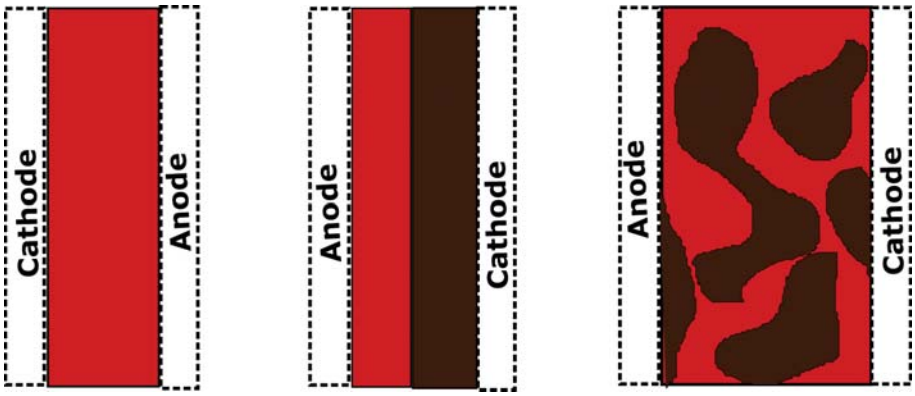

Figure 2.13: Generation of OSC from left to right: Single Layer, Bilayer, Bulk heterojunction, Ordered heterojunction. Exciton dissociation increased from the single layer to the bilayer OSC. In BHJ OSC exciton dissociation efficiency was almost unity but the charge carriers might not reach the electrodes if the active layer morphology does not favour it.

2.7 Morphology of active layer of BHJ organic solar cells

In the above discussion, it is clear that one of the main power conversion efficiency limiting factor in BHJ OSCs is the morphology of the active layer. Exciton from the donor polymer will diffuse to the D/A interface for dissociation. The interface should be within the diffusion length of the exciton which is 5 - 20 nm. After dissociation the electron in the acceptor material and the hole in the donor polymer should also diffuse to their respective electrodes within their respective materials. The donor and the acceptor materials should thus have a continuous path to the electrodes. The desired morphology of the active layer of a BHJ OSC is a continuous interpenetrating networks and separated donor and acceptor phases with a domain size comparable to the exciton diffusion length. The desired morphology looks like the figure below.

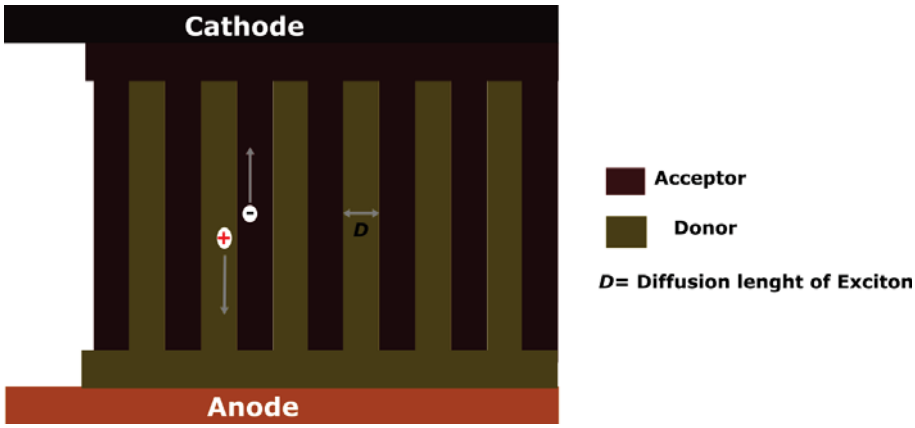

Figure 2.14: Ideal morphology for high performance organic solar cell. In such morphology of BHJ OSC active. layer, the exciton in the donor material will dissociate 100% as the thickness of each donor material pillars is equivalent to the exciton diffusion length. After dissociation, the electron and hole will be drifted to the electrodes by the electric filed in the device [28].

A morphology that is far from the ideal shown in Figure 2.14 decreases the power conversion efficiency of the solar cell. Instead of having pillars of donor and acceptor polymers as in the ideal case, if the morphology is full of intermixed D/A phases exciton dissociation will be ultra-fast ($<$ 100 fs). But if donor and acceptor phases are

separated with large domain sizes, exciton dissociation will be diffusion limited. Such delayed charge generation was reported in P3HT:PCBM OSC prepared using additives [29] and also small molecule solar cells [30]. Howard *et.al.* [31] also reported a morphology related delayed exciton quenching in his work on regioregualr (RR)-P3HT:PCBM and regiorandom (RRa)-P3HT:PCBM OSCs. Thus, charge generation from singlet exciton occurs in a time scale that goes from femto-seconds to tens of picoseconds [29, 30, 32**? ?**]. After the exciton is quenched, the CT exciton and the free charge dynamics will proceed (see Section 2.4). Percolation pathways which are donor and acceptor phases in the morphology affect the CT exciton and free charge carrier recombination dynamics. If CT exciton in such domains cannot diffuse far enough to avoid Coulomb attraction, they might eventually recombine. In cases where they are able to avoid this Coulomb attraction and dissociate into free charge carrier, if there are no uninterrupted pathways to each of the charge carriers that lead to the respective electrodes they will end up recombining before being collected by the external load.

Besides exciton quenching efficiency and free or bound charge carriers recombination, the open circuit voltage and fill factor of an OSC can be influenced by the morphology if the active layer/electrodes interfaces induce extraction barrier due to accumulation of undesired phases.

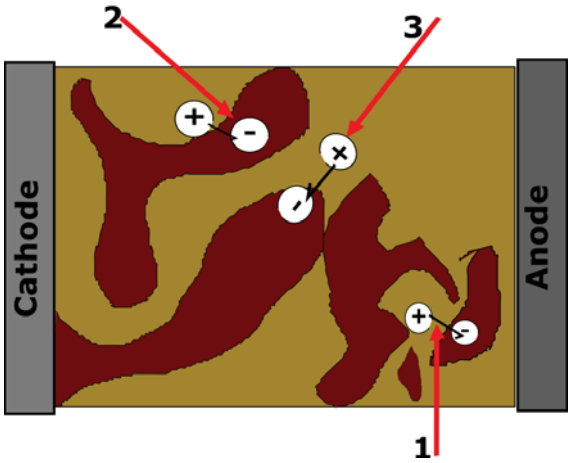

Figure 2.15: A cartoon that shows the effect of morphology on CT exciton and free charge carrier recombinations: the exciton dissociated at the D (light green)/A (brown) interface **1** will recombine readily as they can't diffuse longer to avoid Coulomb attraction between them, **2** free charge carriers will recombine even if they can avoid Coulomb attraction because the percolation path is interrupted before reaching the electrodes and **3** the electron and hole have a chance of being collected

Therefore, the nanomorphology of the active layer of a BHJ OSC is a crucial parameter that needs to be carefully optimized for high power conversion efficiency. Solvent additives and co-solvnets are used as one of the methods to optimize morphology of a BHJ active layer. The solvent additives or co-solvents are usually added in a very small volume ratio to the polymer/fullerene solution before spin coating. An example of the active layer images taken by transmission electron microscopy (TEM) is shown in Figure 2.16 [33]. These images were the active layer of an OSC based on BHJ composite of diketopyrrolopyrrole-quinquethiophene (PDPP5T) copolymer as donor and phenyl-C_{71}-butric-acid-methyl-ester (PCBM71) as fullerene acceptor. For TEM measurements the active layer of the PDPP5T:PCBM71 based OSC was floated from PEDOT:PSS covered indium tin oxide substrate using water to dissolve the PEDOT:PSS layer. The

PDPP5T:PCBM71 layer was deposited on 200 square mesh copper grids. Therefore, the images thus show a depth information. As shown in the Figure 2.16, chloroform (CF) and *o*-dichlorobenzene (*o*DCB) as co-solvents in different volume % was used to dissolve the polymer/fullerene blend. The power conversion efficiency of the OSCs goes from 2%, for without *o*DCB (co-solvent), to more than 5% after adding 3% volume of *o*DCB. The report attributes this drastic increase in power conversion efficiency to the enhanced intermixing of polymer with PCBM71.

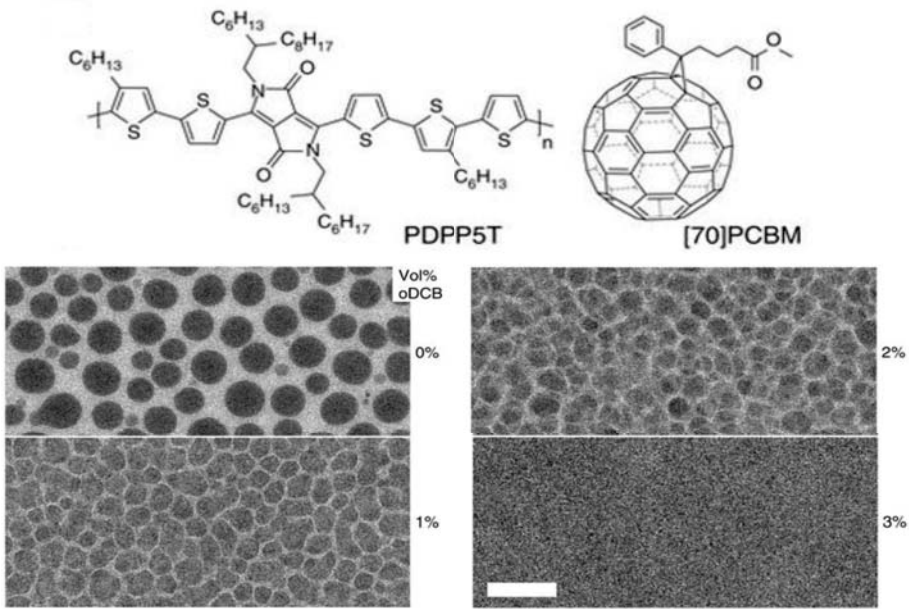

Figure 2.16: Bright-field TEM PDPP5T:PCBM71 (1:2 w/w) films spin coated from CF and *o*DCB (co-solvent). The Scale bar is 600 nm. The intermixing in the active layer has increased as the volume of *o*DCB increases from 0% to 3%. This can be seen by the absence of separated black domains in the active layer [33].

3. Photo-physics, charge generation and recombination dynamics in OSCs

Photo-conversion in any solar cell is determined by the interaction of photon with the semiconductor in the active layer mainly. This interaction is determined by many factors that includes its band gap, optical and electrical properties. In this chapter, I will give a brief introduction to photon-matter interaction processes that are relevant to photo-conversion in OSCs.

3.1 Steady state absorption and fluorescence in copolymers

The first photo-generation step in a solar cell is absorption of solar irradiation. Absorption of photons of energy above the band gap of a material promotes an electron from S_0 to a higher singlet state, S_n, n>0 via allowed transitions. Lambert-Beer law states that the amount of light transmitted through a material is dependent on three parameters: the concentration (c) of the absorbing material, the optical path length (d) the light has to travel thought the sample and the probability of photon of specific energy is absorbed by the material, also called extinction coefficient (ϵ) of the material. The optical density of a material is given by

$$OD = \log \frac{I_0}{I_t} = \epsilon c d, \tag{3.1}$$

where I_0 and I_t are the incident and transmitted light intensities respectively.

The alternation between double and single bonds in the backbone of conjugated polymers lead to $\pi \rightarrow \pi^*$ electronic transitions. There is an additional contribution in D-A copolymers. Jaspersen's *et.al.* [34] work on electronic transitions of a polyflourene (PFO) based copolymer is one of the ice breaking studies. They found the neat PFO polymer has a single absorption peak while the PFO based copolymers consisting of alternating 9,9-ethylhexyl-9H-flourene and 4,7-di-thiophene-2-yl-benzo[1,2,5]thiadiazole units showed two distinct absorption bands. They called this two distinct absorption bands structure a 'camel back' structure. Absorption spectra with two distinct bands, in the short and long wavelength regions, is typical to copolymers. The short wavelength region absorption peak in the neat PFO and the PFO based copolymer was approximately at the same position. Hence, this absorption band is due to the conjugation in the chain that leads to $\pi \rightarrow \pi^*$ transition. They assigned the longer wavelength absorption band to the transition due to the intramolecular charge transfer (ICT) between the D and A units.

Absorption of photons excites an electron form S_0 to S_n, n > 0. The excited electron sits in its Franck Condon state before vibrationally relaxing back to S_1. Then, the electron will relax back to S_0 by emitting photons and this process is called fluorescence (FL). Since FL occurs from a vibrationally relaxed state, its spectrum is red shifted from the absorption spectrum. This shift is called stokes shift.

Solvent effect on absorption and fluorescence spectra

Absorption and FL spectra of a molecule can be affected by the change in the polarity of a solvent. This solvent induced change in the spectra of a molecule is called solvatochromism. The interaction between the solvent and molecules is dipole-dipole interaction which is determined by the polarity of both the solvent and the molecule. Normally a molecule has a higher dipole moment in the excited state (μ_e) than the ground state (μ_g). Therefore, absorption spectrum is usually not affected by the change in polarity of the solvent but FL spectrum is sensitive to this change.

In cases where the molecule is dipolar and the solvents are not, there will be no solvatochromism in FL. The emission of photons will be due to the relaxation of electron from the first singlet excited state called locally excited state (LE) to the ground state. But if the polarity of the solvent is strong enough to interact with the dipolar molecule, the solvent interacts with the exited state dipole moment (μ_e). After photo-excitation the solvent will re-orient itself around 'μ_e' as shown in Figure 3.1, then solvent relaxation will take the molecule from its Franck Condon state to the excited state equilibrium. Emission of photons comes from this relaxed state. In this case, solvent re-orientation and relaxation back to the ground state will be competing processes. If the time for solvent reorientation (τ_R) is longer than the time for relaxation to the ground state (τ_G), the emission occurs from LE state before any solvent reorientation. But if $\tau_R << \tau_G$, the solvent will reorient itself around 'μ_e' before relaxing back to the ground state. The emission will thus be from this relaxed state. Increasing the polarity of the solvent will further lower the relaxed state. Consequently, the FL spectrum will be red shifted with increasing solvent polarity.

The dipole moment of a molecule can increase if the excited states shows partial or full charge separation. In D - A copolymers intramolecular charge transfer between the donor and the acceptor unit can fully/partially separate the charge carriers. As discussed in the above section, their π electronic structure can be described by two mesomeric structures: $D - A \Leftrightarrow D^+ = A^-$, the latter being dipolar. These two mesomeric structures can exist both in the ground and excited states. From our DFT calculation in one monomer unit of one of our copolymers (shown in Figure 2.10), we concluded that the copolymers studied in this work showed a significant charge separation in the excited state than in the ground state. This dipolar excited state will be sensitive to solvent polarity which will bring the equilibrium excited state closer to the ground state. This equilibrium excited state is called intramolecular charge transfer (ICT) state. In such cases, a significant red shift in FL spectra is expected with increasing solvent polarities. But this dipolar character might not be true to all copolymers.

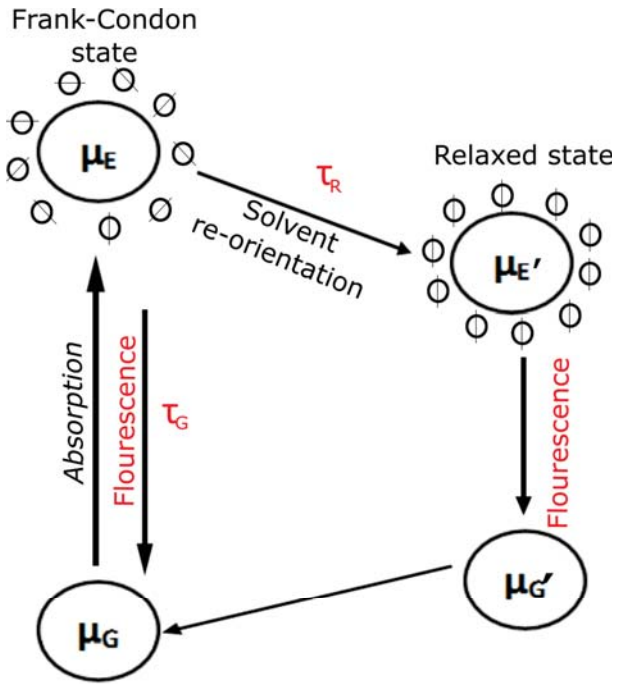

Figure 3.1: Solvent relaxation of a dipolar molecule in a polar solvent takes the molecule from the first excited Franck Condon state to the relaxed state if $\tau_R << \tau_G$. Increasing solvent polarity further lowers the relaxed state which consequently will red shift the FL spectrum. In case of D-A copolymers this relaxed state is ICT state.

3.2 Charge photogeneration in bulk heterojunction OSCs

The D-A copolymer should be blended with an acceptor material, usually fullerene, to serve as an active layer of a BHJ OSC. This active layer is sandwiched between two asymmetric electrodes to finally produce an OSC. The D-A copolymer will here be called a donor material for simplicity. One of the differences between inorganic and organic solar cells as discussed above is the generation of free charge carriers is not straight forward in the latter. After photoexcitation the exciton that reached the donor/acceptor interface will dissociate. But, the electron and hole are still bound as charge transfer (CT) exciton. The existence and the dissociation of CT exciton was controversial. In this section I will present some of experimental reports for the existence of CT exciton and dissociation models. I will also discuss some theories that were applied to similar systems.

3.2.1 Experimental evidence of the presence of inter-facial charge transfer states

The existence of CT states was experimentally shown using techniques that can probe the absorption and emission of this state. The CT state lies below the band gap of the respective donor or acceptor material. Therefore, its emission or absorption is red shifted with respect to the donor or acceptor materials.

Sensitive absorption techniques are needed to probe CT states as the absorption coefficient of this state is very low [35]. A highly sensitive technique to measure external quantum efficiency in the region of CT absorption using Fourier-transform photocur-

rent spectroscopy was successfully used to probe this state [36]. In this technique, a photo-current generation below the band gap of the pristine donor or acceptor materials was observed indicating a new absorbing state is generated in the blend of the donor and acceptor materials.

After photoinduced electron transfer from the excited donor to the acceptor, the electron in the acceptor and the hole in the donor side can recombine radiately, which makes it possible to probe CT states with photo-luminescence(PL) technique. This radiative recombination generates an additional PL signal that is not either in the donor or acceptor materials. Hasharoni *et. al.* in 1997 first reported a weak near infra red PL signal in the blend of MEH-PPV and fullerene [37]. A number of reports came latter in many material combinations. The PL spectra of the blend could be deconvolved into PL from both the pristine donor and acceptor materials and a new red shifted PL from the CT state.

Electroluminescence (EL) spectroscopy was also used to probe emission of the CT state by injecting electrons to the acceptor and holes to the donor materials. Similar to the PL signal, a red shifted additional EL signal to the pristine materials was observed in the blend [38].

3.2.2 Theoretical background of CT states and their dissociation

Before discussing photogeneration in OSCs, it is important to see some theories that were applied to similar systems.

Marcus theory of electron transfer

Marcus theory of electron transfer (ET) was developed in 1956 [39] and has been applied to many chemical systems and conjugated polymer blends [40–42]. In his theory, he considers reactant and product potential energies as parabolic functions of reaction coordinates (see Figure 3.2). ET occurs at the intersection point of the reactant and product potential surfaces. This is to satisfy both the requirements of conservation of energy and Frank Condon principle which states ET occurs very quickly that the nuclear does not get enough time to change its coordinates. In the case of conjugated donor (D) and acceptor (A) polymers, ET occurs at the intersection of the potential surfaces of the excited donor/acceptor (D^*/A) and the charged donor/acceptor (D^+/A^-) as shown in Figure 3.2. ET is an activated process which occurs with an activation energy of $\Delta G^{\#}$. $\Delta G^{\#}$ is a function of Gibbs free energy (ΔG^0) and reorganization energy (λ) and is given by:

$$\Delta G^+ = \frac{(\lambda + \Delta G^0)^2}{4\lambda}. \tag{3.2}$$

The reorganization energy λ, is the energy required to bring the reactant and its surrounding medium to the equilibrium geometry of the product state. This energy can be vibrational contribution due to the change in nuclear geometry as a result of electron transfer or solvent contribution due to the change in polarization of the surrounding medium to stabilize the product.

ET rate constant (k_{ET}) is given by the following equation:

$$k_{ET} = \frac{2\pi}{h\sqrt{4kT\pi\lambda}} V^2 exp(-\frac{(\lambda + \Delta G^0)^2}{4\lambda kT}), \tag{3.3}$$

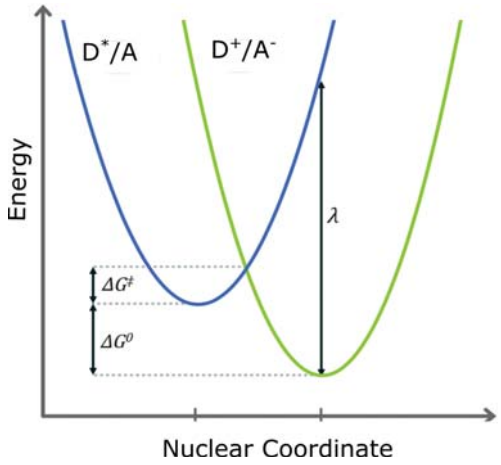

Figure 3.2: Marcus Theory: ET occurs at the intersection of potential surfaces of D*/A and D^+/A^- with an activation energy $\Delta G^{\#}$ which is determined by ΔG^0 and λ.

where V is a matrix element that determines the electronic wave coupling between the reactant and the product or in case of organic solar cells the electronic wave coupling between the donor and acceptor materials. Marcus theory predicts when the free energy for charge separation in D-A systems ($-\Delta G^0$) is equal to λ, ET in such systems will proceed with no barrier. A further increase in $-\Delta G^0$ will decrease the ET by increasing the barrier for charge transfer. This region is called Marcus's inverted region

Marcus theory was successfully used to explain intramolecular charge transfer in solution of donor-acceptor dyads (oligomer-fullerene dyads)[42] and a tree like polymer of donor-acceptor dendimer [41]. The two studies showed as the solvent polarity increases, $D^+ = A^-$ is the charge separated stable structure in the excited molecules. The polarity of the solvent directly influences the reorganization energy of the system. In the above two report on donor-acceptor systems [41, 42], they showed an increase in k_{ET} as the polarity of the solvent increases. The application of Marcus theory to solid films needs a slight modification to include the presence of acceptor bands instead of a molecular level. Van Hal *et. al* [42] also observed a considerable difference in ET kinetics of the donor-acceptor dyads in solids from solutions. They concluded that charge separation in solid films is ultra-fast due to a fast intermolecular charge transfer reaction between adjacent dyad molecules, which is very unlikely to happen in dilute solution. In solid state, the donor and acceptor chromophores of different dyad molecules are in close proximity which makes the intermolecular charge transfer dominate the ET process.

Besides singlet excitons in some polymers usually D-A copolymers, photoexcitaion induces an intramolecular charge transfer (ICT) between the donor and acceptor units within the polymer chain. The influence ICT character of a polymer to the power conversion efficiency of OSCs was not given that much attention until very recently. Singlet excitons were believed to be disociated only when an acceptor material is blended in the OSC active layer. Chen's [43] group reported ultrafast intramolecular exciton splitting into intramolecular charge transfer (ICT) and intramolecular CS states. They reported a linear relation between the population intramolecular CS states and photovoltaic performance of OSC for a series of D-A copolymers. They were able to conclude that ultrafast exciton splitting into partially and fully separated charges within a single copolymer chain lowers the binding energy of exciton which is detrimental to power conversion efficiency of OSC. It is easier to observe ICT state when the polymers are

in dilute solution where there is negligible/no interchain interaction. There are also some reports of ICT state in pristine films [44]. But generally in solid films, there is a strong interchain interaction. Consequently, the charge carriers might rather go to the neighbouring chains. This interchain interaction is usually ultrafast as was reported by Van Hal *et.al.* [42].

Onsager - Braun theory

Geminate recombination of Coulomb bound electron-hole pairs was first quantitatively described by Onsager [45]. He assumes an incident photon with enough energy to ionize molecules in a medium of dielectric constant, ϵ_r, creates a metastable coulomb-bound electron-hole pairs (CT exciton) with a separation, r_0. This CT exciton will undergo a Brownian motion. In the course of this random motion, they will have several attempts of dissociation by the process called auto-ionization or recombine geminately on their first encounter. This is called infinite sink approximation. The model assumes a photon absorption generates localized hole and 'hot' electron. This 'hot' electron will undergo a random motion until it losses it energy at some termalization distance, 'a'. He defined a capture radius also called Onsager radius, r_c, to be the distance at which the coulomb attraction is equal to thermal energy, k_BT and is given by

$$r_c = \frac{e^2}{4\pi\epsilon_r\epsilon_0 k_B T}, \tag{3.4}$$

where e is the charge of an electron, ϵ_r is the dielectric constant of the materials, ϵ_0 is the permittivity of a vacuum, k_B is Boltzmann's constant and T is temperature. The recombination of CT exciton depends on the themalization length, 'a'. If 'a' is larger than the capture radius, r_c, the electron and hole are not bound. In this condition free charge carriers are generated. But, if 'a' is smaller than r_c, recombination to the ground state and escape from the Coulomb attraction become two competitive processes. Therefore, the above equation emphasizes the importance of dielectric constant in the generation of free charge carriers from bound CT excitons. In inorganic materials like Si, ($\epsilon_r > 11$), the capture radius is small. Hence, free charge carriers generation due to photo-excitation is efficient. In contrast, organic semiconductors have a low dielectric constant($\epsilon_r < 4$), which makes the capture radius larger that the electrons that thermalize within this radius will be going through competitive processes between recombination and dissociation into free charge carriers. In dye sensitized solar cells this problem is overcome by using TiO_2 ($\epsilon_r \approx 80$) as an electron transport material.

Onsager formulated the escape probability (P(E)) of a themalized CT exciton as follows. In the presence of electric field (E), the Coulomb potential will be lowered. The escape probability is thus dependent on electric filed (E), thermalization distance 'a', and temperature, T, and is given by the following equation.

$$P(E) = exp(\frac{-r_c}{a})(1 + \frac{er_c}{2k_BT}E). \tag{3.5}$$

In Onsager's 'infinite sink approximation' model, if the separation of the ions reaches zero the CT exciton will recombine irreversibly. This excludes the life time of CT state. Braun latter revised Onsager's model by incorporating a finite life time and reversible recombination dynamics to the CT exciton. The CT exciton can either undergo geminate recombination with a rate $k_{rec} = \tau^{-1}$ to the ground state or dissociate into free

charges with a rate constant of $k_{diss}(E)$. The escape probability in Onsager-Braun model is thus given by

$$P(E) = \frac{k_{diss}(E)}{k_{rec} + k_{diss}(E)} = k_{diss}(E)\tau(E), \tag{3.6}$$

where $\tau(E)$ is the lifetime of CT exciton.

The dissociation rate in Onsager-Braun model is dependent on measurable parameters that include Electric field (E), mobility of electron and hole, μ_e and μ_h respectively, temperature (T) and is give by the following equation.

$$k_{diss}(E) = \frac{3e\,\langle \mu_e + \mu_h \rangle}{4\pi\epsilon_r\epsilon_0 a^3} exp(\frac{-E_b}{k_B T})[1 + b + \frac{b^2}{3} + \frac{b^3}{18} + ...], \tag{3.7}$$

where $E_b = e^2/4\pi\epsilon_r\epsilon_0 a$ is the binding energy of the CT exciton and $b = e^3E/(8\pi\epsilon_r\epsilon_0 k_b^2 T^2)$, where the final summation is the first order approximation of Bessel function.

3.2.3 Dissociation of CT state into free charge carriers

The above discussed theories can be used as a basis for discussing charge photogeneration in OSCs. The main processes involved in charge photogeneration in OSCs are summarized in Figure 3.3. Photo-excitation promotes the electron in donor (D) from the HOMO into the LUMO by generating an S_1 singlet exciton, (D^*). The exciton can be quenched by transferring its electron to the LUMO of the acceptor usually fullerene. At this stage the exciton state evolves to a Coulombically bound electron-hole pairs in a charge transfer (CT) state (D^+/A^-). The initial electron transfer generally creates a 'hot' CT state with excess thermal energy (ΔG_{CT}) due to the energy difference between the excitonic and CT state. The dissociation of the 'hot' CT state depends on the thermalization distance 'a' versus the Coulomb capture radius, r_c as discussed above in Onsager theory. If the CT state thermalizes at $a > r_c$, it will dissociate into free charge carriers in the manifold of charge separated (CS) state. The free charge carriers will diffuse away from each other and if they avoid bimolecular recombination they will be collected by their respective electrodes. But if it thermalizes at, $a < r_c$, the thermalized CT state might undergo a geminate recombination to the ground state, S_0. The long lasting debate in the community of OSCs is whether charge carrier are generated from the 'hot' CT state or the 'relaxed' CT_1 state (see Figure 3.3).

There are two models of photogeneration in OSC: Photo-generation through the 'hot' CT state and Photo-generation through 'relaxed' CT state.

Photo-generation through the 'hot' CT state

If charge carriers are generated through the 'hot' CT state, the competition will be between themalization and dissociation. This process is similar to auto-ionization in intrinsic charge carrier generation from higher lying states in pristine organic semiconductor. The internal conversion process is ultrafast, in the order of 100 fs. The dissociation process should also be at least on the same time scale for charge generation.Grancini *et.al.* report charge generation from 'hot' CT state is extremely fast from 50 fs to a 100 fs regime [47]. In this theory once the 'hot' CT state thermalizes to CT_1, it has no chance of dissociation. It will recombine geminately to the ground state, S_0

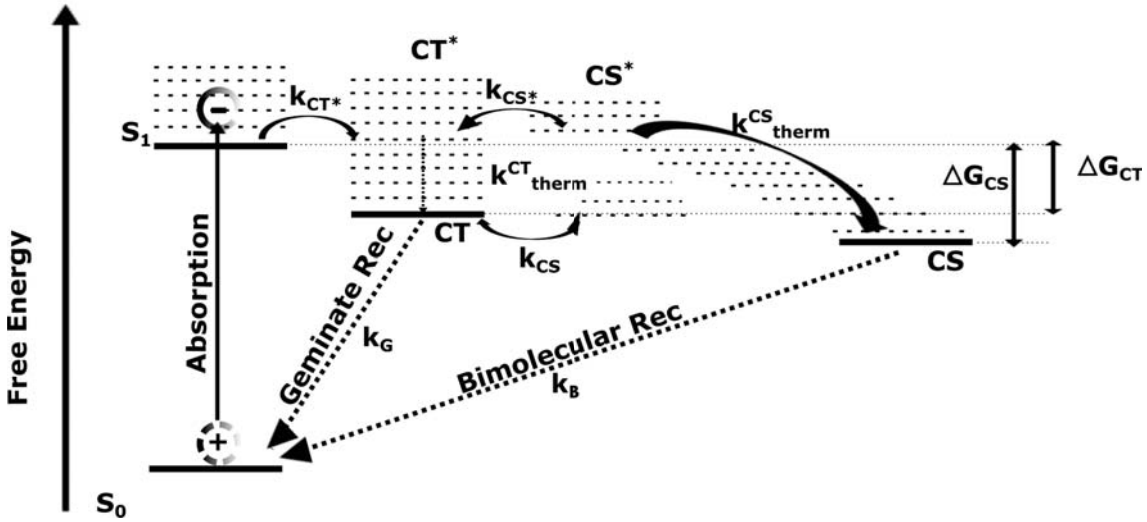

Figure 3.3: Energy levels summarizing charge photogeneration in OSCs. Photoexcitation generates a singlet exciton (S_1). The exciton is quenched at a rate of k_{CT^*} to a 'hot' CT^* state with excess energy of ΔG_{CT}. CT^* will either dissociate into free charges in CS^* at a rate of k_{CS^*} or thermalize to CT at a rate of k^{CT}_{therm}. If this CT state can not separate, it recombines geminately (k_B). The separated charges in CS^* loose the thermal energy (k^{CS}_{therm}) and relax to CS which makes the total energy loss in the system ΔG_{CS}. Finally, if the free charges can not be collected by the electrodes, they will recombine bimolecularily (k_B) [46]

because it doesn't have enough driving force to overcome the Coulomb attraction. The binding energy of this CT state is estimated to be approximately 0.1 - 0.5 eV [48, 49].

Photo-generation through 'relaxed' CT state

If thermalization to CT_1 state is faster than the charge separation process, the CT states will be relaxed. The question is: if charge photogeneration occurs from this relaxed CT state what is the driving force for this dissociation? A number of experimental evidences were reported to support the 'relaxed' CT state theory [31, 50].

A review by Bassler *et. al.* [51] explained charge dissociation through relaxed CT_1 state as follows: the excess energy at the generation of CT state can be used to increase the temperature of the system as it thermalizes. This effectively increases the Boltzmann's factor, which makes the thermalized CT_1 state loosely bound. This loosely bound but relaxed CT_1 state, can escape the Coulomb attraction and contribute to free charge carrier generation. The other plausible hypothesis they gave was, the excess energy might be dissipated in an exothermic process that finally leaves the electron-hole pair loosely bound.

3.3 Geminate versus bimolecular recombination dynamics

Charge carriers are efficiently generated from excitons at the donor - acceptor interface than pristine donor polymers. The free and bound charge carriers (CT excitons) have similar photoinduced absorption spectra. This creates a complication to spectrally identify free and bound charge carriers photoinduced signatures in donor/acceptor

blend films. The CT excitons have a shorter life time due to their higher binding energy than the free charge carrier. The other main difference is their recombination dynamics: recombination dynamics of CT exciton is geminate while the free charge carriers' recombination dynamics is bimolecular.

Geminate recombination is a first order monomolecular recombination, whereas a bimolecular recombination is a second order recombination. Geminate recombination involves recombination of electron and holes generated from the same parent exciton. Recombination of CT exciton is thus classified in this type of recombination. After dissociation of the CT exciton, the electrons and holes are free. These free electrons and holes from different excitons might recombine on their way to the electrodes. This type of recombination is the second order bimolecular recombination. In bimolecular recombination, the free charge carriers should diffuse to their Coulomb capture radius to recombine. But in geminate recombination, the charge carriers recombine because they already are in their Coulomb capture radius.

The geminate recombination rate is independent of the density of charge carrier whereas bimolecular recombination rate is scaled with concentration of holes and electrons. The higher electron/hole concentration, the higher is the probability of bimolecular recombinations. Therefore, as the pump fluence is increased the life time of CT state remains the same. However, the free charge carriers' life time decreases due to the increased probability of recombination with more charge carrier density.

The geminate recombination rate R_G is given by

$$R_G = \frac{n(t)}{\tau_r}, \tag{3.8}$$

where n(t) is the electron(hole) density at some time 't' and τ_r is the life time of CT excitons. A bimolecular recombination includes recombination of mobile charge carriers with trapped charges as well as recombinations of two mobile charge carriers. Hence, the recombination dynamics can be calculated using Langevin theory. Langevin theory can be applied to organic semiconductors because they have low charge carrier mobility. The bimolecular recombination rate, R_B, can be calculated using Langevin theory and is give by

$$R_B = \gamma n(t) p(t), \tag{3.9}$$

with electron (n) and hole (p) density and the Langevin recombination prefactor, γ. The Langevin recombination prefactor γ is given by:

$$\gamma = \frac{e}{\epsilon_r}(\mu_e + \mu_h), \tag{3.10}$$

where e is charge of an electron, ϵ_r is dielectric constant of the organic material and μ_e and μ_h are electron and hole mobilities respectively.

3.3.1 Exciton-exciton annihilation and exciton-charge annihilation

Exciton-exciton annihilation Besides exciton quenching at the D/A interface, exciton can be quenched through exciton-exciton annihilation (EEA). EEA is a process that occurs by excitation energy transfer from one of the excitons to the other. It is a long range interaction through Forster resonant energy transfer [52]. In the process one exciton relaxes back to the ground state (GS) and the other is promoted to higher energy level

(EX*) using the excitation energy of of the other exciton. The excited exciton finally losses its energy through ultrafast internal conversion (EX). The process is summarized as follows and is shown in Figure 3.4:

$$EX_1 + EX_2 \rightarrow \text{GS+EX}_2^* \rightarrow \text{GS+EX}_2.$$

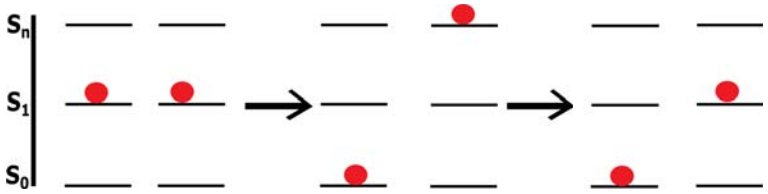

Figure 3.4: EEA scheme: Two EXs interact through Forster energy transfer. One of the EXs is promoted to higher energy level S_n and the other EX relaxes back to the ground state. That leaves an excited EX* while relaxing the other to the ground as shown in the middle. EX* will looses its energy and relax back to S_1 (last).

EEA is determined mainly by the pump fluence rather than morphology of active layer and is a bimolecular process. For EEA, the excitation density should exceed 1.5×10^{17} cm $^{-3}$ [**?**] which is much higher than the operational densities under 1 sun condition. Exciton dynamics at this pump fluence will have a very fast dynamics followed by a longer one. The short dynamics is the intensity dependent EEA and the longer one is the relaxation of excitons back to the ground state and is independent of pump fluence. EEA can be used to determine the diffusion length of an exciton. The rate equation for a singlet exciton in a pristine donor polymer can be written as follows:

$$\frac{dN(t)}{dt} = -\frac{N(t)}{\tau} - \frac{1}{2}\gamma(t)N(t)^2, \tag{3.11}$$

where N(t) is the exciton density at time 't', τ is the exciton life time without EEA, and $\gamma(t)$ is the bimolecular annihilation rate coefficient for EEA. The annihilation rate $\gamma(t)$ is dependent on the dimensionality of the diffusion. Assuming 1D diffusion , $\gamma(t)$ is given by:

$$\gamma(t) = 4\pi DR\frac{R}{\sqrt{2\pi Dt}}, \tag{3.12}$$

where R is the effective interaction radius of singlet excitons, D is the diffusion constant (i.e. $L_D = (D\tau)^{1/2}$)), L_D is the diffusion length [52]. The derivation for $\gamma(t)$ is found in reference [52] and [**?**].

Exciton-charge annihilation Under high pump fluence, excitons specially in a BHJ film are subject to a bimolecular reaction with charges (exciton-charge annihilation (ECA)) in addition to EEA. Charge generation in BHJ films occurs in ultrafast time scale below 100 fs and is efficient. Consequently, ECA is more efficient than EEA in BHJ films. Similar to EEA, ECA is also an interaction through a long range resonant energy transfer between an exciton and a free charge. In this process, the exciton(EX) relaxes back to the ground state (GS) while the free charge (FC) is excited to higher energy levels (FC^*) which then looses it energy rapidly through ultrafast internal conversion.

The process can be summarized as follows:

$EX + FC \rightarrow$GS+FC$^* \rightarrow$GS+FC.

In conclusion, both EEA and ECA are processes that occur at high excitation densities. Both processes do not occur under the normal 1 sun condition.

4. Experimental section

This chapter summarizes organic solar cell sample preparation, the methods used to characterize their performance, morphology of active layers and photophysical study techniques.

4.1 Sample preparation

Solar cell devices were prepared in inverted ITO-free geometry, see Figure 4.1. ITO is one of the costly materials in the production of traditional organic solar cells (OSCs). Besides its cost, it contributes to the degradation of OSCs. ITO etching is one of the degradation mechainisms. Krebs and Norrman observed ITO etching in OSC device (Al/C60/P3OT/ITO)[53]. ITO is coated with PEDOT:PSS to facilitate hole trasfport in the traditional geometry. But ITO can be etched by PEDOT:PSS[54]. Hence, the samples in this work were prepared in inverted ITO-free OSC geometry. Glass slides were cut in a dimension of 2.5 cm width by 1.5 cm length. The glass substrates were cleaned with ultrasonic bath successively with detergent, acetone, iso-propanol and deionized water each 10 min. A solution of ammonia:hydrogen peroxide:deionized water (1:1:5 v/v ratio) was heated to 85°C for final cleaning. The substrates were immersed in the solution for about 5 minutes and rinsed thoroughly with deionized water. Now the substrates are ready for electrode deposition. The substrates were moved to a glove box fitted with a thermal evaporator. Aluminium (80 nm) and Titanium (2 nm) were successively evaporated through a mask at a base pressure of $\approx 10^{-6}$ mbar. The glass/Al/Ti layer was taken out of the glove box for 10 hours to oxidise the Ti layer. Solutions of polymer:PCBM71 in different ratios were prepared using *ortho*-dichlorobenzene (*o*-DCB)solvent. (*o*-DCB) was chosen over chlorobenzene as a solvent because PCBM71 has higher solubility in it. The solutions were stirred for 4-6 hours at 80^0C. The polymer:PCBM71 blend solution was spin coated on glass/Al/TiOx. Then, the samples were taken out of the glove box. Before spin coating the PEDOT:PSS about 2/3 of the Al/TiOx rods were covered with Poly(methyl methacrylate)(PMMA) to protect the bottom electrode contact.

A highly conductive PEDOT:PSS *PH 1000* was mixed with dimethyl sulfoxide (DMSO) and zonyl surfactant in 20:1:0.05 v/v ratio respectively. The mixture is then spin coated outside the glove box at 1000 rpm on top of the glass/Al/TiOx and dried at 60^0C for 5 minutes before it is moved back to the glove box. The thickness of the PEDOT:PSS layer was around 80 nm. The glass/Al/TiOx/Active layer/PEDOT:PSS stack was dried at 60^0C for another 20 mins inside the glove box. The active layer was encapsulated with a glass slide and glue. The glue was cured with solar simulator for 10-15 minutes. Finally, a silver paste was painted on the PEDOT:PSS side before taking the samples out of the glove box for characterization. The area of the solar cells was measured carefully

with optical microscope and was ≈ 4 mm^2.

The thin film samples for transient absorption spectroscopy measurement were prepared on glass substrates. The sample were spin coated on glass substrate either from the pristine polymer or the blend of polymer and PCBM71 solution in *o*-DCB solvent. The substrates were cleaned using the procedure mentioned above. The optical density of the films was kept below 0.4. The solution samples were polymer solution dissolved in *o*-DCB. The concentration of the solutions was in the range where there is no aggregation effect. The optical density of the solutions was about 0.4/cm.

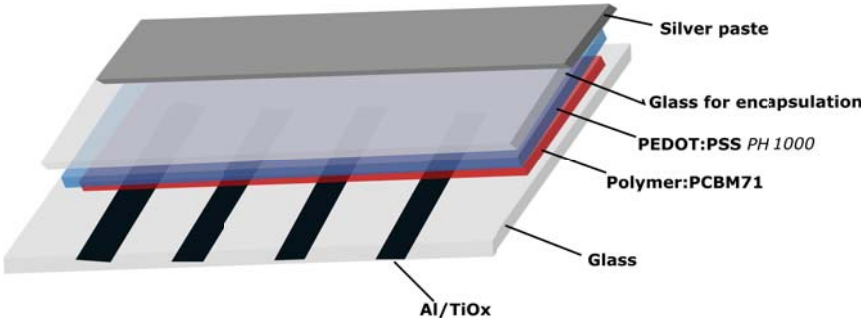

Figure 4.1: ITO-free solar cell architecture: Al/TiO_x rods are thermally deposited on about 2/3 of the length of a clean glass substrate then the active layer composed of polymer:PCBM71 blend is spin coated on about 1/3 of the length of the Al/TiO_x rods. The top electrode, highly conductive PEDOT:PSS *PH 1000*, is spin coated on top of the active layer and the clean glass. The Al/TiO_x/Active layer/PEDOT:PSS stack will be encapsulated with a glass slide. Finally, a silver paste is painted on the uncovered side of PEDOT:PSS for contact.

4.2 Experimental set-ups and characterization techniques

In the following section, characterization techniques used in this work are discussed. A detailed discussion will be spent on the fs-transient absorption set up.

4.2.1 Absorption and fluorescence

Absorption of all polymers were taken in solution, pristine films and polymer:PCBM71 blend films using Thermo Scientific Uv-Vis spectrometer. Fluorescence spectrum was recorded using Perkin Elmer *LS45*. The samples were excited at wavelengths corresponding to absorption maxima of each polymers in solution. The solution should be dilute enough to allow the emission through. Thus, the solution used for fluorescence measurement has an absorbance of ≈ 0.05. The excitation light source and the detector are perpendicular to each other. The incoming light will not directly go to the detector and damage it. The scattered excitation light might reach the detector.

4.2.2 Current-voltage characteristics

A solar simulator model ss-50A from Photo-Emission Tech was used as an illumination source for current-voltage characterization. The illumination was set at one sun (AM 1.5) which corresponds to an intensity of 100 mW/cm^2. Current - voltage evaluation

was taken using Keithley 2400 Source meter. The samples are kept in a dark box for dark I-V characterization.

4.2.3 Fluorescence microscopy

Florescence mapping of polymers and polymer:PCBM71 BHJ films were performed using Carl Zeiss LSM 780 confocal microscope in central analytical facility(CAF) of Stellenbosch University. The exciting laser beam was set at wavelength of 561 nm which is close to absorption maxima of the polymers. A microscope objective of numerical aperture ≈ 1.4 was used both to excite and collect the fluorescence. The laser beam at the output was filtered using a dichroic mirror. Finally, the signal was captured by an avalanche photo diode (APD) and fluorescence images were generated. The fluorescence of a polymer and the polymer:PCBM71 BHJ blend films were taken to get a quantitative idea of exciton quenching in the OSCs. The fluorescence of the pristine polymer is quenched by adding PCBM71 as the electron from the polymer HOMO transfers to the LUMO of PCBM71. Thus, the fluorescence or photoluminescence (PL) quenching efficiency (ΔPL) is given by:

$$\Delta PL = 1 - \frac{PL_{Blend}}{PL_{Pristine}}. \tag{4.1}$$

PL_{Blend} and $PL_{Pristine}$ are the average fluorescence intensity over the area that is measured.

4.2.4 Morphology

Scanning Electron Microscopy (SEM)

A sample hit by beam of electrons emits primary backscattered electrons, secondary and Auger electrons. An electron recorder in SEM picks up the rebounding primary backscattered electrons and secondary electron and record their imprint. These electrons carry information about the sample morphology and chemical composition of materials making up the sample. The information is then translated as a clear image on a screen. The samples for SEM imaging were prepared from solutions of polymer:PCBM71 of the same concentration and spin coating speed as the solar cells. The samples on glass substrate were sputtered with thin gold layer on top for conducting the electrons in the imaging process. The SEM images were taken in CAF-Stellenbosch University. The unit is equipped with a ZEISS EVO MA15VP SEM. A 5 kV electron gun was used. Polymers and fullerenes are both made of carbon: this complicates the assignment of the domains in an SEM image of polymer:fullerene BHJ film to the pure materials. The sample morphology that is recorded with SEM shows the size of the domain sizes. The size of the domains should be comparable to exciton diffusion length (5 - 20 nm) for efficient photogeneration.

Scanning Transmission Electron Microscopy (STEM)

In the case where getting clear SEM images was a challenge, STEM imaging was used for its better resolution. STEM is a transmission electron microscope (TEM). They both use electron beam with short wavelength and they both form images from the information contained in the transmitted electrons. Unlike TEM, STEM uses focused electrons

to a fine spot and the reading is taken in a raster. TEM has been used to study morphology of active layer since 1996 by Yang and Heeger[55] report on MEH-PPV:C60 BHJ active layer. They were able to see a phase segregation between MEH-PPV and C60 by selectively dissolving C60. The dark part of TEM images is usually assigned to PCBM because of its larger proton density. Polymers usually have smaller proton density thus the TEM images of the polymer phase appears lighter. The samples for STEM/TEM should be thin enough to let the electrons through. STEM/TEM samples of the traditional geometry (ITO/PEDOT:PSS/Active layer/Top electrode) OSCs can be prepared by soaking the cells in water to dissolve the PEDOT:PSS layer. The afloat layers will be moved onto copper grids. In the ITO-free solar cells (the geometry mentioned above) detaching the active layer by soaking the samples in water was not possible. Therefore, the solutions were drop cast on a copper grid supported by a polymer film. The STEM images in this work were taken in CAF-Stellenbosch University.

4.2.5 fs-Transient absorption spectroscopy

The macroscopic solar cell parameters in the devices prepared in this work vary with a small change in the structure of the materials. The explanation for these differences can be found in understanding the underlying fundamental photophysical process both in the polymer and the polymer:PCBM71 BHJ films. These photophysical processes include absorption of photons, exciton generation and diffusion to donor/acceptor interface, dissociation of excitons and finally free charge geration and collection by the external circuit. These processes occur on a time scale that spans fs to ms. Therefore a technique that can follow the dynamics in such time scales was important. Transient absorption (TA) spectroscopy can directly follow the population/depopulation of states in the materials in a real time $< 1\mu$s. In our setup, we can follow photophysical process that occur upto < 2 ns. This allows us to see photogeneration and recombination of charge carriers in OSCs within a temporal duration of 150 fs to 2 ns. Conclusions that lead to the improvement/understanding of the fundamental photophysics in OSCs can be deduced from the measurements.

Watching fast events

Fast processes require a measuring tool at least as fast as the dynamics. Fast events like a sport events can be recorded using fast photography with short exposure time of ≈ 0.01 s. Even faster process in the range of picoseconds (ps) or less need the fastest tool available in nature which is light. Time resolution in light can be attained with ultrashort laser pulses. Ultra-short pulses with a temporal duration in the range femtosecond (fs) enable watching fast processes that occur in biological, chemical and physical systems. A fs-laser source thus provides just the measuring tool for dynamics that occur in conjugated polymers and OSCs.

Fs-TA spectroscopy is one of the techniques that enable us to study photo-induced dynamics in organic materials and OSCs. Transient techniques follow the evolution of a process in a real time. Different techniques such as time of flight (ToF) and charge extraction by linearly increasing voltage (CELIV) are widely used to study photoinduced dynamics in OSCs. Fs-TA spectroscopy has a better time resolution to follow dynamics in a fs time regime. In fs-TA spectroscopy, a fs-pump pulse is sent to photoexcite an ensemble of molecules. A second pulse also in fs regime interrogates the

population/depopulation of the states in the excited molecules as in a steady state absorption spectroscopy. The temporal resolution of such a measurement is determined by the convolution of the pump and probe pulses. Since both the pump and the probe have a duration in the fs regime, the TA spectrum will also have a similar resolution. However, such short time scale need a very fast detector that can record data with petahertz repetition rate (1 fs period corresponds to 1 PHz repetition rate). Electronic devises are simply unable to provide access to such ultrafast data recording rate. The available slow detectors can be used in the TA measurement by using a pump-probe set up.

A pump-probe technique can explained by the following example. Suppose you want to make a video of a flying owl in a circus but you only have a conventional camera that has a shutter speed fast enough to take a clear picture of one instance along the course of its flight. The owl is told ”go”, then it starts doing its moves. The word ”go” triggers the dynamic. A series of photographs should be taken along the course to make the video. Since the camera needs some time to reset itself for the next picture, it will not be possible to take as many still pictures that clearly show the dynamics of the circus. This problem can be overcome in a stroboscope photography. In such photography the owl is made to do its circus in a dark room. A stroboscope flashes light with a frequency of sub the frequency at which the owl flatters its wing. The photographer leaves the shutter open and takes pictures every time the stroboscope flashes light. An analogy can already be made between the pump-probe technique and the stroboscope photography. The word ”go” is the pump that triggers the dynamic and the flash light is the probe. The film in the camera is the detector.

One can also take the picture of the owl in the course of the circus by repeating the routine multiple times and take one picture each time at different times of the flight. This can be done provided the owl do identical moves in all the routines. This is impractical.

In a similar way, the dynamics in a photoabsorbing molecule can be triggered by a pump pulse of wavelength corresponding to its transitions. The pump pulse should be able to deposit energy on the molecules to start a photoinduced dynamics. Its temporal resolution should be sufficiently smaller than the dynamics. The excited molecule then relaxes back to the ground state from its excited state by various mechanisms. A probe pulse is sent some time latter to interrogate the excited sample and absorption spectra of the non-equilibrium state is taken. This absorption will then be compared to the ground state spectrum at equilibrium to evaluate the changes that are caused by the pump pulse. The time the excited molecule is probed after excitation is determined by the optical path length difference between the pump and the probe. This optical path difference can be translated into a delay time by dividing it to the speed of light. A data point is recorded by the detector at a fixed time after excitation. Even if it is not ideal to expect the owl to do identical moves every time it is told ”go”, the ensemble molecular dynamics are identical for each pump. Thus, the next data is recorded at a different time by changing the path length difference between the pump and the probe pulses. This is repeated as many times to acquire enough absorption signals that can show the dynamics of the excited molecule clearly. Each data point can be averaged at a fixed position for many iterations to improve sensitivity of the measurement. The number of iterations should be within the sampling time of the detector and the laser repetition rate. Finally, it will be possible to record a change in absorption signal of an excited molecule over time. The evolution of a given dynamics can be extracted by following

a specific signal in time. The temporal profile of the signature will then be fitted with appropriate function to understand the underlying physics behind the dynamics.

Transient absorption spectroscopy set up

A sketch of our transient absorption set up is given in Figure 4.2. A fs-laser source is used to generate both the pump and the probe pulses. The laser is directed to a beam splitter. The position of the beam splitter is used as a reference to the optical path lengths of the pump and the probe pulses. One of the beams enters the non-colinearily phase matched parametric amplifier (NOPA) for near Fourier transformed pump pulse generation while the second beam is sent to a broad band visible white light generation set up. The optical path length difference between the pump and the probe is controlled by a mechanical delay stage. A chopper is incorporated in the set up to acquire a reference absorption signal of the sample in the ground state by blocking every second pump pulse. The pump and the probe pulses are overlapped both spatially and temporally at the sample. The probe pulse heads to the detector while the pump pulse is sent to a beam damp.

The laser source in our set up is a Clark-MXR CPA (chirped pulse amplifier) 2101 amplified femtosecond Titanium:sapphire laser system. It generates a fundamental pulse with a central wavelength of 775 nm, repetition rate of 1 kHz and an output energy ≈ 0.8 mJ. The temporal duration of the fundamental pulse is 150 fs.

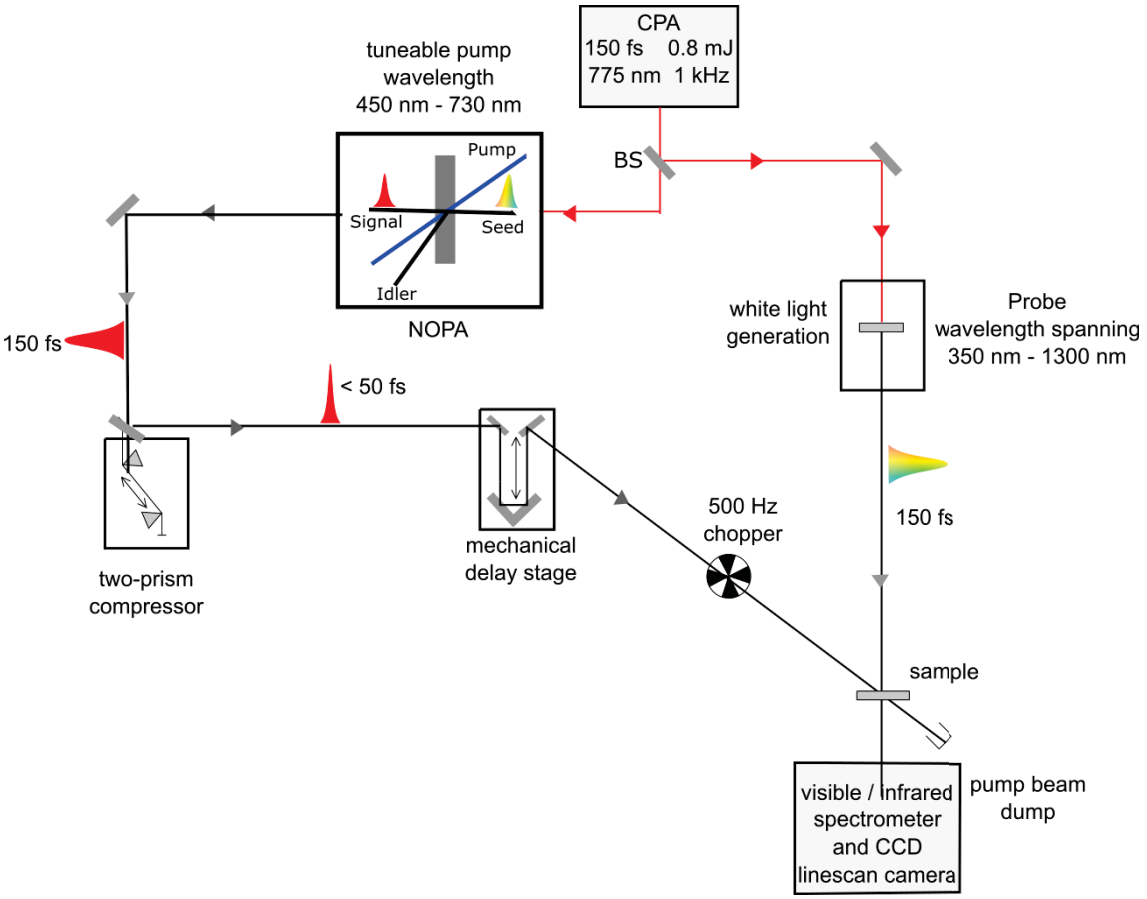

Figure 4.2: Transient absorption set up: the 775 nm fundamental light is split into two using a beam splitter (BS). One of the beams enters the NOPA for pump light generation and the other is directed to a white light generation stage for probe generation. The pump light is compressed using two prism compressor to sub 50 fs. A mechanical delay stage is incorporated to achieve a time resolved measurement. The chopper blocks every second pump pulse. The pump and the probe are overlapped at the sample both spatially and temporally. The transmitted probe light is detected by the spectrometer.

4.2.6 Pump pulse generation: Non-colinearily phase matched optical parametric amplification (NOPA)

Different samples require different pump light to excite the molecule. It is impractical to build a new laser source for each sample. When a high intensity pump pulse with frequency ω_p and a week seed pulse with ω_2 are directed to a non-linear medium, a signal with frequency ω_s and an idler with frequency $\omega_i = \omega_1 - \omega_2$ are generated. This process is called optical parametric amplification. To satisfy energy and momentum conservation, $\omega_p = \omega_i + \omega_s$ and the propagation vector, $k_p = k_i + k_s$. A non-colinearily phase matched optical parametric amplifier (NOPA) is used to generate the colors necessary to excite the samples measured in this study (see Figure 4.2). In our set up, the fundamental light centred around 775 nm is split into two pulses using a beam splitter, one of the beams (30% of the fundamental) goes to the NOPA for pump generation and the other (10% of the fundamental) beam is directed to a white light generation set up. The 30% fundamental light that entered the NOPA is further divided into two beams again using an appropriate beam splitter. One of the beams, which is 90% of the fundamental that enters the NOPA, is directed to a β-barium borate (BBO) crystal for second harmonic generation and a frequency doubled beam centred around 387.5

nm is generated. The rest 10% of the fundamental signal in the NOPA is focused onto a sapphire crystal to generate a white light super-continuum (WLC) seed beam. The frequency doubled 387.5 nm pump is seeded by the chirped WLC. The pump pulse propagates horizontally onto a vertically aligned 2 mm thick BBO crystal which is cut at angle with respect to the optical axis for maximum amplification. The orientation of the BBO-crystal with respect to the pump pulse is set in such an angle to keep the phase matching condition for optical parametric amplification. The pump is seeded with a WLC in non-collinear geometry. This non-collinear geometry allows efficient phase matching between the chirped WLC components and the pump for the entire length of the BBO-crystal. Hence, different components of the white light can selectively be amplified by the 387.5 nm pump to generate a visible light from λ = 450 nm - 730 nm (see Figure 4.3). The k- vector projection the WLC seed along the pump k-vector should be equal for the pulses to remain in phase along the BBO crystal. In such a way, maximum parametric amplification of each component of the white light by the pump can be achieved.

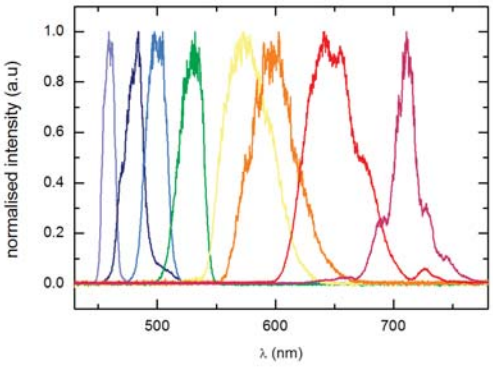

Figure 4.3: Range of pump pulse spectra that can be generated with our NOPA

The amplified visible signal should be in the same direction as the seed and the remaining energy from the pump is damped to an idler signal to satisfy the conditions of conservation of momentum and energy. The idler signal is thus in the infra red region. An amplified signal of energy of upto 10 μJ is obtained in the single stage amplification. The amplified signal is used as a pump pulse in a pump-probe spectroscopy. This pump pulse is compressed to its Fourier limit by using a two prism compressor for better temporal resolution. The duration of this compressed beam is measured with an autocorrelator. An example of an autocorrelation signal for 515 nm probe pulse is shown in Figure 4.4. A Gaussian fit of the autocorrelation signal has a full width half maximum (FWHM) of 46 fs which corresponds to 33 fs pulse duration.

4.2.7 Probe Pulse generation

A 10% of the fundamental is directed to white light generation set up. Non-linear phenomena broadens the femto-second pulse propagating through a medium from its Fourier transform limited pulse in spectrum and a WLC is generated. The WLC in our set up is generated using one of the three crystals: a 3 mm thick sapphire (400 nm - 700 nm) , a 5 mm thick CaF_2 (340 nm - 700 nm) and 3 mm thick yttrium aluminium

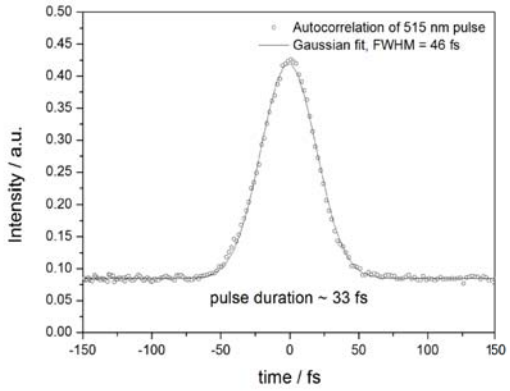

Figure 4.4: Autocorrelation signal of a compressed 515 nm pump pulse. The FWHM of the Gaussian fit is 46 fs which corresponds to a pump temporal duration of 33 fs

garnet (YAG) (850 nm to $\approx$ 1300 nm). The WLC spectrum in our set up has a total spectral bandwidth from about 350 nm - 1300 nm. An appropriate filter is used on the probe line to block the fundamental. The WLC spectrum generated using the above three crystals together with appropriate filters is shown in Figure 4.4.

A normal group velocity dispersion (GVD) of the white light as it propagates through the aforementioned crystals creates a positive chirp. Due to this chirp, the temporal duration of the WLC from teh blue light to the red is about 1 ps. Since the temporal duration of each colors in the WLC is determined by the fundamental pulses, the temporal duration of each color is 150 fs. To compensate for the chirp in the WLC, the time zero of each wavelength at the sample is shifted manually. The temporal resolution of the pump-probe set up is determined by the convolution of the pump pulse and the spectral components of the WLC probe pulse at time zero on the sample. The temporal resolution of our set up is below 200 fs.

4.2.8 Time resolved absorption spectra

The power of the pump-probe experiment relies on its ability to follow evolution of a photoinduced process in time. This temporal evolution is achieved by delaying the probe light from the pump at the sample. The pump light is sent to a retro-reflector mounted on a computer controlled motorized mechanical delay stage (Newport). The delay stage has a length of 30 cm which correspond to 2 ns, as the pump light travels back and forth. The movement of the delay stage is as accurate as 1 μm which corresponds to $\approx$ 3 fs. Since temporal resolution of our pump-probe set up is below 200 fs, few fs error from the movement of the delay stage does not limit the temporal resolution of the measurements.

The pump and the probe pulses are temporally and spatially overlapped at the sample. The pump pulse initiates the photo-induced process in the molecule. A delayed probe pulse is sent to interrogate the changes caused by the pump on the molecule. The probe pulse should be narrower in width to make sure an excited samples is probed. The transmitted probe light through the sample is sent to two grating spectrometers sensitive either to the visible or near-infra red region of the spectrum. The transmitted pump light will be directed to a beam dump. Some scattered light might reach the grating spectrometer, if the sample is scattering. Data is collected with a line scan charge

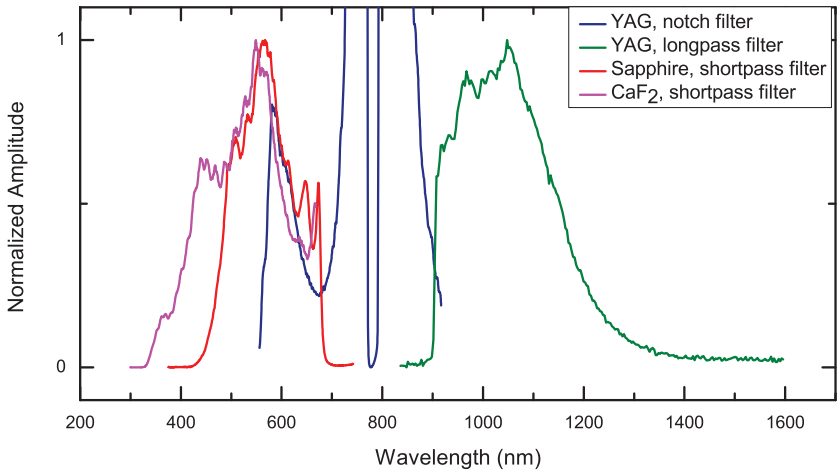

Figure 4.5: Spectrum of WLC generated using three different crystals: A total probe spectral bandwidth from below 350 nm to 1300 nm can be generated by selectively changing the crystals in the white light generation set up. An appropriate filter is used to block the fundamental from reaching the detector

coupled device (CCD) camera in the visible or near infra red region. A combined spectral region of below 350 nm and 2500 nm can be recorded. The readout rates of the cameras is 1 KHz (Entwicklungsbüro Stresing Gmbh). This read out rate is equivalent to the frequency of the pulse train produced by the CPA. Thus, every shot is recorded individually.

In a steady state absorption spectroscopy, a reference spectrum (of the solvent and the cuvette if solution, of the substrate if a thin film) is taken to measure the absolute absorption of the molecule. Similarly, a simple referencing technique is used in transient absorption spectroscopy by blocking the pump light every other time and measure the ground state absorption which is the reference spectrum. A mechanical chopper operating at 500 kHz, half the frequency of the CPA output, is incorporated in the pump line to block every second pulse to measure the reference spectrum. The intensity of light that reaches the cameras is periodically transmitted light intensity of the excited sample (I_{exc}) and the unexcited sample (I_{unexc}). The change in absorption (optical density), ΔOD, of the molecule due to the pump can be given as follows:

$$\begin{aligned} \Delta OD(\lambda) &= OD(\lambda)_{exc} - OD(\lambda)_{unexc} \\ &= -\log \frac{I_{exc}}{I_0} + \log \frac{I_{unexc}}{I_0} \\ &= -\log \frac{I_{exc}}{I_{unexc}}. \end{aligned} \tag{4.2}$$

The incident probe pulse intensity, I_0, does not influence the change that is induced by the pump pulse. The $\Delta OD(\lambda)$ of each wavelength will be measured along the length of the delay stage. The resulting transient absorption spectrum will be the change in optical density measured for each wavelength as a function of time, $\Delta OD(\lambda, t)$. Each measurement is averaged over 6000 laser shots to reach a sensitivity below 10^{-3}.

The samples should relax back to ground state before the second pump arrives to avoid heating and some optical non-linear processes like two photon absorption. A

solution sample is pumped through a flow cell to provide a new sample for each pump pulse. A thin film is mounted on a rotating sample holder. But if the sample relaxes back within the period of the pump pulse which 1 ms, this might not be necessary.

Data analysis of transient absorption spectrum

Let us use a simple energy level diagram of a hypothetical molecule as an example to understand contributions to transient absorption spectrum (see Figure 4.5a).

The pump pulse excites some of the hypothetical molecules from their ground state to the excited state (solid blue arrow in Figure 4.5a). The concentration of the absorbing molecules in the ground state will thus be reduced. The probe pulse that comes after the pump sees less absorbing molecules at the ground state absorption wavelength. Consequently, the change in absorption at this wavelength will be negative. The spectral shape and position of this contribution is identical to the steady state absorption spectra. This contribution to the transient absorption spectrum is called **ground state bleaching (GSB)**.

The other contribution to the TA spectra is **fluorescence by stimulation emission**. The probe pulse stimulates emission(SE) of photons by relaxing the excited molecules back to the ground state (broken blue arrow in Figure 4.5a). When the chopper is open the pump light passes through, assuming no absorption and when the chopper unblocks the pump light, the photon that reaches the detector will be the sum of the photons that impinge on the sample and the stimulated emission. Consequently, SE will have a negative change in absorption because $I_{exc} > I_{unexc}$. SE has an identical spectral shape like the steady state fluorescence.

Many molecules have $S_1 \rightarrow S_n$, n > 1 allowed transitions. An excited molecule by the pump can be promoted to one of these higher states by absorbing photons (broken red arrow in Figure 4.5a). The **absorption of the excited states (ESA)** when compared to the ground state absorption is positive.

In a more complex molecule, the first excited state might evolve into a newly generated state called intermediate state. The change in absorption of this intermediate state is also positive. The signal evolution can be seen if the generation time is above the temporal resolution of the transient absorption set up.

A raw transient absorption signal (shown in Figure 4.6b) is given as wavelength in the ordinate, delay time between the pump and the probe in the abscissa and ΔOD as a color-map. Blue part of the spectrum shows negative ΔOD which means either GSB or SE. A red part shows an ESA. A vertical line is taken out to closely analyse the ΔOD spectrum profile at a specific time of interest. The profile can provide a clue or sometimes full information about the type of spectral signatures either using complementary measurements like steady state absorption and fluorescence or by itself (see Figure 4.6c). An additional information about the spectral signatures can be found by taking a horizontal line out from the raw TA spectrum to see the evolution of a specific spectral signature in time. The ΔOD Vs time curves will be fitted with appropriate functions to get time constants for specific dynamics in the material (see Figure 4.6d).

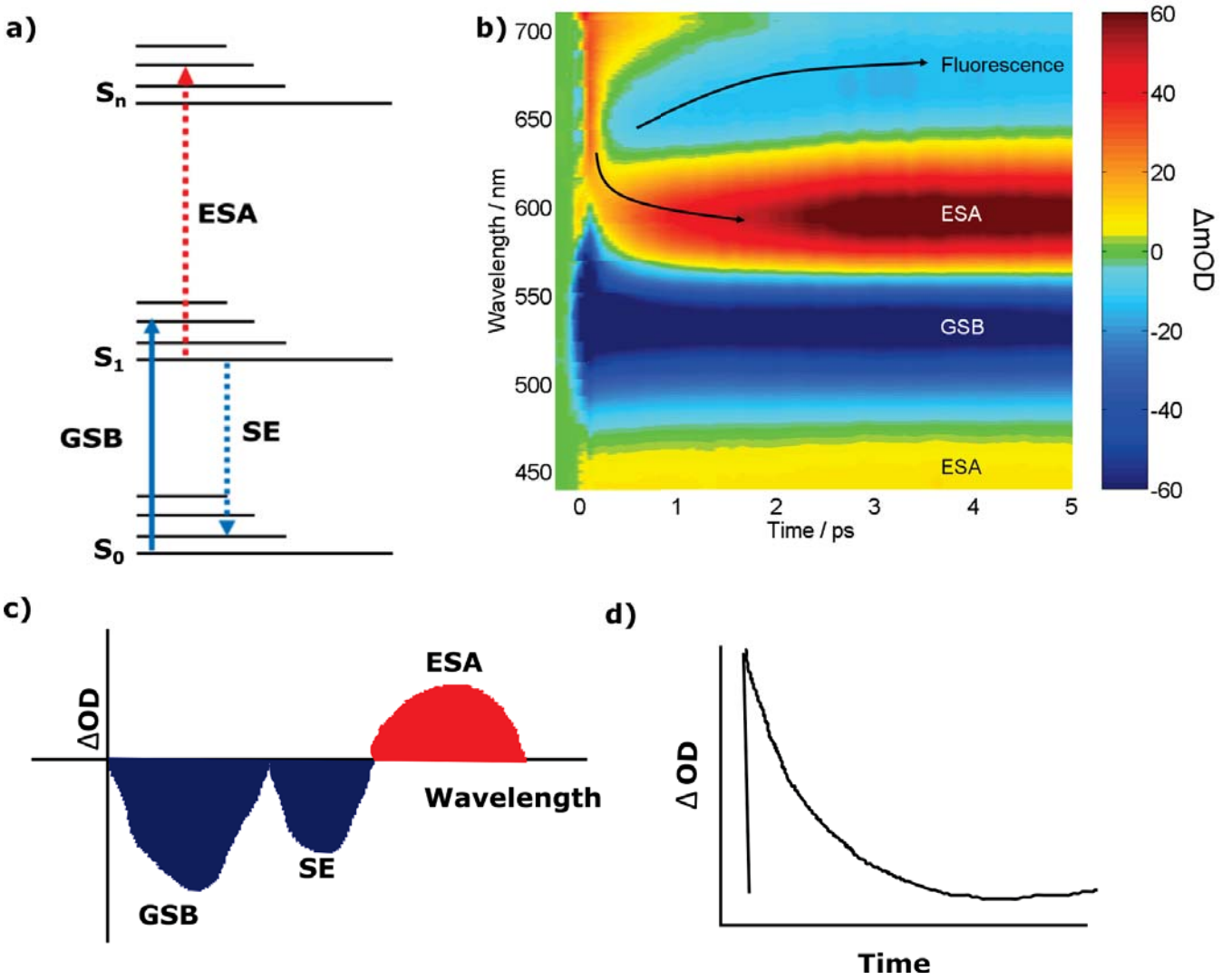

Figure 4.6: (a) Contributions to transient absorption signal: A pump light excites the molecule to a higher excited state. The probe light will see a lower absorption due to the bleaching of the ground state (GSB). The probe light also stimulates emission (SE). The molecule can also be excited to higher states, ESA. (b) Raw transient absorption spectrum [56], ΔOD is given as a color map. Blue shows a negative ΔOD which corresponds to either GSB or SE, the red color represents a positive ΔOD which is absorption of product or intermediate states c) a vertical line out of the raw transietn absorption spectra in (b) gives the spectrum at a specific time d) a horizontal line out is taken at a fixed wavelength to analyze the temporal evolution of a signal of interest.

5. Photophysics of bithiophen-isoindigo (P2TI) copolymer and its performance in ITO-free solar cells

5.1 Introduction

Organic solar cells (OSCs) have exceeded the commercial goal of 10% both in single [8, 9] and multi-junction solar cells[27]. This is mainly through improvements in material synthesis and device architecture. The active layers of highly performing OSCs were composed of bulk heterojunction (BHJ) composites of low band gap polymeric materials and fullerene derivatives. The broad absorption of such low band gap polymeric materials contributed to the higher short circuit current which resulted in a higher efficiency. One of the challenges in OSCs is that photoexcitation creates a tightly bound electron-hole pairs. A highly electron deficient material usually fullerene is added in the BHJ active layer to dissociate the exciton from the polymer. The exciton can thus be quenched by transferring its electron to the LUMO of the acceptor material. Energy is lost to dissociate these exciton. Consequently, OSCs suffer from low open circuit voltage. Copolymers have a dipolar character which enables an internal partial/full charge dissociation. This lowers the exciton binding energy.

In this work, both steady state spectroscopy and fs-transient absorption (TA) spectroscopy were used to study photophysics of a bithiophen-isoindigo (**P2TI**) copolymer in solution, pristine film and **P2TI**:PCBM71 BHJ film. We started fs-TA spectroscopy measurement with photoinduced charge transfer in a copolymer chain followed by a solid pristine film where there is a significant inter-chain interaction. The result showed a fast generation of an intramolecular charge transfer state (ICT) in the copolymer chains. In a fs-TA spectroscopy measurement on **P2TI**:[6,6]-Phenyl-C71-Butyric-Acid-Methyl Ester (PCBM71) BHJ film, long living charge carriers were found. The application of the copolymer for solar cell was studied using an ITO-free solar cell geometry: Al/TiO_x/**P2TI**:PCBM71/PEDOT:PSS.

5.2 Result and discussion

5.2.1 Steady state spectroscopy

The steady state absorption spectroscopy of **P2TI** is studied both in solution and thin film. The Uv-Vis absorption spectrum in chloroform (CF) solution (red), the pristine film (black) and **P2TI**:PCBM71 BHJ film (green) is shown in Figure 5.1. The absorption spectrum of **P2TI** in CF solution shows two distinct absorption bands: one which

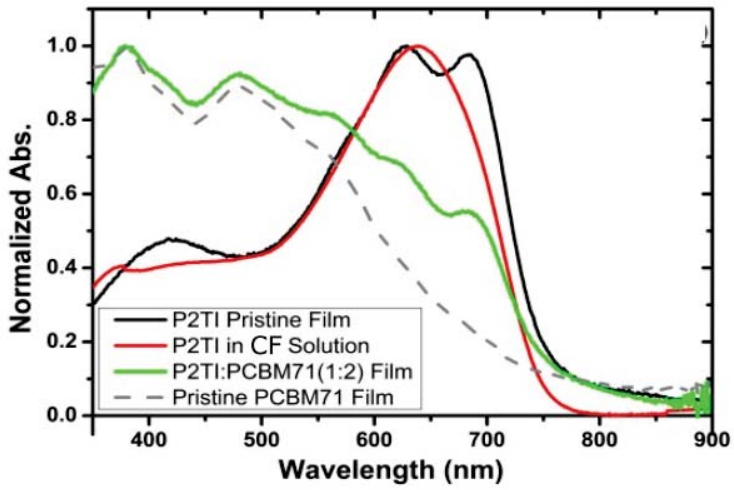

Figure 5.1: Steady state absorption spectra of **P2TI** in CF solution (red), pristine film (black) and **P2TI**:PCBM71 (1:2) BHJ film (green). The absorption spectra of **P2TI** both in chloroform solution and pristine film have the "camel" back structure which is a signature of copolymers. The absorption of the BHJ film is the superposition of the absorptions of the pristine **P2TI** and pristine PCBM71 films(dashed gray line)

peaks at 638 nm and a shoulder below 500 nm. This two absorption bands sturcture also called "camel" back structure[34], is common in D-A copolymers. The absorption coefficient of **P2TI** in CF solution at the 638 nm is 96 L/g cm. This high absorption coefficient is essential for high photo-current generation. The absorption spectrum of pristine **P2TI** film is slightly red shifted compared to the solution spectrum. This shift is due to $\pi - \pi$ stacking in the solid films which is important for charge mobility. Similar to the solution spectra, the pristine **P2TI** film also has two distinct absorption bands. The lower wavelength region absorption band is more noticeable in the pristine film.

The absorption band between 600 nm and 700 nm is due to the $S_1 \leftarrow S_0$ transition. This band has peaks at 630 nm and 685 nm which are vibrational states in the manifold of S_1. Considering the characteristics of D-A copolymers discussed in section 2.2.2, the low band gap of copolymers usually is due to intramolecular charge transfer (ICT) between the donor and acceptor units (bithiophene and isoindigo units in this case). Therefore, the first absorption band is presumably assigned to a transition that leads to ICT state. The position of the low wavelength absorption band peak is similar to the maximum of absorption spectrum of a polythiophene [57]. Jespersen *et.al* [34] also observed the low wavelength maxima of a polyfluorene based D-A copolymer is similar to the absorption maxima of a donor polymer. Form this observation it can be concluded that the low wavelength peak below 500 nm is due to $\pi - \pi^*$ transition which is common in conjugated polymers due to the alternating single and doubles bond along the backbone. This transition is thus to higher states than the first singlet excited state.

The absorption of **P2TI**:PCBM71 BHJ film is a simple superposition of the absorption of the pristine **P2TI** and pristine PCBM71 (shown in gray in Figure 5.1) films. The solar harvest of the **P2TI**:PCBM71 BHJ film has a contribution from PCBM71 as it compensates the low absorption of **P2TI** below 500 nm . This is one of the reasons PCBM71 was chosen over [6,6]-Phenyl C61 butyric acid methyl ester (PCBM61). Be-

sides its higher absorption in the visible region of the solar spectrum, PCBM71 has also a slightly lower LUMO level which gives a higher driving force for exciton dissociation in the blend. To further understand the properties of the excited states in **P2TI**,

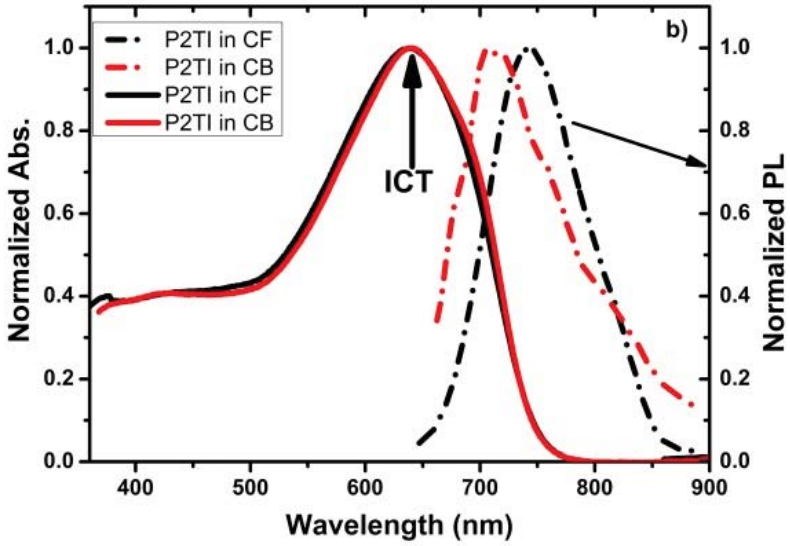

Figure 5.2: Steady state PL spectra of **P2TI** in CB (red) and CF (black) solution (red). A red shift in PL is seen with increasing solvent polarity which indicates relaxation from ICT state

photoluminescence (PL) spectrum of **P2TI** in CF (polarity index = 4.1) solution was recorded at excitation of 630 nm. The PL spectrum was stokes shifted by 114 nm. This large stokes shift shows a significant structural change of the polymer upon excitation. A copolymer can be found in two mesomeric structures: D - A and $D^+ = A^-$. Therefore the ground state of **P2TI** has D-A structure but the excited state evolves to its mesomeric structure: $D^+ = A^-$ which has higher dipole moment. The higher dipole moment in $D^+ = A^-$ structure shifts the PL spectrum significantly. Thus, the high stokes shift also confirms the ICT character of the excited state in **P2TI** in solution. To further confirm this assumption, the absorption and the PL spectra of **P2TI** in two solvents of different polarity (CF and chlorobenzene(CB)(polarity index = 2.7)) was compared, see Figure 5.2. The absorption spectra of **P2TI** in both solvents were almost identical but the PL spectrum was red shifted as the polarity of the solvent increased. This shows the excited state is dipolar. Consequently, the increase in solvent polarity enables access of lower states, in this case the ICT state. The result is consistent with the assignment of the first absorption band with an ICT character. The optical properties of **P2TI** in solution and film is summarized in Table 5.1.

Table 5.1: Optical properties of **P2TI**.

copolymer	Abs. Max Film		Abs. Max Soln.		Abs Shift from Soln to Film		$E_g^{Opt}(eV)$
	λ_{max1}	λ_{max2}	λ_{max1}	λ_{max2}	$\Delta\lambda_{max1}$	$\Delta\lambda_{max2}$	
P2TI	417	629 / 685	–	638	–	-9 / 47	1.56

5.2.2 Photovoltaic performance and morphology

Photovoltaic performance

ITO-free solar cells were fabricated using **P2TI** as a donor polymer and PCBM71 as an acceptor. Keep in mind that the polymer **P2TI** has an intermolecular D - A coupling but in solar cells it is blended with another acceptor material usually C60 derivatives to serve as an active layer. The internal D - A coupling within the polymer plays important role in reducing the exciton binding energy due to its ICT character. The energy levels of the polymer and the fullerene determine the charge flow within the solar cell. Therefore, electro-chemistry of **P2TI** was studied using square wave voltammetry and the HOMO -LUMO levels of -5.4 ev and -3.7 ev respectively were found [20]. The LUMO level offset of **P2TI** from PCBM71 (LUMO = 4.0 eV) is 0.3 eV, which is in the range of the empirically suggested value of (0.3 - 0.4 eV) [58]. Back to the solar cells, the ITO-free **P2TI**:PCBM71 BHJ solar cells were prepared in three ratios of **P2TI** to PCBM71 in a geometry of Al/TiO_x/ Active Layer / PEDOT:PSS. A total of 8 devices were prepared for each stoichiometry and the best performing cell is presented.

The current density - voltage characteristics of **P2TI**:PCBM71 based BHJ ITO-free solar cells under simulated AM 1.5 illumination is shown in Figure 5.3a and the photovoltaic performance of each ratios is summarized in Table 5.2. The performance of the solar cells is lower than expected. The main reason for this low performance of the cells is the short circuit current density (J_{SC}) in the three devices. A high current density was expected due to its low band gap, broad absorption and high extinction coefficient measured in solution. The expected current density based on its band gap is about 10 mA/cm^2 (see section 1.3).

Comparing among the three devices, J_{SC} increases with increasing PCBM71 ratio. This is due to the higher absorbance of the active layer in the visible region below 500 nm with increasing PCBM71. The open circuit voltage, V_{OC}, shows almost no change. The open circuit voltage of an OSC is mainly determined by the HOMO level of the donor polymer and the LUMO of the acceptor. Besides this, the work function of electrodes and LUMO offset between the polymer and the fullerene also affect the V_{OC} of an OSC. A report by Tang *et. al.* [59] showed ITO- free solar cells of the aforementioned geometry have lower V_{OC} than the traditional geometry: ITO/PEDOT:PSS/Active layer/ Al. An empirical value for a maximum attainable V_{OC} of an OSC was formulated to be : $eV_{OC} = E_g$ - 0.6 V [60]. The open circuit voltages of **P2TI**:PCBM71 based BHJ ITO-free solar cells were only 0.2 V below the maximum value. This value is high for ITO free solar cells which inherently have lower V_{OC}.

The fill factor (FF) shows a larger difference with increasing PCBM71 loading than J_{SC} and V_{OC}. FF of the solar cells decreased with increasing PCBM71 loading. FF is measure of recombination within a solar cell. This recombination can be due to some holes in the preparation. Thus, the shunt resistances in the cells can give a measure of the leakage current. A dark current density -voltage characteristics was measured to analyse the difference in FF. As shown in Figure 5.3b, the dark current increased with increasing PCBM71 loading. Therefore, the shunt resistance decreases with increasing PCBM71 loading which accounts for a decrease in FF.

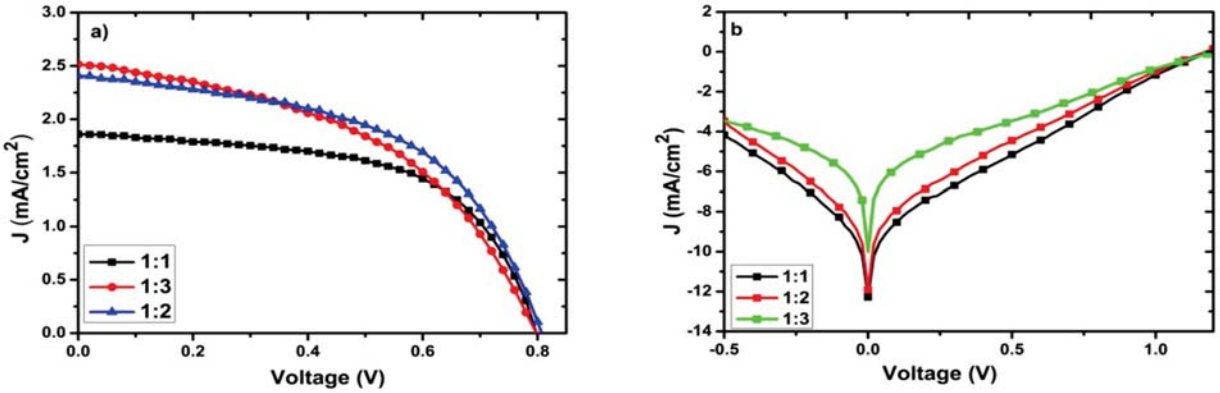

Figure 5.3: Current density-voltage curves of ITO-free **P2TI**:PCBM71 based BHJ solar cells in different ratios of **P2TI** to PCBM71 (a) under simulated AM 1.5 sun illumination (b) in dark. The best performance was found in 1:2 ratio of **P2TI**:PCBM71. The FF is improved with decreasing PBCM71 loading due to the decreasing in leakage current (b)

Table 5.2: Summary of Photovoltaic properties of Al/TiO_x/**P2TI**:PCBM71/PEDOT:PSS OSCs

P2TI:PCBM71 ratio	J_{sc} (mA/cm^2)	V_{OC} (V)	FF	Eff (%)
1:1	1.9	0.80	58.4	0.87
1:2	2.4	0.81	52.3	1.02
1:3	2.5	0.80	46.8	0.94

Morphology

From the broad absorption spectra pristine of **P2TI** film and high extinction coefficient of **P2TI** in solution, a high short circuit current density was expected. But the short circuit current density of the cells studied was only about 24% of the expected value. In addition to the solar spectral coverage of the pristine **P2TI** and its extinction coefficient, the efficiency of the exciton dissociation and the percolation of the charges to the electrodes determine the photogeneration in the cell. To interrogate the active layer morphology in the quest for answer to the low J_{sc}, a morphology study of the active layer of the best performing cell was done using scanning electron microscope (SEM). The sample for SEM measurement was prepared on a thin microscope cover slide. The thickness of the active layer was kept similar to the solar cells by using the same spin coating speed and concentration of the **P2TI**:PCBM71 in *o*-DCB solution. The SEM image of **P2TI**:PCBM71 (1:2) on a cover slide has domain sizes exceeding 100 nm as shown in Figure 5.4. These domains can be copolymer only or the blend of the copolymer and PCBM71.

Let us see each of the two cases separately in relation to charge photogeneration. Suppose the domains are only polymers. Then, the excitons created in this volume neglecting the ones at the surface can not dissociate because the domain size is almost 10 times the typical exciton diffusion length (5 - 20 nm). If the domain consists of the blend of the two, exciton dissociation will be efficient within the domains, but since the polymer/fullerene separated phase is interrupted the free charges do not have efficient percolation path that leads to the electrode. Hence, the large domains in the active layer have an adverse effect in the current generation. The main reason for poor performance

of **P2TI**:PCBM71 based BHJ ITO-free solar cells is the loss of percolation path for free charge carriers to the electrodes.

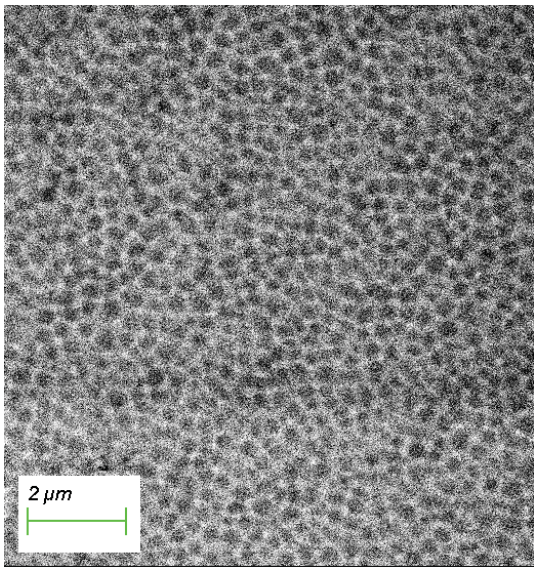

Figure 5.4: SEM images of **P2TI**:PCBM71(1:2) BHJ film. The domain sizes exceed 100 nm. The large size of domain size is the reason for poor J_{sc} in the device

5.2.3 fs-Transient absorption spectroscopy of P2TI in solution

The charge dynamics of an organic solar cell starts with the dynamics within the polymer. The polymer interaction can be intrachain or interchain with the adjacent polymer chains. To understand the full solar cell dynamics, we start from the dynamics within a stand alone polymer chain. fs-Transient absorption(TA) measurement was taken on a dilute solution of **P2TI** in CB that has an OD = 4/cm at the maximum absorption. Steady state absorption measurement was taken by varying the concentration of the solutions to see any aggregation effect. The steady state absorption spectra have identical profiles, therefore dynamics related to interchain interaction can be excluded in the analysis of the TA measurements. A pump pulse of 630 nm generated using our NOPA was used to excite the copolymer. The pump beam was compressed using a two prism compressor to sub 50 fs temporal duration. The solution was pumped through a 100 μm thin quartz cuvette to provide a new sample for each laser shot.

The TA spectrum of **P2TI** in CB solution shown in Figure 5.5 has three spectral features: A broad negative ΔOD signal between 550 nm and 700 nm, two positive ΔOD signals above 700 nm. The ΔOD spectra are taken out at selected delay times between the pump and the probe (shown in Figure 5.5(bottom)) to closely look into the above three spectral features. The negative ΔOD spectral feature has two maxima whose position correspond to the maxima in the steady state absorption and PL spectra respectively. Thus, these signals are attributed to ground state bleaching (GSB) and stimulated emission (SE) from the excited state by the probe respectively. One thing to note here is the GSB shows almost negligible refill in the first about 8 ps. One of the two positive ΔOD spectral features has a peak at about 750 nm. This signal rises in the first 8 ps. Remember the GSB shows almost no change in this time scale which means the state at 750 nm is not directly populated from the ground state. The state is thus

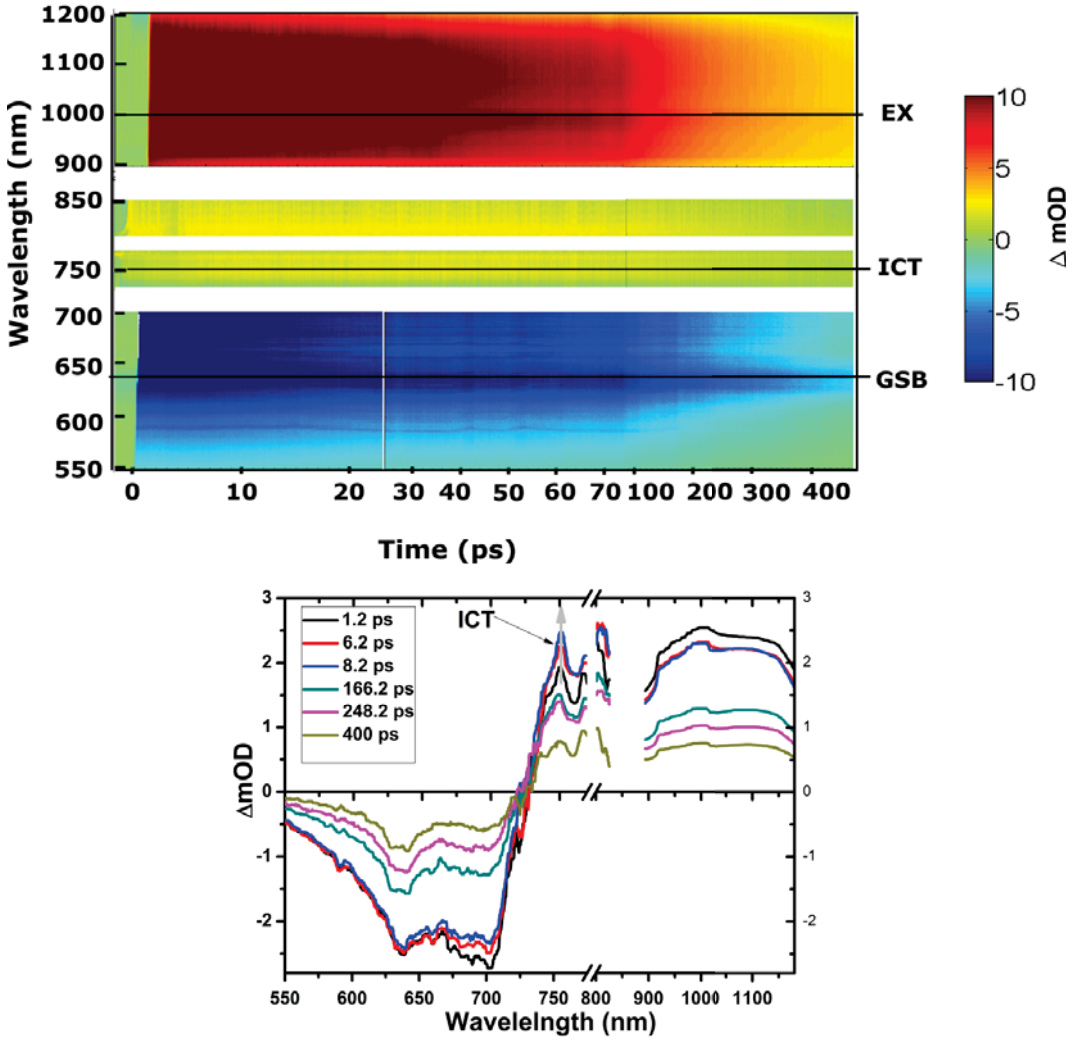

Figure 5.5: (Top) TA spectrum of **P2TI** in CB solution. The blue part of the TA spectrum shows a negative change in absorption which is due to GSB and SE. The light yellow and red regions (positive change in Absorption) is due to ESA. (bottom) ΔOD curves taken out at selected delay times. The negative Δ OD peaks at positions corresponding to the steady state absorption and emission of **P2TI** in solution. An increasing positive signal at 750 nm shows the generation of an ICT state. The broad positive signal is due to EX. The spectra below 700 nm and above 900 nm are divided by 6 for clarity.

an intermediate state. From the steady state PL measurement, this intermediate state is assigned to the ICT state. The other positive ΔOD spectral feature is a broad signal above $\approx$ 900 nm. This signal was generated with the temporal resolution of the set up $\approx$ 150 fs. The GSB signal has also the same rising time constant. The broad positive signal is either directly populated from the ground state or is populated from the first excited singlet state in $\approx$ 150 fs. The first excitation in organic materials is exciton. An intersystem crossing can lead to the formation of triplets from singlet excitons. But in conjugated polymers since the materials are made of light atoms, spin-orbit coupling is not efficient. Hence, triplets are not generated as fast ($<$ 150 fs) and they also have a life time longer than ns [61]. Therefore, this signal is assigned to exciton (EX) absorption which is $S_1 \rightarrow S_n$ transition.

To understand the dynamics **P2TI** in CB solution, the temporal evolution of the GSB (630 nm), the ICT state absorption (750 nm) and the EX absorption (1000 nm) were fitted with a sum of exponential functions. The fit results are shown on Figure 5.6(left)

and also given in Table 5.3. The ICT state rises with a time constant of τ_{ICT1} = 2 ps. The signal then decays with a time constant of τ_{ICT2} = 180 ps. A 27% of the signal stays longer than 500 ps. The EX absorption rises immediately with our temporal resolution and 10% of the signal has fast decay time constant of τ_{EX1} = 2.1 ps. The rest of the signal decays with time constant of τ_{EX2} = 190 ps. A similar EX life time is reported in many conjugated polymers [31, 43]. The GSB signal recovers with time constants of 20 ps (24%), 590 ps (63%) and 13% stays longer than 600 ps.

The rise time constant of the ICT state matches well with the first decay time constant of the EX absorption. This clearly shows the ICT state is generated from the EX.

The ICT state has three time constants corresponding to three processes. The rise time constant is the time that it is generated from the EX. A similar fast ICT generation time was reported in a D - A type polyflourene copolymer [62]. As shown in the absorption spectra of **P2TI** in solution (Figure 5.1), the oscillator strength at the wavelength assigned to the ICT state transition is significantly stronger than the $\pi - \pi^*$ transition. It is known that the ICT state transition is determined by the transition from HOMO to the LUMO of the copolymer. The HOMO and LUMO of the copolymer is formed from the hybridizations of the HOMOs and LUMOs of the donor and the acceptor units in the copolymer respectively. A stronger ICT oscillator strength indicates efficient charge transfer between the units [63]. Therefore, isoindigo has a strong electron withdrawing property when it is coupled with a bithiophene donor unit as in **P2TI**. This facilitates the ICT generation rate becuase the excited state will have stronger dipole moment. The second and third time constants are assigned to relaxation of the ICT to the ground state. The ICT state has thus two relaxation channels. Remember there is no interchain interaction in the dilute solution we measured. The first time constant (180 ps) is assigned to the normal direct relaxation of the ICT state in the chain. The second process takes longer ($>$ 500 ps). This process is due to a recombination of two ICT states along the chain as the polymer chain recoils and self-aggregates [43]. The first process is geminate recombination but the second process is due to two charge carriers from different ICT states, thus it is bi-molecular recombination.

Comparing the life time of EX and ICT state, the ICT state has a 27% contribution that lives longer than 500 ps. This longer life time of ICT state is due to the partial separation of electron-hole pairs. Thus, exciton binding energy can be reduced in ICT state which is beneficial for the performance of OSCs based on such copolymers.

The photodynamics in copolymer **P2TI** chain is sketched in Figure 5.6(Right) and can be summarized as follows: the 630 nm pump pulse excites the copolymer to the first singlet excited state and EX state is generated. This EX state has two channels by which it decays. One of the channels is the normal relaxation channel to the ground state (190 ps) and the other channel is internal conversion that will generate the ICT state (2.1 ps). The ICT state relax back to the ground state by geminate and non-geminate recombination channels.

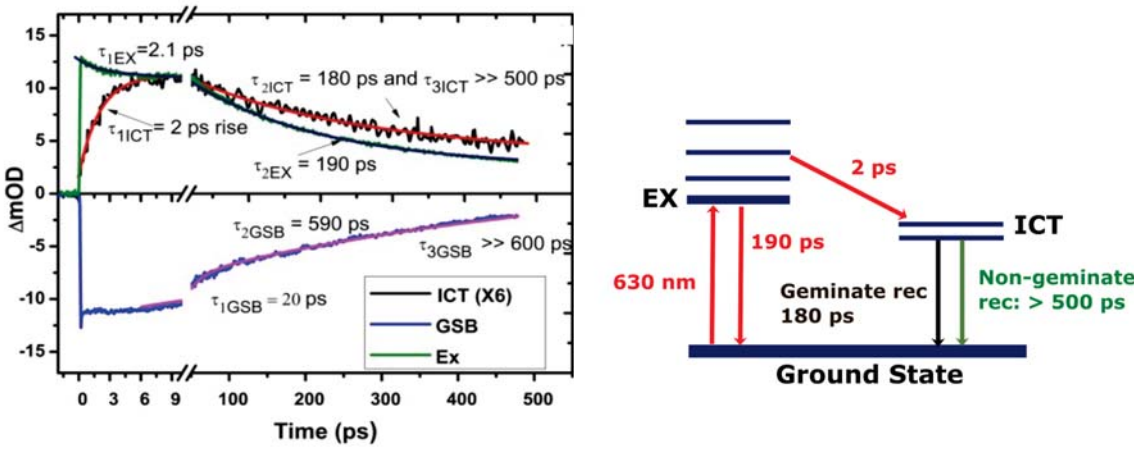

Figure 5.6: (left) The temporal evolutions of GSB, ICT and EX absorption fitted with a sum of exponential functions. The time constant are shown in the figure. The ICT state absorption was multiplied by 6 for clarity. (right) A dynamics sketch of **P2TI** in CB solution. A 630 nm pump excites the copolymer generating EX immediately. Part of the EX will then relax to ICT state with an internal conversion. Finally the rest of the EX and the ICT state will relax back to the ground state.

5.2.4 fs-Transient absorption spectroscopy of pristine P2TI and BHJ films of P2TI:PCBM71

After understanding the dynamics of **P2TI** in a dilute solution, we proceed to TA measurement of the pristine **P2TI** and **P2TI**:PCBM71 (1:2) BHJ films as the real working solar cell condition is based on thin films. In OSCs, the polymer is the main photoabsorber but fullerene is added to facilitate exciton dissociation and charge transport within the device. Excitons from fullerene are normally neglected. Therefore, both films were excited with a pump pulse of 630 nm which is the absorption maxima of **P2TI**. The pump pulse was compressed using two prism compressor to a temporal duration of sub 50 fs.

fs-Transient absorption spectroscopy of pristine P2TI

The dynamics in the pristine **P2TI** film is a basis for understanding the dynamics in the OSC.

The TA spectrum of the pristine **P2TI** is shown in Figure 5.7. A change in absorption spectra at different times were taken out to facilitate the assignment of the signals, see Figure 5.7(bottom). The spectra have two negative ΔOD signals peaking at 640 nm and 690 nm and one broad positive signal above 730 nm. The two negative signals' position matches well with the two steady state absorption peaks in the low energy band side of the pristine **P2TI** film (see Figure 5.1). Therefore, these two spectral contributions are due to GSB. The broad positive signal has a maximum at 1175 nm. The signal is generated immediately with the temporal resolution of our set up.

To understand the dynamics within the pristine film, we fitted the GSB and the signal at 1175 nm with a sum of exponential functions. The time constant are shown in the graph (Figure 5.8) and also summarized in Table 5.3. Both the signal at 1175 nm and the GSB are generated in < 150 fs. The signal at 1175 nm decays with a time constant 38 ps (42%) and 265 ps (58%). The broad positive signal is thus assigned to exciton (EX)

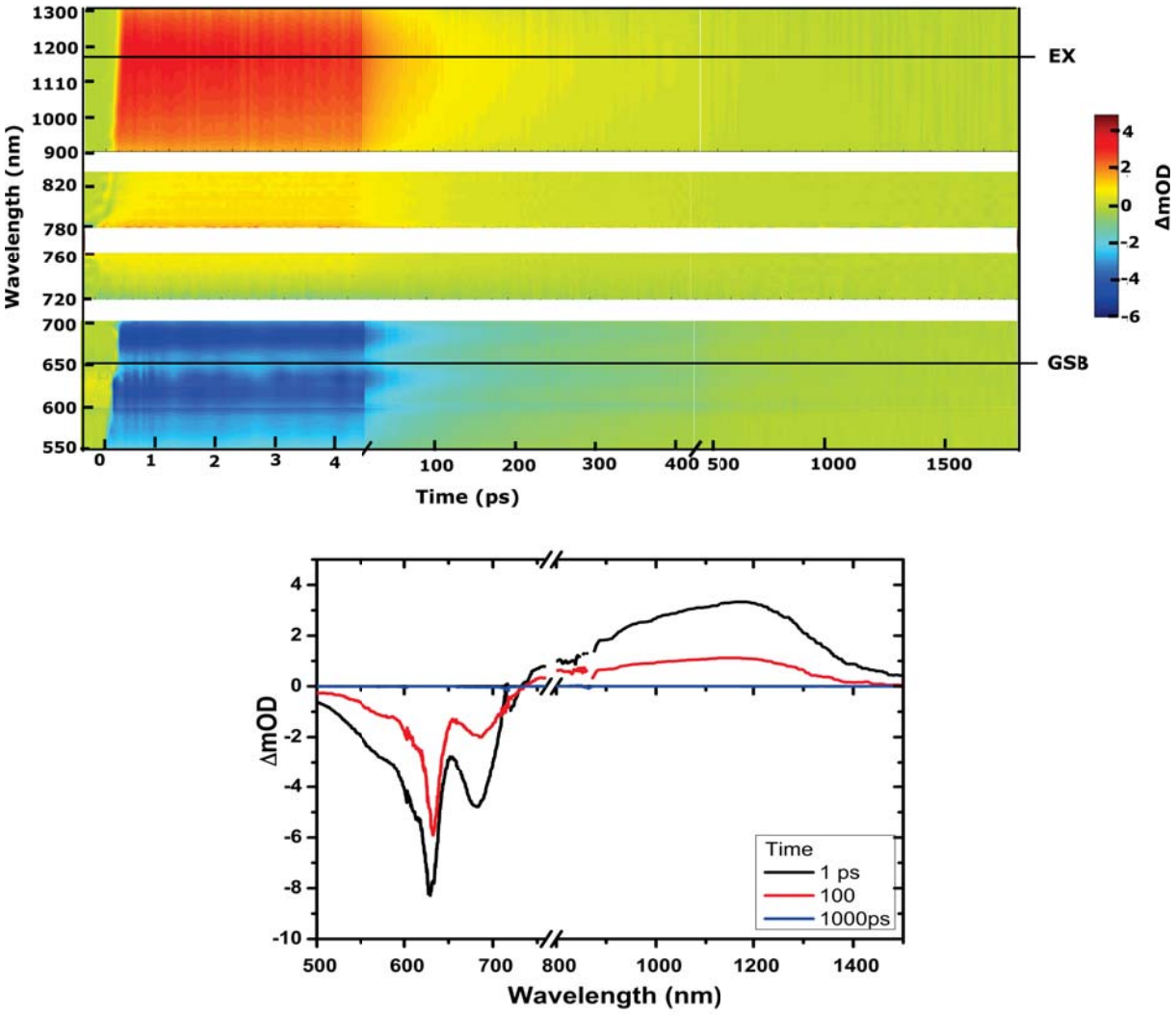

Figure 5.7: Top)TA spectrum of prisitne **P2TI** film. The blue part of the spectrum shows a negative change in absorption which is due to GSB. The broad light yellow and red regions (positive change in Absorption) is due to ESA. bottom) ΔOD curves taken out at selected delay times. The negative ΔOD peaks at positions corresponding to the maxima of the ground state absorption of pristine **P2TI** film in the low energy region thus the signal is due to GSB. The broad positive signal is due to EX.

absorption($S_1 \rightarrow S_n$). Triplet states can be excluded as the state is generated in < 150 fs and decays in < 1 ns. The GSB and the EX absorption have similar time constants. This shows there is no or negligible intermediate states that can be assigned to charge transfer state or free charge carrier absorption.

In the TA spectrum of pristine **P2TI** film, there was no growing signal that shows the generation of ICT state as in **P2TI** in solution. According to Marcus theory, electron transfer rate between the excited donor and acceptor increases with increasing reorganization energy of both the materials and the solvent. The electron transfer from the excited donor to the acceptor thus increases with increasing solvent polarity. This is the case with **P2TI** copolymer in solution. But in the case of solid films with strong interchain interaction, the excited donor would rather transfer its electron to the adjacent acceptor. Van Hal *et. al.*[42] studied electron transfer rate in donor-acceptor dyads. In their study, they were able to measure the electron transfer rate in dilute dyad solution samples but not in solid films. They concluded charge separation in solid films is ultra-

fast due to intermolecular charge transfer reaction between adjacent dyad molecules. Similarly, a strong interchain interaction due to π-π staking in the **P2TI** pristine film might dominate the intramolecular interaction. Thus, it won't be possible to see ICT formation in the pristine films.

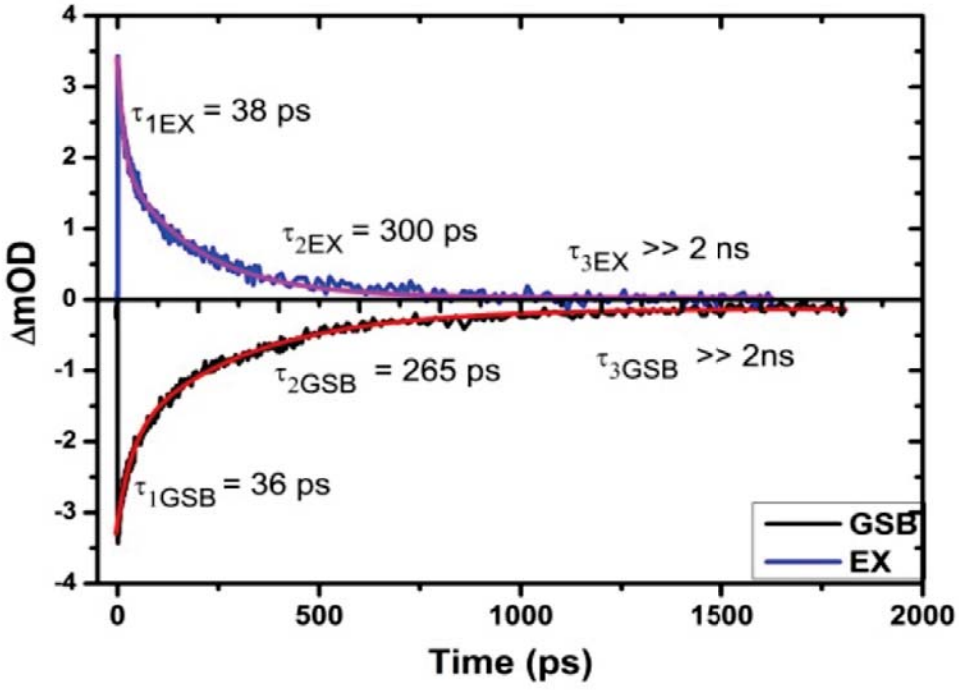

Figure 5.8: The temporal evolution of GSB and EX absorption are fitted a sum of exponential functions. The time constants of the EX and GSB signals (shown in the figure) are similar which indicates there is no or negligible intermediate state.

fs-Transient absorption spectroscopy of P2TI:PCBM71 BHJ film

The BHJ film of **P2TI**:PCBM71 (1:2) was studied as it is the active layer of the best performing cell among the different stoichiometries prepared (see above). The charge dynamics in this film determine the entire charge generation and recombination of the solar cell excluding charge extraction by the electrodes. The photodynamics in the BHJ film follow from the pristine **P2TI** film. The pump pulse excites the copolymer since PCBM71 has a negligible absorption at 630 nm.

TA spectrum of the BHJ film is shown in Figure 5.9. The spectrum has two negative signals at the same position with the pristine **P2TI** film which is assigned to the GSB of the copolymer. The broad positive signal is assigned to excited state absorption (ESA).

Photogeneration in an OSC starts with exciton (EX) generation in the polymer. The EX will then be quenched by the nearby acceptor and form a charge transfer (CT) state. Finally, the CT excitons if they separate, will generate free charge carriers in the manifold of charge separated (CS) states. Hence,the broad ESA is the sum of the absorption of EX, CT and CS states.

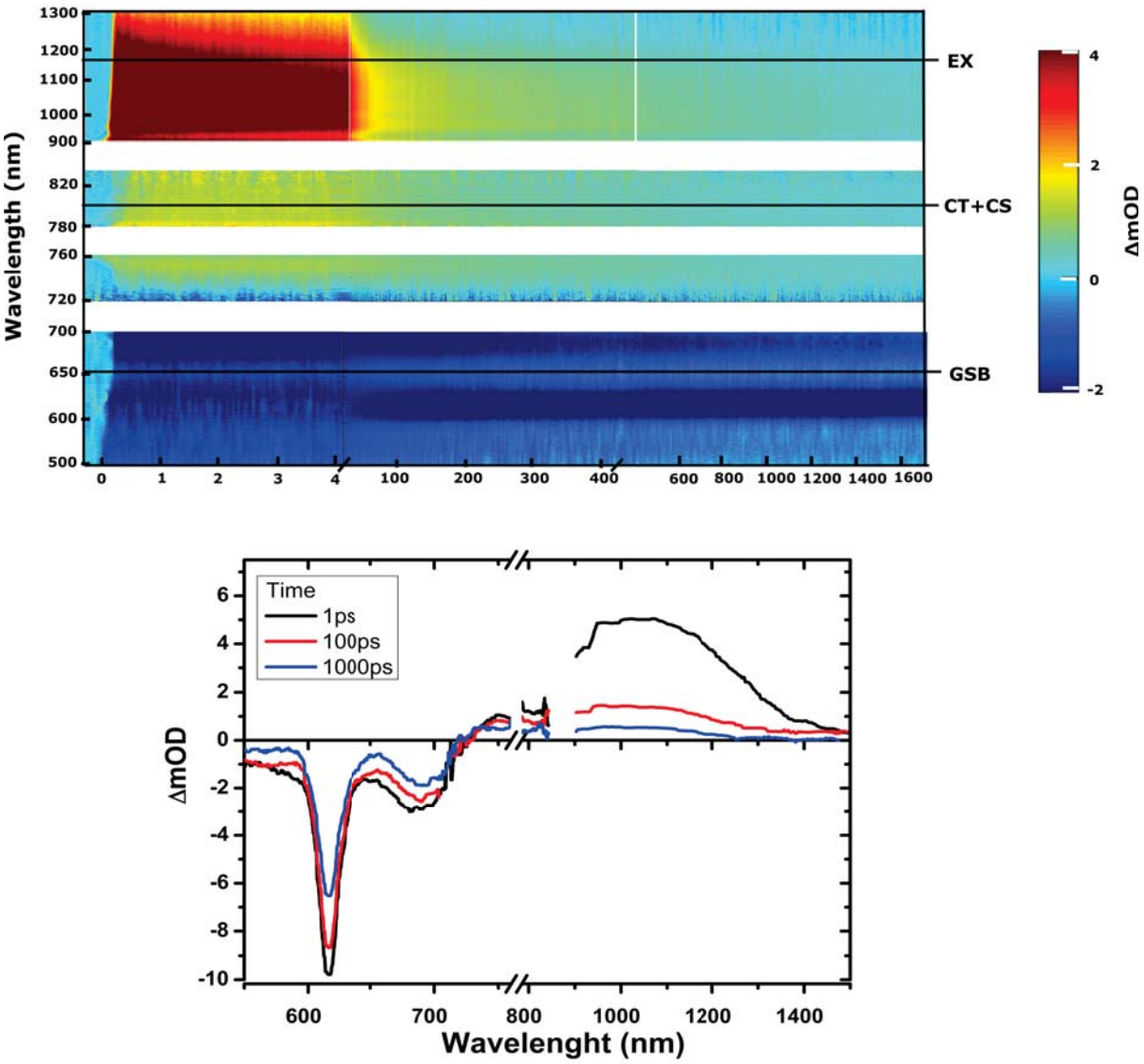

Figure 5.9: Top) TA spectrum of **P2TI**:PCBM71 (1:2) BHJ film. The blue part of the spectrum shows a negative change in absorption which is due to GSB. The broad light yellow and red regions (positive change in Absorption) is due to ESA. bottom) ΔOD curves taken out at selected delay times. The negative ΔOD peaks at positions corresponding to the ground state absorption of pristine **P2TI** film. The broad positive signal is due to EX+CT+CS states absorption. The ESA has a similar profile after 1 ps which shows all the states are populated below this time scale

Looking closely to the ESA part of the TA spectrum of the BHJ film, the spectra have similar profile after 1 ps. Thus, all the states are generated in < 1 ps. This is in agreement with ultra-fast exciton quenching in OSCs.

It was not easy to spectrally identify the three states in the TA spectrum. To simplify the process we started with the signals that we already have prior knowledge. From the pristine **P2TI** film, it is known that the EX absorption is at 1175 nm. Thus, a temporal trace at 1175 nm was fitted with a sum of exponential functions. The majority of the absorption at 1175 nm (63%) decays with a time constant of 10.5 ps and 29% of the signal decays with a time constant of 200 ps, a very small part (8%) of the signal stays longer than 2 ns. Comparing the absorption signal at 1175 to the GSB, its time constants vary considerably. The GSB has a 39% contribution that lives longer than 2 ns. Clearly,

there must be some intermediate states in the ESA. Therefore, a temporal trace was taken at the other end (805 nm) of the ESA to avoid the contribution of EX absorption as much as possible. The temporal evolution and the sum of exponential fits of the selected spectral signatures are shown in Figure 5.10. The trace at 805 nm was fitted with a sum of exponential functions and compared with GSB (see Table 5.3). The signal rises with a time constant of 250 fs and decays (56%) with a time constant of 120 ps. The signal has a 44% contribution that lives longer than 2 ns. This signal has a similar temporal profile to the GSB (see Table 5.3). The signal at 805 nm rises with a time constant longer than the resolution of the set up, this excludes the assumption of EX absorption in this signal. The signal is thus the sum of absorptions of CT excitons and free charge carriers in CS state. Hence, both CT and CS states are generated with a time constant below 250 fs. The CT state decays with time constant of 120 ps and the CS state lives longer than 2 ns. The absorption signal at 1175 nm on the other hand has three contributions: 63% EX which decay in time constant of 10.5 ps, and CS state that lives longer than 2 ns but the 200 ps time constant can be either CT state or EX decay. The time constant is in the order of EX life time. It also is close to the CT state life in 120 ps. The photodynamics is sketched in Figure 5.11.

The contribution of absorption of charge carrier bound or free can be analysed using the signal at 805 nm. This signal hence dictates the charge generation and recombination dynamics in **P2TI**:PCBM71 BHJ solar cell. The signal rises in a short time scale (250 fs), which shows efficient exciton quenching but in about 1 ns almost 60% of the signal decays. This explains the poor performance of the solar cell. This is due to the coarse morphology of the active layer as seen in the large domain sizes of SEM images. Since exciton quenching is efficient, loss of percolation pathways for free charge carriers to propagate to their respective electrodes is the reason for poor performance of the **P2TI**:PCBM71 based OSCs. The assumption that the domains in the SEM images are mixture of donor and acceptor is also confirmed with TA measurement.

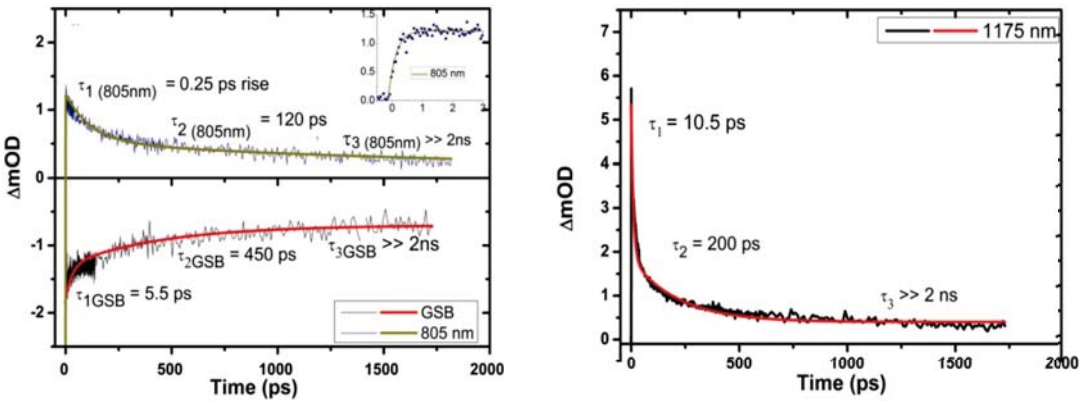

Figure 5.10: (left)The temporal profiles of GSB and signal at 805 absorption and (right) absorption signal at 1175 nm in **P2TI**:PCBM71 BHJ film are fitted with a sum of exponential functions. Both the GSB and the signal at 805 nm have a large portion that lives longer than 2 ns. The signal at 805 nm is due to CT and CS states absorption.

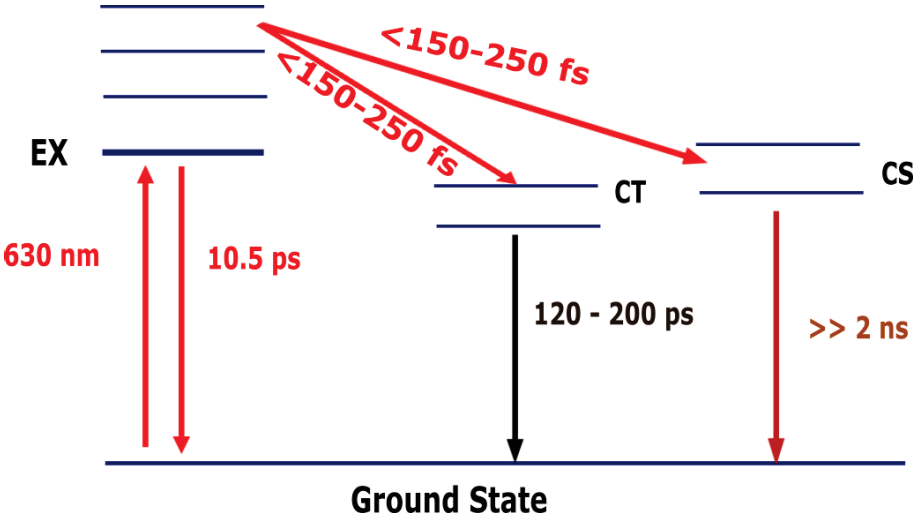

Figure 5.11: Sketch of Photodynamics in BHJ film of **P2TI**:PCBM71(1:2). The EX in the copolymer is quenched by PCBM71 in < 250 fs and a CT and CS states are generated. The free charges will then be collected with their respective electrode if they avoid bimolecular recombination.

Table 5.3: Time constants obtained by fitting each signal with a sum of exponential functions. The amplitude of each signal is normalized in percentage where $A = A_i/(A_1 + A_2 + A_3)$ X 100%.

Polymer	Signal	A_1 (%)	τ_1 (ps)	A_2 (%)	τ_2 (ps)	A_3 (%)	τ_3 (ps)
P2TI in CB	760 nm	—	2 (rise)	73	180	27	> 500
	1000 nm	10	2.1	90	190	—-	—-
	650 nm	24	20	62	590	14	> 600
P2TI Film	1175 nm	40	38	58	265	2	$>> 2000$
	650	37	36	59	300	4	$>> 2000$
P2TI:PCBM71(1:2) film	1175 nm	63	10.5	29	200	8	$>> 2000$
	805 nm	–	0.25 (rise)	56	120	44	$>> 2000$
	650 nm	19	5.5	43	450	38	$>> 2000$

5.3 Conclusion

In conclusion, a copolymer with bithiophene as a donor and isoindigo as an acceptor unit, **P2TI**, was studied. The absorption of the copolymer spans from below 350 to about 780 nm. The band gap of the polymer was 1.56 eV. A moderated solar cell efficiency of 1.02% with relatively high open circuit voltage of 0.81 V was obtained in an ITO-free solar cell based on a bulk heterojunction active layer of **P2TI**:PCBM (1:2). A steady state fluorescence measurement with two solvents of different polarity confirmed the presence of intramolecular charge transfer state in the relaxation channel of **P2TI** in solution. fs-Transient absorption spectroscopy measurement of **P2TI** in solution showed that this state was generated from the first singlet excited state with a time constant of 2 ps. Transient absorption measurement was also done on pristine **P2TI** and **P2TI**:PCBM71 (1:2) films. In pristine **P2TI** film, the photodynamics is mainly due to singlet excitons. Interchain interaction in **P2TI** pristine film dominates the charge transfer process. Consequently, intramolecular charge transfer state could not be observed. In the bulk heterojunction film, free charge carriers were formed in ultrafast time scale but only 44% of the charge carriers lived longer than 2 ns. This is due to the poor mor-

phology of the film. In such morphology, even if exciton quenching is fast, the loss of continuous percolation pathways to each of the charge carriers in their respective phases will have an adverse effect in the photogeneration. The poor current density from such a copolymer with a broad band absorption and high extinction coefficient is thus due to the loss of percolation pathways. Therefore, optimizing the morphology of the active layer can enhance the solar cell by creating uninterrupted pathways for charge carriers in their respective medium all the way to the electrodes.

6. Effect of side chain on photophysics and photovoltaic properties of two terthiophene-isoindigo copolymers

6.1 Introduction

Organic solar cells (OSCs) are mainly fabricated with solution processable techniques like spin coating, doctor blade coating and roll-to-roll printing. Hence, solubility of these polymers is a crucial step in the fabrication process. The use of side chains is essential to make polymers soluble enough for OSC application [13, 64]. For a long time, the use of side chains was believed to improve the solubility of the polymer without changing its opto-electronic properties. The band gap of a polymer can be tuned by adding side chains [13]. These side chains might induce steric hinderance in the backbone of the polymer. Consequently, the band gap increases. The position of the side chains can also change its opto-electical property [65]. Besides, side chains play an important role in the planarity of polymers [65] which is crucial for charge mobility. Some side chains like alkyl-substituted aromatic side groups can extend the π conjugation from the backbone to the lateral substituents leading to 2D conjugated system [66].

Most of the reports focus on the effect of side chains on the crystallization, opto-electronic properties, morphological structures of polymers and their photovoltaic properties when blended in a BHJ composite with fullerene derivatives. But side chain modulation can also directly affect the ICT character of a copolymer. Understanding the ICT character of a copolymer is important to further optimize their structure for increasing the performance of OSCs. Therefore, a systematic study of side chain engineering on the ICT character is essential to understand the structure-property relationship of D-A type copolymers for OSC application.

In this work, two copolymers (Figure 6.1) with terthiophene as a donor and isoindigo as an acceptor were designed and synthesized by direct arylation polycondensation method (see section 2.3). The difference in structure between the two copolymers is the length of the alkyl side chains on the terthiophene unit. The copolymer **P3TI-1** has an octyl side chain (C_8H_{17}) and **P3TI-2** has a longer dodecyl ($C_{12}H_{25}$) side chains at positions 3 and 4 of the first and the last thiophene units of the terthiophene donor units respectively. It is found that the length of the alkyl side chains can change the optical property, energy levels and photovoltaic property. We also studied charge dynamics of the copolymer using TA spectroscopy. The results showed that the length of alkyl side chains has a significant effect on ICT generation rate of the copolymer, exciton life time and charge carrier dynamics in pristine and copolymer/PCBM71 BHJ films.

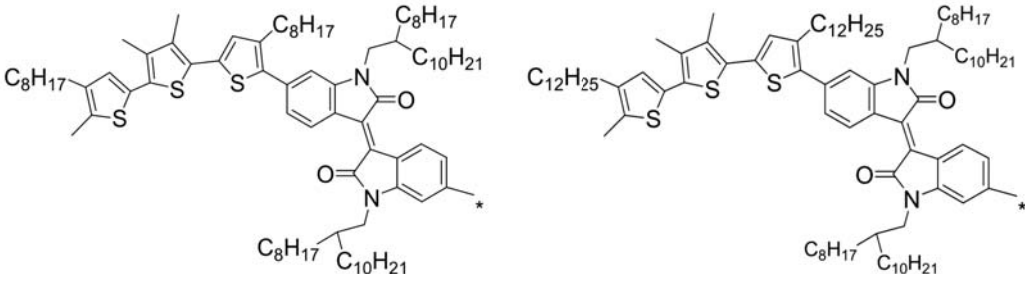

Figure 6.1: Chemical structures of **P3TI-1** (left) and **P3TI-2** (right) copolymers. The only difference in their structure is the length of the side chains.

6.2 Result and discussion

6.2.1 Steady state spectroscopy

Absorption spectra

Absorption spectra of the two copolymers are expected to be similar as their backbone structure is the same. Any difference observed can simply be attributed to the length of alkyl side chains on the terthiophene unit. Absorption spectra of **P3TI-1** and **P3TI-2** were taken both in solution and spin coated films. Absorption spectra of the two copolymers in CF solution ,shown in Figure 6.2a and b(black), has the so called "camel back" structure which is a finger print of D-A copolymers [34]. The low energy band from 580 nm to 650 nm is usually composed of a transition to an ICT state. This charge transfer character is due to intra-molecular charge transfer between the terthiophene and the isoindigo unit. The high energy band between 380 nm and 420 nm is due to the $\pi - \pi^*$ transition. This $\pi - \pi^*$ transition is common in π -conjugated polymers due to the alternating single and double bonds. This band is de-localized along the chain of the copolymers. The change in the length of the side chains on the terthiophene unit did not create a noticeable change in the absorption spectra of the copolymers in CF solution.

The absorption spectra of the two copolymers in films(Figure 6.2a and b (red)) have similar shapes but were broader than the respective absorption spectra in solution. This indicates a good molecular packing in solid states. Optical band gaps of the copolymers calculated from the absorption onset of the polymers were 1.63 and 1.56 eV for **P3TI-1** and **P3TI-2**, respectively. The band gap of the copolymers is in the ideal region for photovoltaic application[58]. The length of alkyl side chains on the terthiophene unit of the copolymers has negligible effect on the band gap of the copolymers. The absorption spectra of the two copolymers blended with PCBM71 is a simple superposition of the absorption spectra of the copolymers and PCBM71. The fullerene derivative PCBM71 has a better absorption below 500 nm and lower LUMO level that enables lower driving force for exciton dissociation than PCBM61. In the BHJ films of **P3TI-1** or **P3TI-2** blended with PCBM71, the contribution of PCBM71 to the total absorption is insignificant as both copolymers have a good absorption below 500 nm. But a BHJ film of copolymer:PCBM71 has a better exciton dissociation efficiency than the BHJ films of polymer:PCBM61 because PCBM71 has a lower LUMO level[18].

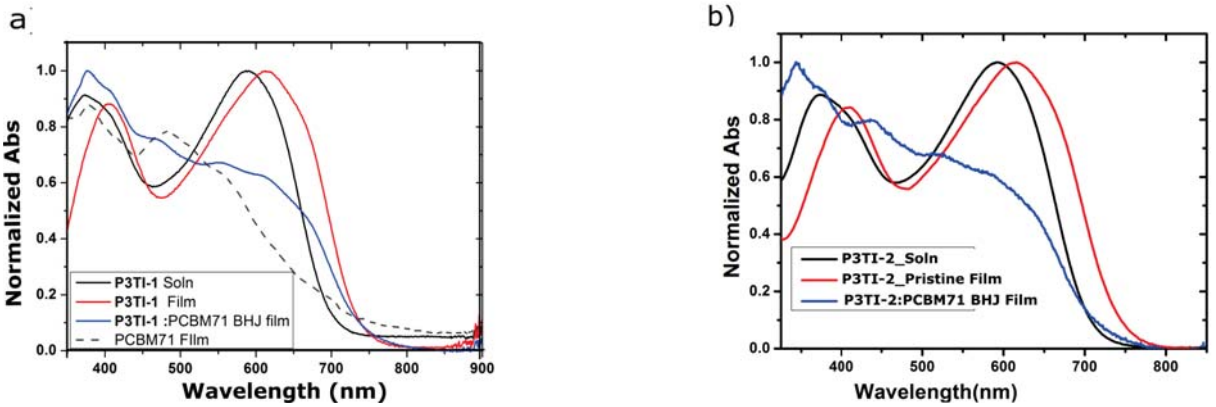

Figure 6.2: Steady state absorption spectra of **P3TI-1**(a) and **P3TI-2** (b) in CF solution(black), pristine film (red) and BHJ blends with PCBM71 (blue). The absorption spectra of both copolymers in solution and Pristine film has the so called 'camel' back structure. The BHJ absorption spectra have negligible contribution from PCBM 71 (shown in gray dashed line in a).

Table 6.1: Optical properties of **P3TI-1** and **P3TI-2**.

copolymer	Abs. Max Film		Abs. Max Soln.		Abs Shift from Soln to Film		$E_g^{Opt}(eV)$
	λ_{max1}	λ_{max2}	λ_{max1}	λ_{max2}	$\Delta\lambda_{max1}$	$\Delta\lambda_{max2}$	
P3TI-1	404	611	375	591	29	20	1.63
P3TI-2	411	615	373	592	38	23	1.59

Photoluminescence (PL)

The PL spectra of both copolymers in CF solution were recorded at excitation of both the absorption maxima of the respective copolymers. PL spectra recorded after exciting at the higher wavelength of each copolymers resulted in a stokes shift of 155 nm (0.44 eV) for **P3TI-1** and 149 nm (0.42 eV) for **P3TI-2** copolymer. These large stokes shifts can be due to significant structural changes of the copolymers upon excitation. Upon excitation, a molecule will be in its Frank-Condon excited state, then the molecule's nuclear geometry rearranges itself to a more stable configuration which is the excited state equilibrium. The electronic structure of a sample therthiophene-isoindigo copolymer was calculated using DFT calculations both in the ground and excited state (see Figure 2.10). In the DFT calculations, we found that the electronic structure of these type of copolymers goes from D - A in the ground state to $D^+ = A^-$ equilibrium excited state. This creates a significant structural change that is accompanied by a large stokes shift.

To better understand the relaxation channels in the copolymers chains, we further studied their PL in two solvents with different polarity: CB (polarity index = 2.1) and CF (polarity index = 4.1) with excitations at the longer wavelength absorption maximum of each. The PL and absorption spectra of both copolymers in CB and CF solution are shown in Figure 6.3. The PL spectra of both copolymers in two solvents showed a red shift with increasing solvent polarity but the absorption spectra remains the same. A solvent-solute interaction depends on the nature of the solute and the polarity of the solvent. If a molecule has a higher dipole moment in the excited state than the ground state ($\mu_e > \mu_g$), a polar solvent can interact with the dipoles in the excited state in such a way that it lowers its energy. The increase in polarity of the solvent enables

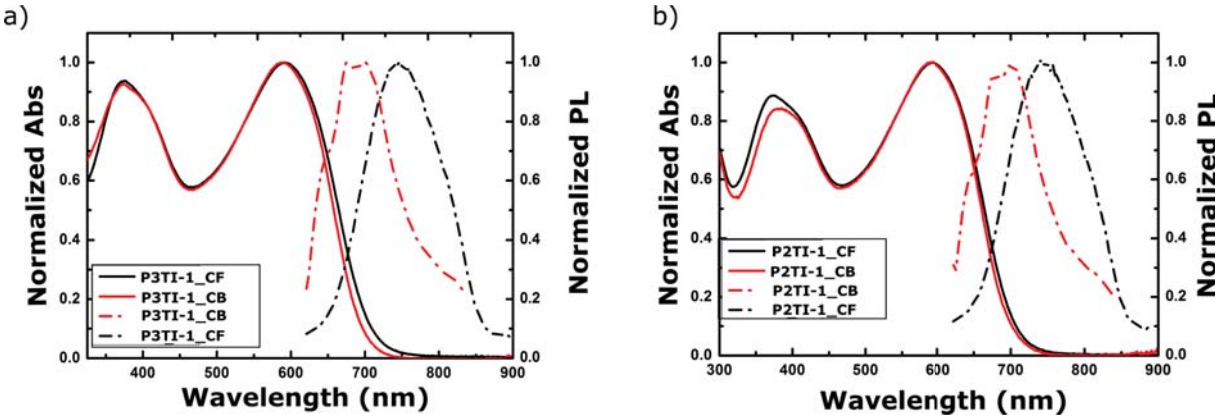

Figure 6.3: PL and Absorption spectra at excitation of the higher wavelength absorption maxima of **P3TI-1** (a) and **P3TI-2** (b) in CB (red) and CF (black). A red shift in PL in both copolymers confirms presence of ICT state in their relaxation channels

access this lower state. In the case of copolymers, the donor-acceptor coupling creates a dipole due to the intramolecular charge transfer. The red shift in PL of copolymer **P3TI-1** and **P3TI-2** with increasing solvent polarity hence confirms the presence of ICT state in the relaxation of these copolymers.

The PL spectra was also recorded at excitation of 374 nm (Figure 6.4). The PL spectra of **P3TI-1** (Figure 6.4a) has a negligible PL in the lower wavelength region but **P3TI-2** (Figure 6.4a) has two distinct PL regions. This shows the higher wavelength region relaxation is the dominant relaxation channel in the copolymer **P3TI-1**. Therefore in **P3TI-1**, the ICT state is the dominant relaxation channel. But copolymer **P3TI-2** has two relaxation channels of which the low wavelength region emission is stronger. This low wavelength transition is due $\pi - \pi^*$ transition.

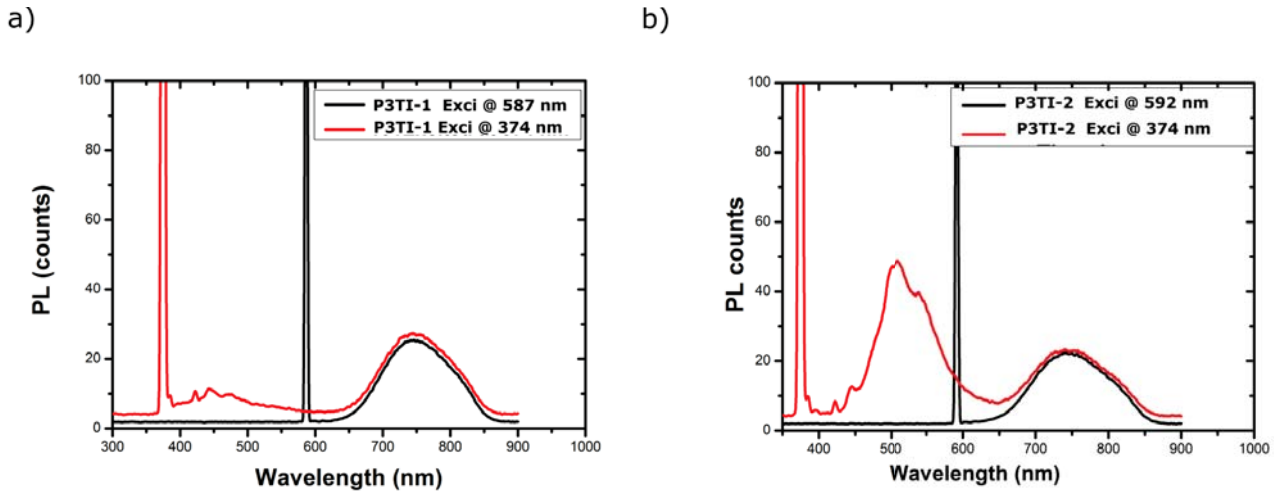

Figure 6.4: PL spectra of (a)**P3TI-1** and (b) and **P3TI-2** exited at higher wavelength (black) absorption maxima and lower wavelength (red) absorption maxima. ICT state is the dominant relaxation channel in **P3TI-1** but **P3TI-2** has an additional relaxation channel. The sharp peaks in the figure are the scattered pump light.

6.2.2 Photovoltaic performance and morphology

Photovoltaic Properties

OSCs in an ITO free geometry (Al/TiO_x/ Active layer /PEDOT:PSS *PH 1000*) were prepared. The active layer was a BHJ composite of **P3TI-1** or **P3TI-2** copolymers blended with PCBM71. The detail of the sample preparation is given in chapter 4.

The photovoltaic performance of a given solar cell is the product of open circuit voltage, short circuit current and fill factor under 1 sun condition. The efficiency of **P3TI-1**:PCBM71 and **P3TI-2**:PCBM71 BHJ OSCs were 0.93% and 0.67%. The efficiency decreased by 28% as the length of the alkyl side chains in the thertiophene units of the copolymer is longer by 4 methyl units. The photovoltaic parameters of the two solar cells are summarized in Table 6.2. Short circuit current of a solar cell is determined by many factors that include spectral overlap of the copolymer's absorption with the solar spectrum, charge transport, and morphology of the active layer. The amount of solar irradiance that can be absorbed is determined by the broadness of the absorption spectra of the copolymers and its absorption coefficient. In copolymers **P3TI-1** and **P3TI-2**, there was almost no difference in their spectral coverage of the solar spectrum. The absorption coefficient is also another parameter to be considered. But in the preparation of the solar cells, the thickness of the cells is optimized for best performance. Hence, the difference in their absorption coefficient is compensated. A LUMO offset between the copolymers and PCBM71 of 0.3 - 0.4 eV is needed to overcome exciton binding energy in OSCs [58]. The LUMO offset of **P3TI-2**:PCBM71 is 0.3 eV but for **P3TI-1**:PCBM71 it is 0.2 eV (Figure 6.6a). The lower LUMO offset in **P3TI-2**:PCBM71 might contribute to its smaller short circuit current due to poor exciton quenching. But in the case of copolymers, exciton binding energy can be lower due to their dipolar character. To see if the LUMO offset is the reason for lower short circuit current in **P3TI-2**:PCBM71 OSCs, we took fluorescence(FL) images of the pristine copolymers and the BHJ films of the copolymer:PCBM71 (see Figure 6.5). FL quenching efficiency is calculated as:

$$\Delta FL = 1 - \frac{FL_{Blend}}{FL_{Prisitne}}, \tag{6.1}$$

where FL_{Blend} and $FL_{Prisitne}$ are the average FL over the measured area of the blend or the pristine copolymer films.

A ΔFL value of 90.1% for **P3TI-1**:PCBM71 and 81% for **P3TI-2**:PCBM71 was found. Therefore, exciton quenching is more efficient in **P3TI-1**:PCBM71.

Open circuit voltage tells us the energetics in the entire solar cell. The HOMO and LUMO levels of both copolymers was measured using square voltammetry and is shown in Figure 6.6a[20]. Open circuit voltage is mainly determined by the difference in the effective band gaps i.e $\Delta E = E_{HOMO}^{polymer} - E_{LUMO}^{PCBM71}$ of the device. The effective band gap (ΔE) is similar for both copolymers because they have similar HOMO levels. The open circuit voltage differ by only 5 mV.

The fill factor (FF) of the OSCs based on BHJ of **P3TI-1**:PCBM71 and **P3TI-2**:PCBM71 is the main difference among the two devices. It increases almost by 2 fold as the length of the alkyl side chains on the terthiophene unit of the copolymers becomes shorter by 4 methyl unit. FF is a measure of recombination in a solar cell. Therefore, the 2-fold difference in FF of the OSCs shows charge recombination losses in **P3TI-2**:PCBM71 OSCs are worse than **P3TI-1**:PCBM71 OSCs. This indicates that long alkyl side chains in the copolymers create a barrier on charge carrier transport to the electrodes. The long alkyl

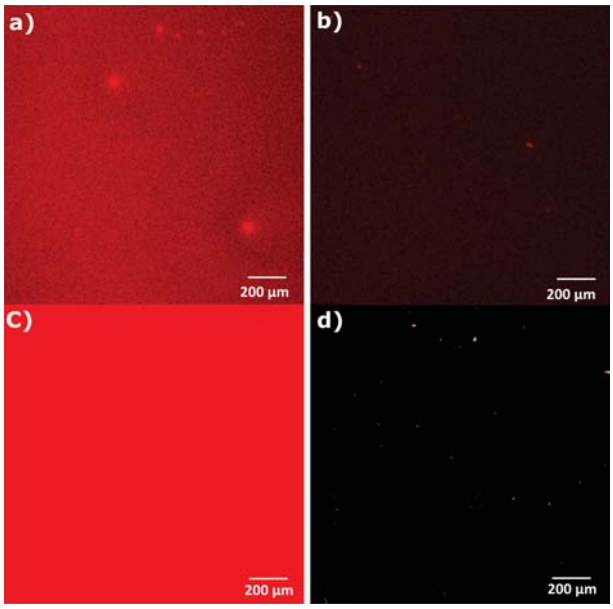

Figure 6.5: Florescence imaging of (a) Pristine **P3TI-2** film (FL_{av} = 7.5 counts/3 mm^2 $\times 10^6$ pixels) (b) **P3TI-2**:PCBM71 BHJ Film (FL_{av} = 39.5 counts/3 mm^2 $\times 10^6$ pixels) (c) Pristine **P3TI-1** film (FL_{av} = 58.9 counts/3 mm^2 $\times 10^6$ pixels) (d) **P3TI-1**:PCBM71 BHJ Film (FL_{av} = 5.4 counts/3 mm^2 $\times 10^6$ pixels). The redder images show higher FL while the darker images represent reduced FL. Exciton quenching is more efficient in **P3TI-1**:PCBM71.

side chains might create traps that will induce higher recombination losses in the cells. This observation is the motivation for further studying the effect of length of alkyl side chains on charge transfer dynamics that occur within the copolymer chain, when the copolymer chains can interact in solid pristine films and when it is in the actual solar cell active layer i.e BHJ film of copolymer:PCBM71. These will be discussed in the next sections.

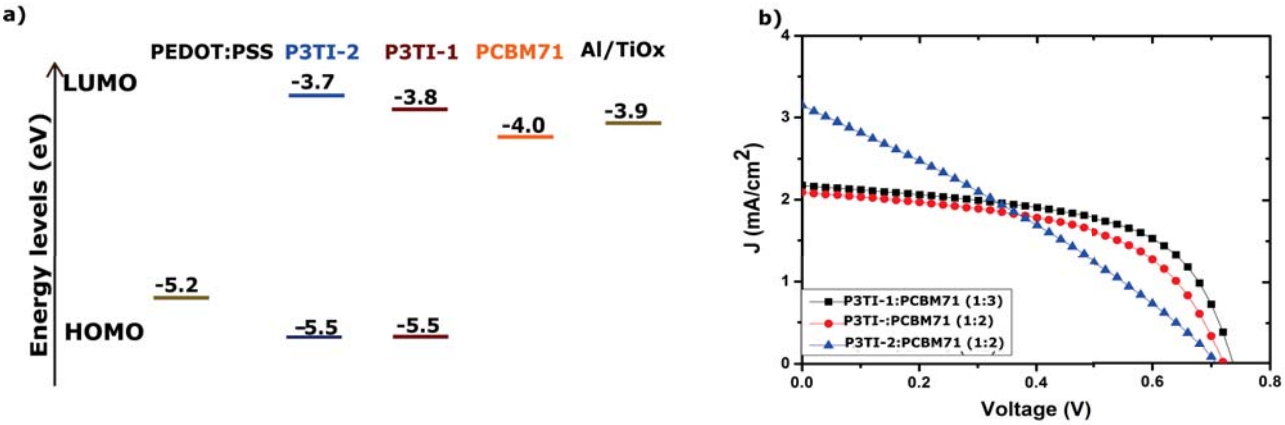

Figure 6.6: a) Energy levels and b) J-V curves of Al/TiO_x/ **P3TI-1**(**P3TI-2**):PCBM71/PEDOT:PSS OSCs. The fill factor is the main difference in the two solar cells. The fill factor increased by 48% when the length of the alkyl side chains on the donor unit of the copolymers is shortened by 4 methyl units.

Table 6.2: Summary of photovoltaic properties of Al/TiO_x/**P3TI-1**:PCBM71/PEDOT:PSS and Al/TiO_x/**P3TI-2**:PCBM71/ PEDOT:PSS OSCs

Copolymer	Copolymer to PCBM71 Ratio	$J_{sc}(mA/cm^2)$	$V_{oc}(V)$	FF (%)	Eff(%)
P3TI-1	1:2	1.9	0.74	58	0.81
P3TI-1	1:3	2.2	0.74	58.1	0.93
P3TI-2	1:2	3.2	0.	30.2	0.67

Morphology

The short circuit current in both solar cells is lower than expected from their broad absorption. We studied the morphology of the active layer in these solar cells using scanning transmission electron microscopy (STEM) (Figure 6.7). The active layers in both solar cells are full of large domains that exceed 200 nm. The images can not give a comparative value between the two solar cells as the size of the domains in both solar cells is much much larger than the typical exciton diffusion length (5- 20 nm). The result emphasizes the importance of better intermixing between the copolymer and PCBM71 for photogeneration. Exciton created in the copolymer should get to PCBM71 molecule within its diffusion length for dissociation. The dissociated charge carriers should also have un-interrupted pathway to the electrodes. The morphology of the active layers of both **P3TI-1**:PCBM71 and **P3TI-2**:PCBM71 OSCs are poor for efficient photogeneration and collection of charge carriers. Therefore, the short-circuit current in both OSCs is low compared to what is expected from their broad absorption. Solvent additives like 1,8-diiodooctane are usually used to improve the intermixing between the copolymers and PCBM71. This can enhance the short circuit current. We recommend morphology optimization for the OSCs studied in this work.

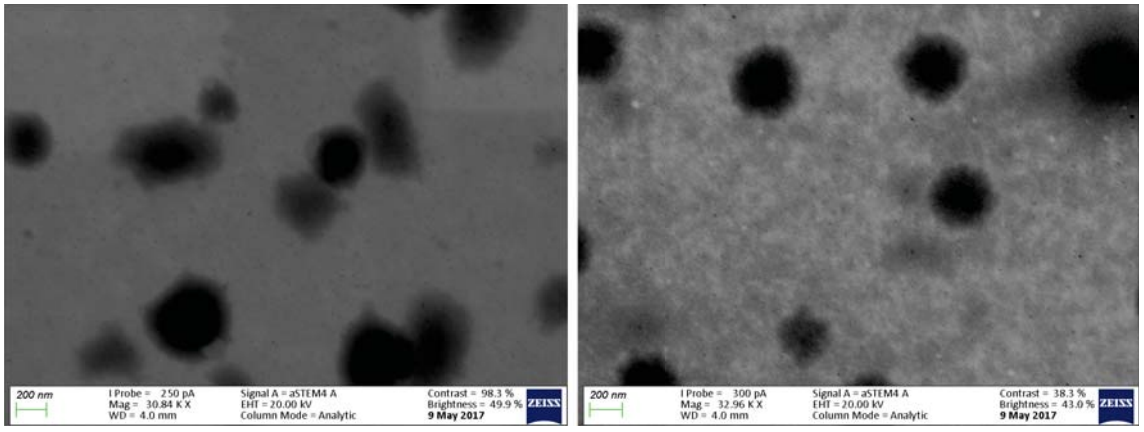

Figure 6.7: STEM images of **P3TI-2**:PCBM71 (1:2) (left) and **P3TI-1**:PCBM71 (1:3) (right). The active layers are full of domain sizes exceeding 200 nm which is more than 10 times the typical exciton diffusion length.

6.2.3 Charge dynamics in copolymer chains

fs-Transient absorption(TA) spectroscopy measurement were taken in dilute solutions of the copolymers in CB solvent. We first took steady state absorption spectra of the copolymers solutions to see any aggregation effect in the concentrations studied for

TA measurement. There was no spectral shift that would indicate aggregation in both solutions. Therefore, any interchain interaction in data analysis of fs-TA measurement in solution can be excluded.

The fs-TA spectra of both copolymers (Figure 6.8) in CB solution have positive ΔOD signals above 900 nm, a negative ΔOD signal below 650 nm and an overlapping positive and negative ΔOD signal around 680 and 685 nm for **P3TI-1** and **P3TI-2** respectively. The negative ΔOD signals in both copolymers can be assigned to ground state bleaching (GSB) unambiguously because of their spectral matching to the absorption maxima of the corresponding copolymers as shown in Figure 6.2. This signal has also the contribution of scatter pump light. The positive signal above 900 nm is assigned to exciton absorption as it is generated within our temporal resolution ($<$ 150 fs). The last spectral signature in both copolymers evolves from a negative signal to a positive absorption signal and grows upto 30 ps and 40 ps for **P3TI-1** and **P3TI-2** respectively. The spectral position of these signatures coincide with the emission of the respective copolymers (see Figure 6.3). These signatures might be either overlapping

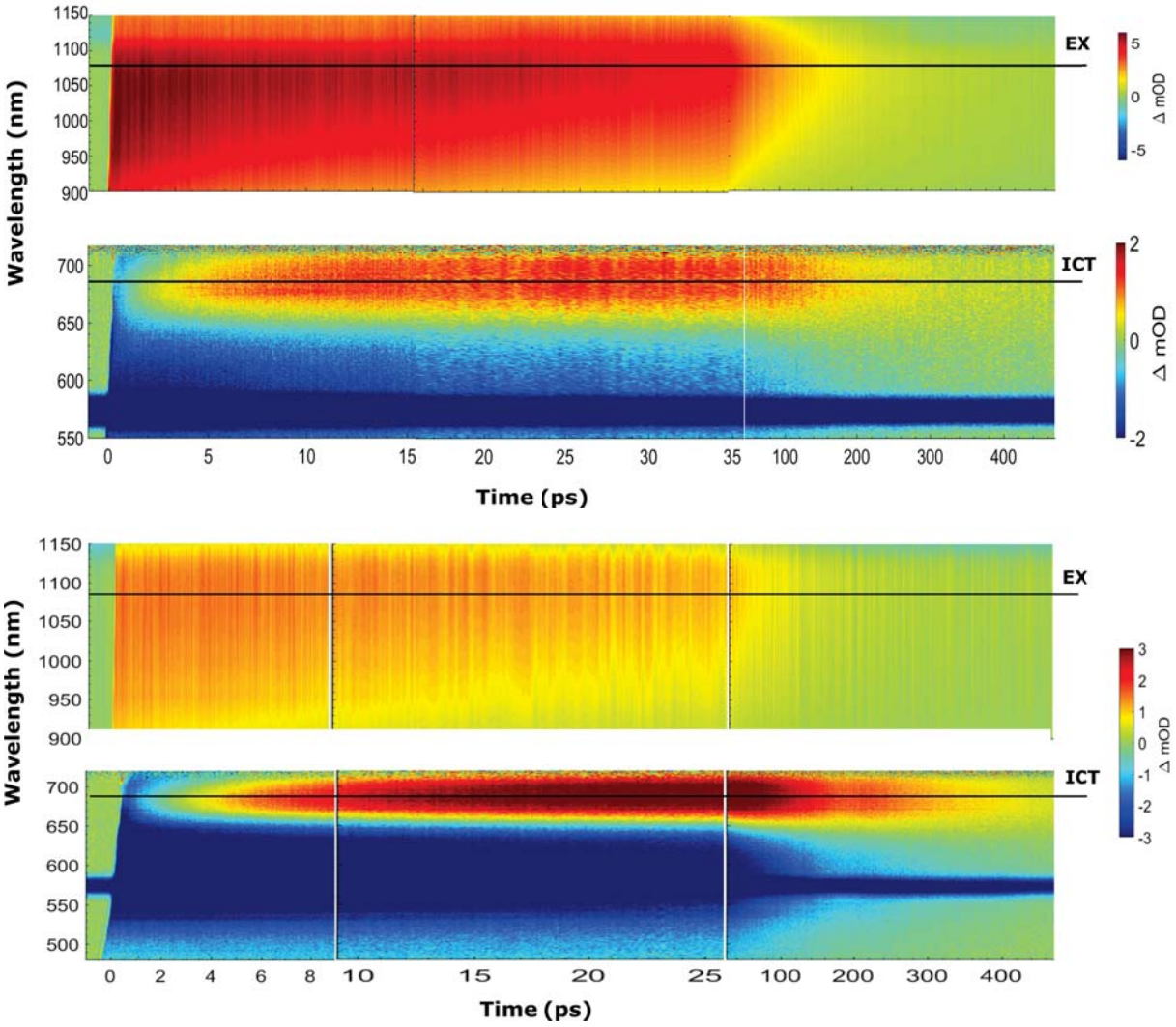

Figure 6.8: Transient absorption spectra (top) **P3TI-1** (bottom) **P3TI-2** in CB solution. Both TA spectra show a growing ICT signal around 680 nm and exciton absorption above 900 nm.

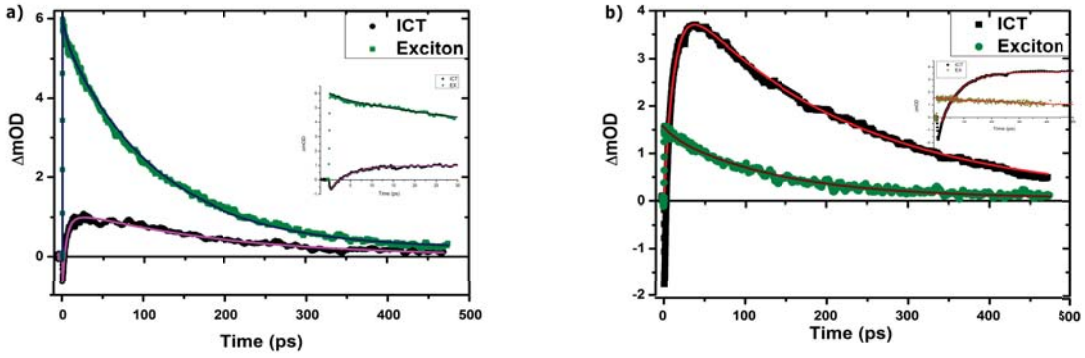

Figure 6.9: Temporal profile and fitting of ICT and exciton absorption of (a) **P3TI-1** (b) **P3TI-2** copolymer in CB solution

signatures of stimulated emission and growing intermediate states or growing intermediate states that quenches the emission of the respective copolymers. In either cases, the signatures have contributions from intermediate states. From the steady state spectroscopy measurement and DFT calculations, we know ICT state participates in the relaxation of the copolymers in solution. Therefore, this intermediate state is assigned to ICT state. To understand the photodynamics of each copolymer, we took line outs at the ICT and exciton absorption signals. We fitted the temporal evolution of each spectral signature with sum of exponential functions. The fit results are shown in Figure 6.9 and summarized in Table 6.3. The ICT state grows with a time constant of 4.5 ps and 13 ps for **P3TI-1** and **P3TI-2** respectively. The rise time constants of each ICT states and the short decay time constants of corresponding exciton absorptions correlate well. The ICT state generation rate in **P3TI-1** copolymer is faster by almost 3-fold than the rate in **P3TI-2** copolymers. The shorter side chains in **P3TI-1** copolymer enhance the ICT character between the donor and the acceptor units. This is also observed in its lower LUMO level. The LUMO of the copolymers are the result of orbital coupling of the LUMOs of the donor terthiophene unit and the acceptor isoindigo unit. The acceptor units are similar in both copolymers. Therefore, the lower LUMO level in **P3TI-1** shows an effective electron transfer from the donor to the acceptor unit. On the contrary, the long side chains in **P3TI-2** create a barrier for charge transfer between the donor and the acceptor units. This might be because of poor orbital coupling between the donor and acceptor units in the copolymer. The PL measurement with excitation at lower wavelength absorption maximum of **P3TI-2** shown in Figure 6.4 also supports this conclusion. The dominant relaxation channel in this copolymer was the lower wavelength region.

Table 6.3: Summary of fit results of copolymer **P3TI-1** and **P3TI-2** in CB solution

Copolymer	Signal	A_1	τ_1(ps)	A_2	τ_2(ps)	y_0
P3TI-1	ICT	–	4.5 (rise)	1.6	180	0
P3TI-1	Exciton	0.45	4.5	5.4	115	0.2
P3TI-2	ICT	–	13.1 (rise)	4.6	212	0.07
P3TI-2	Exciton	0.13	13	1.37	135	0

6.2.4 Charge dynamics in pristine copolymer films

Unlike copolymers in solution where the chains of the copolymers are isolated, there is interchain interaction in the solid films as could be seen from the broadening of the steady state absorption spectra in solids films compared to the solution (see Figure 6.2). This interchain interaction influence the TA spectroscopy measurement.

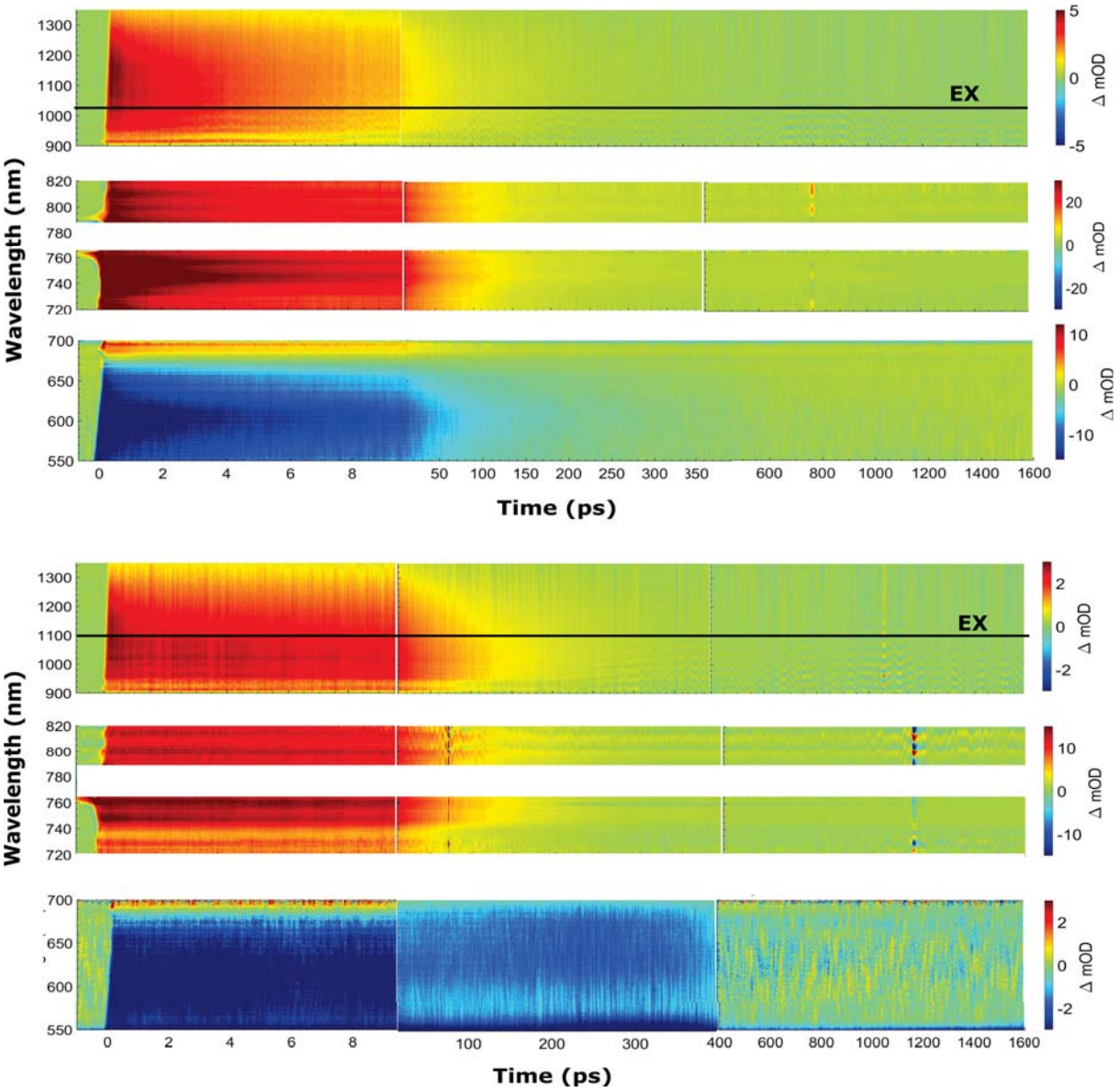

Figure 6.10: TA spectra **P3TI-1** (top) and **P3TI-2** (bottom) pristine films. The TA spectra of the pristine films are different from TA spectra of the respective copolymers in CB solution.

The TA spectra of **P3TI-1** and **P3TI-2** copolymers pristine films are clearly different from their respective TA spectrum in solution (see Figure 6.10). The TA spectra of both copolymers in pristine films have negative signals below 720 nm and a broad positive signals above it. There was no growing signal within our temporal resolution. The ESA was populated within our temporal resolution. This ESA signal in the TA spectrum of the pristine conjugated polymer films is dominated by excitons especially in short time scale less than 1 ns. To find out if there is any other contribution to ESA signal in

addition to exciton absorption, we took line outs at different wavelength regions for both copolymers as shown in the Figure 6.11.

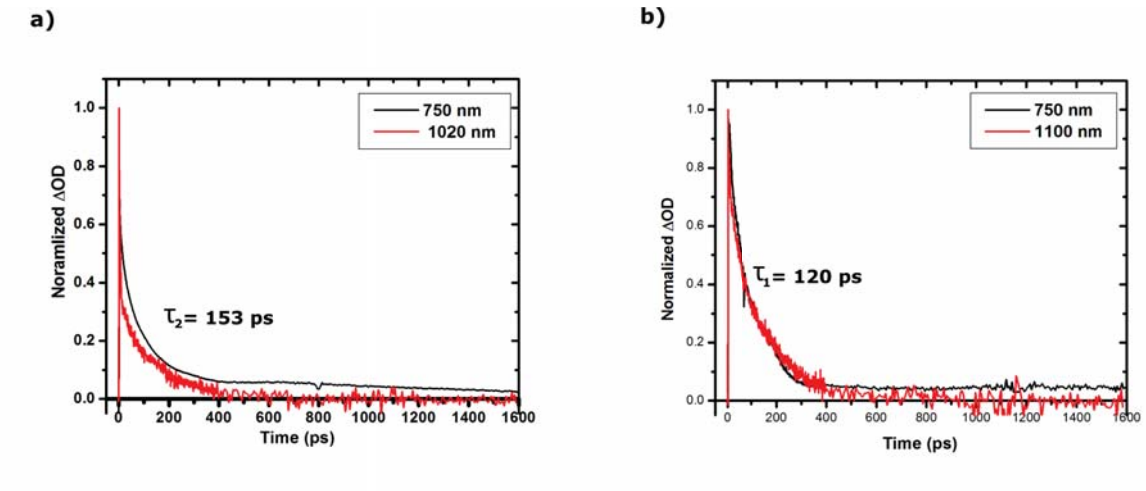

Figure 6.11: Temporal profile of line outs taken at different wavelengths of the TA spectra of (a) **P3TI-1** (b) **P3TI-2** in pristine film. The line out have similar temporal evolution. This shows there is only one spectral signature in the ESA.

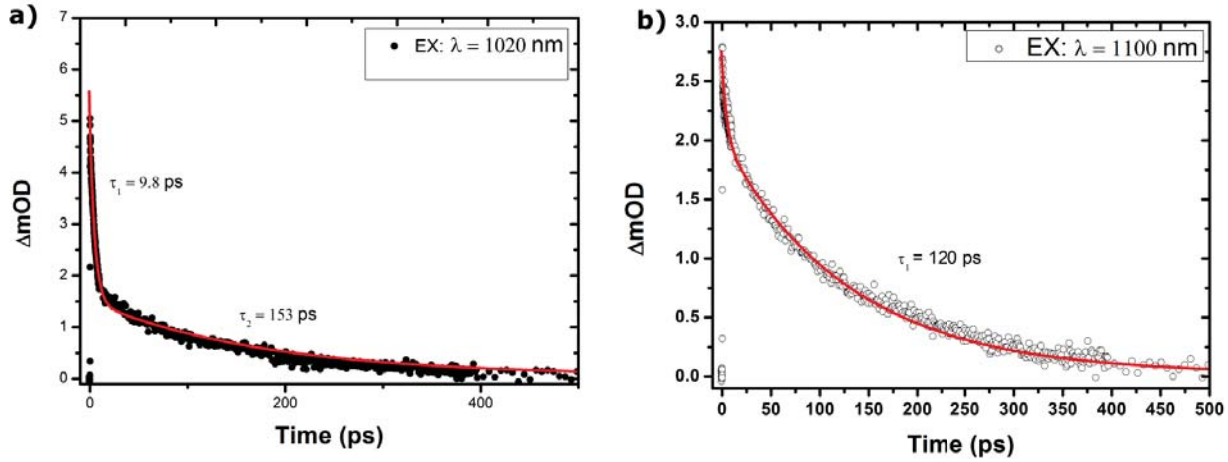

Figure 6.12: Temporal profile of exciton in (a) **P3TI-1** and (b) **P3TI-2** copolymer pristine film. Longer alkyl side chains shortens exciton life time.

We didn't observe a significant difference in the life time of the signals taken at different positions of the TA spectra of both copolymer pristine films (Figure 6.11). Thus, exciton absorption is the reasonable assignment for the broad ESA signal observed in both copolymer pristine films. The exciton in **P3TI-1** and **P3TI-2** decays with time constants of 153 ps and 120 ps respectively (Figure 6.12). The stronger ICT character of the excitons in the copolymer-**P3TI-1** might contribute to its longer exciton life time.

Intensity dependent dynamics in pristine copolymer films

In the quest of an answer for the 2 fold difference in FF between **P3TI-1**:PCBM71 and **P3TI-2**:PCBM71 solar cells, we further studied intensity dependent dynamics of exciton in each copolymer pristine films. At excitation densities exceeding 10^{17} photons/cm^3 in conjugated polymers, excitons will have high probability of meeting each other which can prompt exciton-exciton annihilation (EEA)[**?**]. In EEA, the energy of one of the excitons is transferred to the other. Consequently, the first exciton will relax back to the ground state while the second is excited to higher states. The product of EEA is thus an excited exciton ($S_1 \rightarrow S_n$) at an expense of relaxing one exciton ($S_0 \leftarrow S_1$). The excited exciton will relax back by an ultrafast internal conversion: $S_1 \leftarrow S_n$ [52]. For EEA the excitons should diffuse a distance where there can be Forster Energy transfer. Thus, diffusion length and life time are the important parameters in EEA. The pump fluence was increased from 160 nJ to 240 and finally to 500 nJ with a beam size of approximately 100 μm diameter. Assuming a thickness of 100 nm for each copolymer films, the excitation density is calculated to be 6.5×10^{16}, 8.5×10^{16}, and $1.8 * 10^{17}$ photons/cm^3. EEA annihilation is a fast process thus short time scale measurement upto 10 ps were taken.

For copolymer-**P3TI-2**, there was no intensity dependent dynamics for pump fluence from 2 to 3.06 mJ/cm^2. A faster decay dynamics was observed as the fluence was further increased to 6.4 mJ/cm^2 (Figure 6.13a). The faster decay dynamics with increasing fluence shows an intensity dependent dynamics has come to play. This intensity dependent dynamics is bimolecular. The short time dynamics in a pristine polymer film is mainly due to excitons. Charge carriers (bound or free) if generated dominate in longer time scales. Consequently, the bi-molecular dynamics is related to the dynamics that involves only excitons which are exciton relaxation and EEA. EEA is thus the only possible bimolecular dynamics.

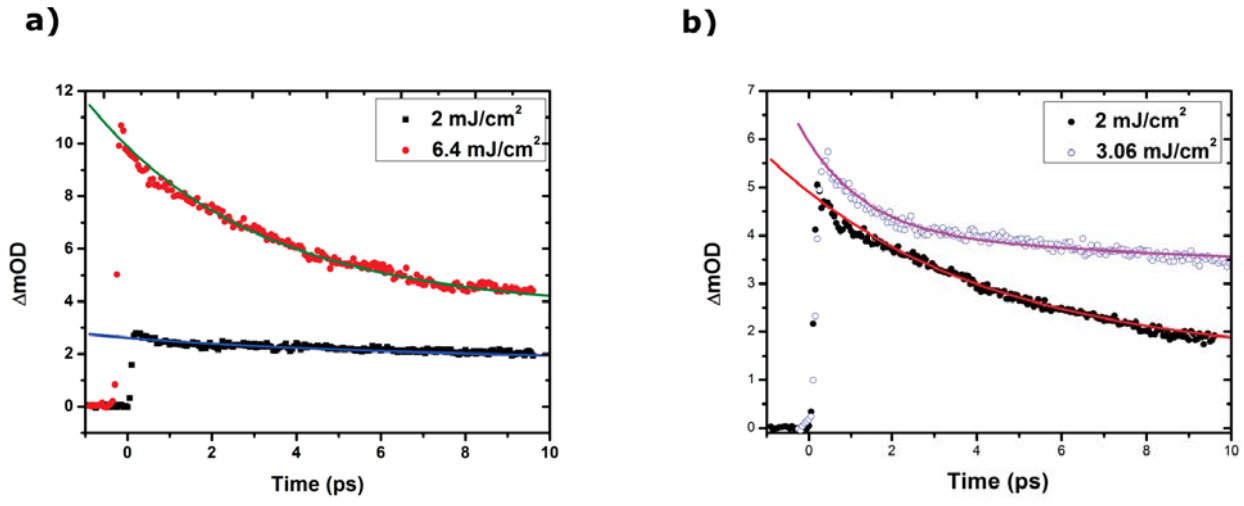

Figure 6.13: Temporal evolution and sum of exponential fits of EX in a) **P3TI-2** and b) **P3TI-1** copolymer pristine film with different pump fluence. EEA started at lower excitation density in **P3TI-1** than **P3TI-2**. Exciton diffusion is more efficient in **P3TI-1**

Comparing the temporal profile of pristine copolymer **P3TI-1** and **P3TI-2** films at a pump fluence of 2 mJ/cm^2 (160 nJ), the latter has negligible decay in the first 10 ps. But **P3TI-1** shows a significant loss (36%) within the first 10 ps. In this short time scale, no

or negligible loss of excitons is expected in conjugated polymers. In copolymer-**P3TI-1**, this loss becomes faster as we increase the pump fluence to 3.06 mJ/cm^2 (240 nJ), thus we assign this loss for EEA.

Assuming each photon generates an exciton, the exciton density can be approximated to the excitation density. Thus, the exciton density to initiate EEA in copolymer-**P3TI-1** was one order lower than copolymer-**P3TI-2**. This shows effective exciton diffusion in copolymer-**P3TI-1**. The excitons in **P3TI-2** have shorter diffusion length due to the longer alkyl side chains. This lowers the probability of their interaction for EEA in lower excitation density. Alkyl side chains can change the morphology or packing of the copolymer films. The degree of crystallinity in the films creates a difference in coupling between chromophores which in turn affects the diffusion length of excitons. A study on Poly 3-hexylthiophen(P3HT) showed diffusion length increases with increasing crystallinity. The diffusion length of a highly crystalline regio-regular-P3HT (RR-P3HT) is 20 nm which is 4 times longer than the diffusion length of an amorphous regiorandom P3HT (RRa-P3HT) [52]. The longer alkyl side chains in **P3TI-2** copolymer therefore traps exciton by creating a barrier to interchain interaction in the pristine copolymer film. A poor interchain interaction in **P3TI-2** pristine film is detrimental to the charge mobility in the respective solar cell which is one of the important parameters for power conversion efficiency.

Table 6.4: Summary of fit results of copolymer **P3TI-1** and **P3TI-2** pristine films with different pump fluence.

Copolymer	Fluence (mJ/cm^2)	A_1	τ_1(ps)	A_2	τ_2(ps)
P3TI-1	2	17	9.8	2	153
P3TI-1	3.06	1.6	7.3	3.2	153
P3TI-2	2	–	–	2.2	120
P3TI-2	6.4	5.4	4	4.2	120

6.2.5 Dynamics in BHJ films of copolymers blended with PCBM71

The BHJ composite of P3TI-1 or P3TI-2 copolymers and PCBM71 serves as the active layer of the photovoltaic cell. The dynamics that we observe in these films collectively contribute to the internal quantum efficiency(IQE) of the solar cell. The efficiency of a given solar cell is a result of multiple process from absorption of photons to charge collection by the asymmetric electrodes. The charge generation process is discussed in chapter 3. The charge generation process starts with exciton (EX)generation. The EX will be quenched at the copolymer/PCBM71 interface and generate charge transfer (CT) excitons. Finally, the CT excitons will dissociate into free charges in the manifold of charge separated (CS) states. The TA spectra of BHJ films of the copolymers with PCBM71 is shown in Figure 6.14. The ESA signal in these BHJ films will have a contribution EX, CT states and CS states. It is difficult to spectroscopically separate each of these signal. The signals usually overlap, it will be possible to deconvolve them with a pre-knowledge of the absorption of at least two signals. The measurement in the pristine polymer can give us information about EX absorption. And an additional

measurement on oxidized sample of the copolymers can help determine the absorption of the CS state.

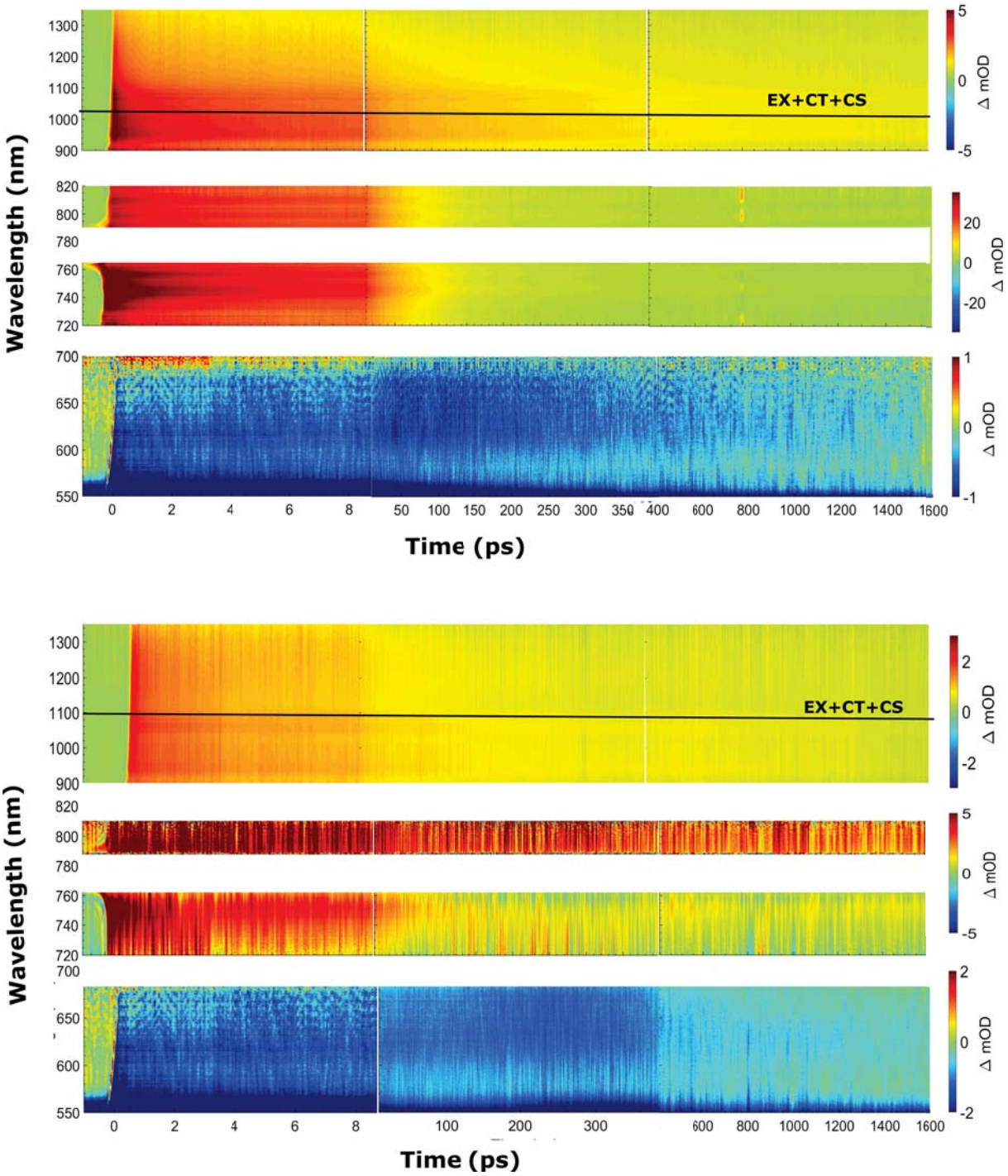

Figure 6.14: TA spectra **P3TI-1**:PCBM71(1:2)(top) and **P3TI-2**:PCBM71 (1:2) (bottom) BHJ films. The broad ESA is due to EX, CT and CS states.

The other possibility is to take line outs at different spectral regions of the TA spectrum and analyse their temporal evolution. In doing so, we might be able to get a signal with contributions from one or two of the three excited states. We were able to use this assumption for **P2TI**:PCBM71 BHJ film in the previous chapter. We also tried taking

line outs at different wavelength regions of the ESA for the two copolymer:PCBM71 BHJ films studied here. Unfortunately, the temporal profile of each of the line outs are similar. Hence, we took line outs at the EX absorption wavelengths of each of the copolymers and analysed the temporal evolutions of the signals. We fitted the temporal profiles with a sum exponential functions (Figure 6.15 and 6.16). A time constant of τ_1 = 1.5 (3.2) ps, τ_2 = 15 (0) ps, τ_3 = 300 (200) ps and $\tau_4 >> 2$ ns was found for **P3TI-1** (**P3TI-2**) respectively at a pump fluence of 2.6 mJ/cm^2.

These signals for both BHJ films was populated within our temporal resolution. This instantaneous population can mean: 1. the signal is purely exciton 2. the signal is due to exciton and the charge related species (CT ans CS) which means the CT and CS states are also generated instantaneously. 3. The signal is due to absorption of charge related species due to fast quenching of excitons below our temporal resolution. The signal has a measurable (20 to 30%) contribution that lives longer than 2 ns. Therefore, it clearly has a contribution from absorbing charge related species. It also has a decay time constants below 5 ps, which should be assigned to exciton related dynamics. Therefore, the second assumption which says the signal is due to EX, CT and CS state seems a plausible assumption. This assumption also is supported by the morphology images taken by STEM (Figure 6.7). The large domain sizes can suppress the exciton dissociation at the interface and/or the percolation of free charge carriers. This poor morphology creates a bunch of life times for excitons in the different part of the domains. The excitons created at the interface will be quenched below our temporal resolution, the excitons created at a distance which is lower or equal to the exciton diffusion length will be quenched latter. The rest of the excitons which are far from the interface will have no chance of dissociation thus relax back within their life time.

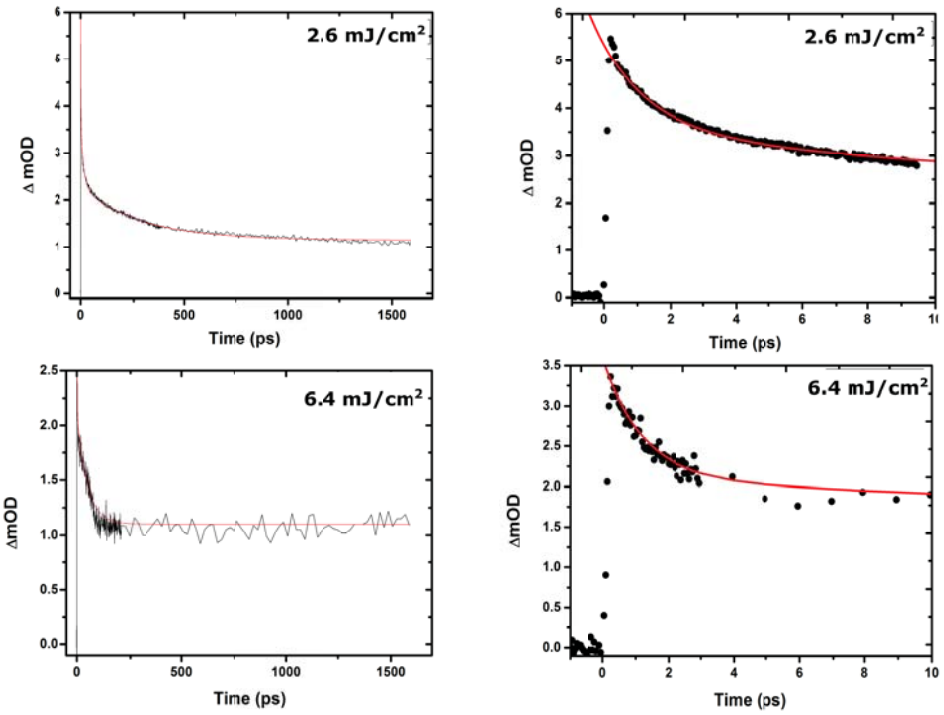

Figure 6.15: Temporal profile and fit of a line out at $\lambda = 1020nm$ of TA spectra **P3TI-1**:PCBM71 at different pump fluence. The signal has a contribution that lives $>>$ 2 ns. This is due to the contribution of charge related species.

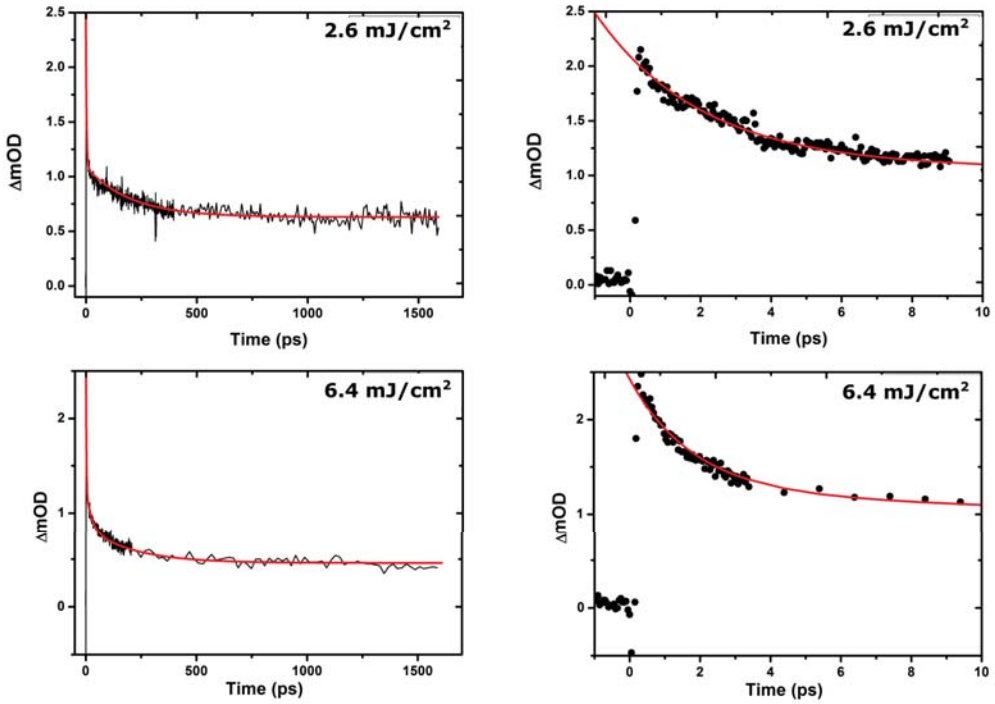

Figure 6.16: Temporal profile and fit of a line out at $\lambda = 1100nm$ of TA spectra **P3TI-2**:PCBM71 at different pump fluence. The signal has a contribution that lives $>>$ 2 ns. This is due to the contribution of charge related species.

Therefore, we have to be careful when assigning the time constants to a specific process in the BHJ films. To help the assumption of the time constants we measured the dynamics with two pump fluence (see Figure 6.15 and 6.16). As summarized in Table 6.5, the fit results have 3 to 4 time constant. The last time constants can safely be assigned to charge separated states. The 3rd time constant is longer than the life time of excitons. It can be assigned to either charge transfer or charge separated states. In **P3TI-2**:PCBM71 BHJ film, the 3rd time constant, τ_3, almost doesn't change with pump fluence. This indicates the geminate nature of the dynamics. Therefore, this time constant can be assigned to the decay of CT states. The third time constant in **P3TI-1**:PCBM71 BHJ film disappears as we increase the pump fluence, so it can not unambiguously be assigned.

Even if we could partially understand the dynamics in each BHJ films, it was not possible to draw a conclusion that can support the difference in the efficiency of the solar cell devices prepared using these BHJ films. The increase in pump fluence decreased the contribution of the long living component (Free charge) from 30 to 21% in **P3TI-2**:PCBM71 BHJ film. On the contrary this contribution grows in **P3TI-2**:PCBM71 film from 20 to 30% with increasing the pump fluence. A precise measurement of the thickness will enable the possibility of the comparison between the two solar cells.

Table 6.5: Summary of fit results of **P3TI-1**(**P3TI-2**):PCBM71 BHJ films

Copolymer	Fluence (mJ/cm^2)	A_1	τ_1(ps)	A_2	τ_2(ps)	A_3	τ_3(ps)	y_0
P3TI-1	2.55	1.8	1.5	1.3	15	1.1	300	1.15
P3TI-1	6.4	1.5	1.2	1	48	–	–	1.1
P3TI-2	2.55	1	3.2	–	–	0.48	200	0.63
P3TI-2	6.4	0.8	1	0.45	22	0.38	210	0.46

6.3 Conclusion

Structure - property relation study of organic semiconductors to optimize structure of polymers for highly performing solar cells is an ongoing research. In this study, the structures of two copolymers (**P3TI-1** and **P3TI-2**) were changed by only elongating the alkyl side chains of **P3TI-2** by 4 methyl units. The two copolymers were successfully designed and synthesized by a direct arylation polycondensation method. The two copolymers have similar HOMO levels of 5.2 eV. The LUMO levels of **P3TI-1** and **P3TI-2** are 3.8 eV and 3.7 eV respectively. Organic solar cells were prepared using each copolymers and PCBM71 bulk heterojunction blend as the active layer in a geometry Al/TiO_x/Active layer /PEDOT:PSS *PH 1000*. The efficiency and fill factor of the organic solar cells increased by 28% and 48% respectively as the length of the alkyl side chains is shortened by 4 methyl units. A steady state fluorescence measurement with solvents of different polarity showed the presence of intra-molecular charge transfer state. A steady state fluorescence spectroscopy measurement was also taken by exciting the copolymers at their lower wavelength absorption maxima. The results showed that **P3TI-2** has two dominant relaxation channels but **P3TI-1** has one dominant relaxation channel which is in the higher wavelength region. This indicates efficient ICT formation in **P3TI-1**. fs-Transient absorption spectroscopy measurement was taken on dilute solutions of the two copolymers in chlorobenzene. The measurement confirmed the presence of intramolecular charge transfer states in the relaxation of the copolymer chains. The ICT generation time were 4.5 ps and 13 ps for **P3TI-1** and **P3TI-2** respectively. The shorter alkyl side chains foster intra-molecular charge transfer between the donor and the acceptor units of the copolymer-**P3TI-1**. The longer side chains in copolymer-**P3TI-2**, on the contrary localizes the charge carriers and takes a longer time to transfer charges between the donor and acceptor units. The exciton life time in **P3TI-1** pristine film was longer than **P3TI-2**. An intensity dependent fs-transient absorption spectroscopy measurement on each pristine films showed exciton diffusion is more efficient in **P3TI-1**. In addition to the intramoleular interaction, longer alkyl side chains also inhibit interchain interaction. The dynamics in the bulk heterojunction films could not give a clear comparative information. The morphology of these bulk heterojunction films was full of large domain sizes exceeding 200 nm. This poses a complication in understanding the dynamics and assigning time constants to specific processes. In the bulk heterojunction films, 20 to 30% of the signal lives longer than 2 ns. In comparison to the pristine films and the copolymers in chlorobenzene solution, the bulk heterojunction film has a larger amount of contribution that lives longer than 2 ns. The STEM images taken for both bulk heterojunction composites show a domain size exceeding 200 nm which is more than 10 times longer than the typical exciton diffusion length (5 - 20 nm). We recommend morphology optimization for both bulk heterojunction films in the preparation of organic solar cells and study of transient absorption spectroscopy to

better understand the difference in recombination mechanisms. Fluorescence imaging taken on both the pristine copolymers and bulk heterojunction films showed exciton quenching is more efficient in **P3TI-1**:PCBM71 films than **P3TI-2**:PCBM71.

7. Outlook and summary

A thorough understanding of structure-property relation is important to understand efficiency limiting factors in organic solar cells. Photovoltaic performance of three organic solar cells based on similar copolymers as donor material and PCBM71 as an acceptor material was studied. The structures of the copolymers differ only on the donor side of the copolymers. The photovoltaic performance of the three copolymers was low. The current density in all the three solar cells was lower than expected. All the copolymers have band gaps < 1.7 eV, which is in the ideal region for photovoltaic application. The current density was expected to be higher because of their broad absorption. We found morphologies of the bulk heterojunction films of each OSCs play important role in charge photogeneration. Domain sizes exceeding exciton diffusion length is the reason for low current density in the solar cell devices.

Photogeneration in OSCs is a multi-step process. We studied photodynamics of each of the copolymers in solution, pristine film and BHJ films using fs-transient absorption spectroscopy. We found intramolecular charge transfer state in all the copolymers. We also found longer side chains lower the rate of intramolecular charge transfer state generation by studying two copolymers which have a structural difference of only length of side chains on their donor units. This intramolecular charge transfer state is essential to lower the binding energy of excitons. Side chains are crucial for solubility of polymers in common solvent for organic solar application. But the length of this side chains should be optimized to enhance both intra/inter-molecular charge transfer interactions. Longer side chains create barrier on intra/inter-chain interactions. This barrier is detrimental to charge mobility in the bulk heterojunction organic solar cell based on such copolymers.

In Summary, intramolecular charge transfer characterisics were found in the three copolymers studied. Even if side chains are important for solubility of copolymers, their lenght has to be optimized to facilitate both intra- and inter-molecular interaction. This is essential for charge transport in organic solar cell devices. The mobility of charge carriers in the active alayer of an organic solar cell limits the power conversion efficiency.

Exciton binding energy and exciton diffusion length play an important role in power conversion efficiency of OSCs. We recommend exciton dynamics studies on series of polymers to further optimize the structure of polymers for higher performance.

While doing this work, we were aware of the drastic efficiency increase of organic solar cells that are fabricated using fullerene free acceptors. The use of fullerene acceptors has its own drawbacks that include weak absorption and restricted energy levels. The energy level of non-fullerene acceptors can be tuned to achieve high open circuit voltage. The non-fullerene acceptors also have the advantage of a strong absorption. The excitons in the non-fullerene acceptors can not be neglected. The charge dynamics in these kinds of organic solar cells are determined by the excitons that are generated

both from the donor polymer and the non-fullerene acceptor. We therefore recommend a charge dynamics study in non-fullerene organic solar cells to understand the fundamental photophysical processes that are relevant for charge photogeneration using fs-transient absorption spectroscopy.

Bibliography

[1] Mazzio, K.A. and Luscombe, C.K.: The future of organic photovoltaics. *Chemical Society Reviews*, vol. 44, no. 1, pp. 78–90, 2014.

[2] Chapin, D.M., Fuller, C. and Pearson, G.: A new silicon p-n junction photocell for converting solar radiation into electrical power. *Journal of Applied Physics*, vol. 25, no. 5, pp. 676–677, 1954.

[3] Shockley, W. and Queisser, H.J.: Detailed balance limit of efficiency of p-n junction solar cells. *Journal of applied physics*, vol. 32, no. 3, pp. 510–519, 1961.

[4] Fu, R., Chung, D., Lowder, T., Feldman, D., Ardani, K. and Margolis, R.: Nrel us solar photovoltaic system cost benchmark q1 2016 report. Tech. Rep., National Renewable Energy Laboratory-Data (NREL-DATA), Golden, CO (United States); National Renewable Energy Laboratory, 2016.

[5] REN21: *Renewables 2017 Global Status Report*. Paris: REN21 Secretariat, 2017.

[6] Chiang, C.K., Fincher Jr, C., Park, Y.W., Heeger, A.J., Shirakawa, H., Louis, E.J., Gau, S.C. and MacDiarmid, A.G.: Electrical conductivity in doped polyacetylene. *Physical review letters*, vol. 39, no. 17, p. 1098, 1977.

[7] Tang, C.W. and VanSlyke, S.A.: Organic electroluminescent diodes. *Applied physics letters*, vol. 51, no. 12, pp. 913–915, 1987.

[8] Chen, J.-D., Cui, C., Li, Y.-Q., Zhou, L., Ou, Q.-D., Li, C., Li, Y. and Tang, J.-X.: Single-junction polymer solar cells exceeding 10% power conversion efficiency. *Advanced Materials*, vol. 27, no. 6, pp. 1035–1041, 2015.

[9] Zhao, W., Qian, D., Zhang, S., Li, S., Inganäs, O., Gao, F. and Hou, J.: Fullerene-free polymer solar cells with over 11% efficiency and excellent thermal stability. *Advanced Materials*, vol. 28, no. 23, pp. 4734–4739, 2016.

[10] Landerer, D., Bahro, D., Röhm, H., Koppitz, M., Mertens, A., Manger, F., Denk, F., Heidinger, M., Windmann, T. and Colsmann, A.: Solar glasses: A case study on semitransparent organic solar cells for self-powered, smart wearable devices. *Energy Technology*.

[11] Sze, S.M. and Ng, K.K.: *Physics of semiconductor devices*. John wiley & sons, 2006.

[12] Kürti, J., Surján, P., Kertész, M. and Frapper, G.: Design of small gap conjugated polymers. *Synthetic metals*, vol. 57, no. 2-3, pp. 4338–4343, 1993.

[13] Jayakannan, M., Van Hal, P.A. and Janssen, R.A.: Synthesis and structure-property relationship of new donor–acceptor-type conjugated monomers and polymers on the basis of thiophene and benzothiadiazole. *Journal of Polymer Science Part A: Polymer Chemistry*, vol. 40, no. 2, pp. 251–261, 2002.

[14] Salzner, U., Lagowski, J., Pickup, P. and Poirier, R.: Comparison of geometries and electronic structures of polyacetylene, polyborole, polycyclopentadiene, polypyrrole, polyfuran, polysilole, polyphosphole, polythiophene, polyselenophene and polytellurophene. *Synthetic Metals*, vol. 96, no. 3, pp. 177–189, 1998.

[15] Wang, E., Mammo, W. and Andersson, M.R.: 25th anniversary article: Isoindigo-based polymers and small molecules for bulk heterojunction solar cells and field effect transistors. *Advanced Materials*, vol. 26, no. 12, pp. 1801–1826, 2014.

[16] Puchalska, M., Połeć-Pawlak, K., Zadrożna, I., Hryszko, H. and Jarosz, M.: Identifica-

tion of indigoid dyes in natural organic pigments used in historical art objects by high-performance liquid chromatography coupled to electrospray ionization mass spectrometry. *Journal of mass spectrometry*, vol. 39, no. 12, pp. 1441–1449, 2004.

[17] Mei, J., Graham, K.R., Stalder, R. and Reynolds, J.R.: Synthesis of isoindigo-based oligothiophenes for molecular bulk heterojunction solar cells. *Organic letters*, vol. 12, no. 4, pp. 660–663, 2010.

[18] Ma, Z., Dang, D., Tang, Z., Gedefaw, D., Bergqvist, J., Zhu, W., Mammo, W., Andersson, M.R., Inganäs, O., Zhang, F. *et al.*: A facile method to enhance photovoltaic performance of benzodithiophene-isoindigo polymers by inserting bithiophene spacer. *Advanced Energy Materials*, vol. 4, no. 6, 2014.

[19] Zhu, L., Wang, M., Li, B., Jiang, C. and Li, Q.: High efficiency organic photovoltaic devices based on isoindigo conjugated polymers with a thieno [3, 2-b] thiophene π-bridge. *Journal of Materials Chemistry A*, vol. 4, no. 41, pp. 16064–16072, 2016.

[20] Zelalem, A.: *synthesis and characterization of small molecules and conjugated polymers for organic photovoltaic application*. Ph.D. thesis, Addis Ababa: Addis Ababa University, 2014.

[21] Cook, S., Furube, A. and Katoh, R.: Analysis of the excited states of regioregular polythiophene p3ht. *Energy & Environmental Science*, vol. 1, no. 2, pp. 294–299, 2008.

[22] Weinberger, B., Akhtar, M. and Gau, S.: Polyacetylene photovoltaic devices. *Synthetic Metals*, vol. 4, no. 3, pp. 187–197, 1982.

[23] Antoniadis, H., Hsieh, B., Abkowitz, M., Jenekhe, S. and Stolka, M.: Photovoltaic and photoconductive properties of aluminum/poly (p-phenylene vinylene) interfaces. *Synthetic Metals*, vol. 62, no. 3, pp. 265–271, 1994.

[24] Tang, C.W.: Two-layer organic photovoltaic cell. *Applied Physics Letters*, vol. 48, no. 2, pp. 183–185, 1986.

[25] Halls, J.J., Pichler, K., Friend, R.H., Moratti, S. and Holmes, A.: Exciton diffusion and dissociation in a poly (p-phenylenevinylene)/c60 heterojunction photovoltaic cell. *Applied Physics Letters*, vol. 68, no. 22, pp. 3120–3122, 1996.

[26] Yu, G., Gao, J., Hummelen, J.C., Wudl, F. and Heeger, A.J.: Polymer photovoltiac cells: Enhanced efficiencies via a network of internal donor-acceptor heterojunctions. *Science*, vol. 270, no. 5243, p. 1789, 1995.

[27] Nian, L., Gao, K., Liu, F., Kan, Y., Jiang, X., Liu, L., Xie, Z., Peng, X., Russell, T.P. and Ma, Y.: 11% efficient ternary organic solar cells with high composition tolerance via integrated near-ir sensitization and interface engineering. *Advanced Materials*, vol. 28, no. 37, pp. 8184–8190, 2016.

[28] Ma, Z.: *Studies of Morphology and Charge-Transfer in Bulk-Heterojunction Polymer Solar Cells*. Ph.D. thesis, Linköping University Electronic Press, 2013.

[29] Solanki, A., Wu, B., Salim, T., Lam, Y.M. and Sum, T.C.: Correlation between blend morphology and recombination dynamics in additive-added p3ht: Pcbm solar cells. *Physical Chemistry Chemical Physics*, vol. 17, no. 39, pp. 26111–26120, 2015.

[30] Sharenko, A., Gehrig, D., Laquai, F. and Nguyen, T.-Q.: The effect of solvent additive on the charge generation and photovoltaic performance of a solution-processed small molecule: perylene diimide bulk heterojunction solar cell. *Chemistry of Materials*, vol. 26, no. 14, pp. 4109–4118, 2014.

[31] Howard, I.A., Mauer, R., Meister, M. and Laquai, F.: Effect of morphology on ultrafast free carrier generation in polythiophene: fullerene organic solar cells. *Journal of the American Chemical Society*, vol. 132, no. 42, pp. 14866–14876, 2010.

[32] De, S., Pascher, T., Maiti, M., Jespersen, K.G., Kesti, T., Zhang, F., Inganäs, O., Yartsev, A. and Sundström, V.: Geminate charge recombination in alternating polyfluorene copolymer/fullerene blends. *Journal of the American Chemical Society*, vol. 129, no. 27, pp. 8466–8472, 2007.

[33] Van Franeker, J.J., Turbiez, M., Li, W., Wienk, M.M. and Janssen, R.A.: A real-time study of

the benefits of co-solvents in polymer solar cell processing. *Nature communications*, vol. 6, p. 6229, 2015.

[34] Jespersen, K.G., Beenken, W.J., Zaushitsyn, Y., Yartsev, A., Andersson, M., Pullerits, T. and Sundström, V.: The electronic states of polyfluorene copolymers with alternating donor-acceptor units. *The Journal of chemical physics*, vol. 121, no. 24, pp. 12613–12617, 2004.

[35] Gao, F. and Inganäs, O.: Charge generation in polymer–fullerene bulk-heterojunction solar cells. *Physical Chemistry Chemical Physics*, vol. 16, no. 38, pp. 20291–20304, 2014.

[36] Goris, L., Poruba, A., HodÁkova, L., Vaněček, M., Haenen, K., Nesládek, M., Wagner, P., Vanderzande, D., De Schepper, L. and Manca, J.: Observation of the subgap optical absorption in polymer-fullerene blend solar cells. *Applied physics letters*, vol. 88, no. 5, p. 052113, 2006.

[37] Hasharoni, K., Keshavarz-K, M., Sastre, A., González, R., Bellavia-Lund, C., Greenwald, Y., Swager, T., Wudl, F. and Heeger, A.: Near ir photoluminescence in mixed films of conjugated polymers and fullerenes. *The Journal of chemical physics*, vol. 107, no. 7, pp. 2308–2312, 1997.

[38] Tvingstedt, K., Vandewal, K., Gadisa, A., Zhang, F., Manca, J. and Inganas, O.: Electroluminescence from charge transfer states in polymer solar cells. *Journal of the American Chemical Society*, vol. 131, no. 33, pp. 11819–11824, 2009.

[39] Marcus, R.A.: On the theory of oxidation-reduction reactions involving electron transfer. i. *The Journal of Chemical Physics*, vol. 24, no. 5, pp. 966–978, 1956.

[40] Bredas, J., Beljonne, D., Cornil, J., Calbert, J.P., Shuai, Z. and Silbey, R.: Electronic structure of π-conjugated oligomers and polymers: a quantum–chemical approach to transport properties. *Synthetic metals*, vol. 125, no. 1, pp. 107–116, 2001.

[41] Petrella, A., Cremer, J., De Cola, L., Bäuerle, P. and Williams, R.M.: Charge transfer processes in conjugated triarylamine- oligothiophene- perylenemonoimide dendrimers. *The Journal of Physical Chemistry A*, vol. 109, no. 51, pp. 11687–11695, 2005.

[42] Van Hal, P., Meskers, S. and Janssen, R.: Photoinduced energy and electron transfer in oligo (p-phenylene vinylene)-fullerene dyads. *Applied Physics A: Materials Science & Processing*, vol. 79, no. 1, pp. 41–46, 2004.

[43] Rolczynski, B.S., Szarko, J.M., Son, H.J., Liang, Y., Yu, L. and Chen, L.X.: Ultrafast intramolecular exciton splitting dynamics in isolated low-band-gap polymers and their implications in photovoltaic materials design. *Journal of the American Chemical Society*, vol. 134, no. 9, pp. 4142–4152, 2012.

[44] Gao, B.-R., Qu, J.-F., Wang, Y., Fu, Y.-Y., Wang, L., Chen, Q.-D., Sun, H.-B., Geng, Y.-H., Wang, H.-Y. and Xie, Z.-Y.: Femtosecond spectroscopic study of photoinduced charge separation and recombination in the donor–acceptor co-oligomers for solar cells. *The Journal of Physical Chemistry C*, vol. 117, no. 9, pp. 4836–4843, 2013.

[45] Onsager, L.: Initial recombination of ions. *Physical Review*, vol. 54, no. 8, p. 554, 1938.

[46] Clarke, T.M. and Durrant, J.R.: Charge photogeneration in organic solar cells. *Chemical reviews*, vol. 110, no. 11, pp. 6736–6767, 2010.

[47] Grancini, G., Maiuri, M., Fazzi, D., Petrozza, A., Egelhaaf, H., Brida, D., Cerullo, G. and Lanzani, G.: Hot exciton dissociation in polymer solar cells. *Nature materials*, vol. 12, no. 1, pp. 29–33, 2013.

[48] Blom, P.W., Mihailetchi, V.D., Koster, L.J.A. and Markov, D.E.: Device physics of polymer: fullerene bulk heterojunction solar cells. *Advanced Materials*, vol. 19, no. 12, pp. 1551–1566, 2007.

[49] Hallermann, M., Haneder, S. and Da Como, E.: Charge-transfer states in conjugated polymer/fullerene blends: Below-gap weakly bound excitons for polymer photovoltaics. *Applied Physics Letters*, vol. 93, no. 5, p. 290, 2008.

[50] Lee, J., Vandewal, K., Yost, S.R., Bahlke, M.E., Goris, L., Baldo, M.A., Manca, J.V. and Voorhis, T.V.: Charge transfer state versus hot exciton dissociation in polymer- fullerene

blended solar cells. *Journal of the American Chemical Society*, vol. 132, no. 34, pp. 11878–11880, 2010.

[51] Bässler, H. and Köhler, A.: Hot or cold: how do charge transfer states at the donor–acceptor interface of an organic solar cell dissociate? *Physical Chemistry Chemical Physics*, vol. 17, no. 43, pp. 28451–28462, 2015.

[52] Tamai, Y., Ohkita, H., Benten, H. and Ito, S.: Exciton diffusion in conjugated polymers: from fundamental understanding to improvement in photovoltaic conversion efficiency. *J. Phys. Chem. Lett*, vol. 6, no. 17, pp. 3417–3428, 2015.

[53] Krebs, F.C. and Norrman, K.: Analysis of the failure mechanism for a stable organic photovoltaic during 10 000 h of testing. *Progress in Photovoltaics: Research and Applications*, vol. 15, no. 8, pp. 697–712, 2007.

[54] De Jong, M., Van Ijzendoorn, L. and De Voigt, M.: Stability of the interface between indium-tin-oxide and poly (3, 4-ethylenedioxythiophene)/poly (styrenesulfonate) in polymer light-emitting diodes. *Applied Physics Letters*, vol. 77, no. 14, pp. 2255–2257, 2000.

[55] Yang, C. and Heeger, A.: Morphology of composites of semiconducting polymers mixed with c 60. *Synthetic metals*, vol. 83, no. 2, pp. 85–88, 1996.

[56] Minda, I.: *Charge Dynamics in Hybrid and Organic-Inorganic Light Harvesting Thin Films followed with Femtosecond Transient Absorption Spectroscopy*. Ph.D. thesis, Stellenbosch: Stellenbosch University, 2017.

[57] Fuks-Janczarek, I., Kityk, I., Miedziński, R., Gondek, E., Danel, A. and Zagorska, M.: Specific features of uv–vis absorption spectra of cis-and trans-polythiophenes. *Spectrochimica Acta Part A: Molecular and Biomolecular Spectroscopy*, vol. 64, no. 1, pp. 264–271, 2006.

[58] Scharber, M.C., Mühlbacher, D., Koppe, M., Denk, P., Waldauf, C., Heeger, A.J. and Brabec, C.J.: Design rules for donors in bulk-heterojunction solar cellstowards 10% energy-conversion efficiency. *Advanced materials*, vol. 18, no. 6, pp. 789–794, 2006.

[59] Tang, Z., Andersson, L.M., George, Z., Vandewal, K., Tvingstedt, K., Heriksson, P., Kroon, R., Andersson, M.R. and Inganäs, O.: Interlayer for modified cathode in highly efficient inverted ito-free organic solar cells. *Advanced Materials*, vol. 24, no. 4, pp. 554–558, 2012.

[60] Veldman, D., Meskers, S.C. and Janssen, R.A.: The energy of charge-transfer states in electron donor–acceptor blends: Insight into the energy losses in organic solar cells. *Advanced Functional Materials*, vol. 19, no. 12, pp. 1939–1948, 2009.

[61] Guo, J., Ohkita, H., Benten, H. and Ito, S.: Near-ir femtosecond transient absorption spectroscopy of ultrafast polaron and triplet exciton formation in polythiophene films with different regioregularities. *Journal of the American Chemical Society*, vol. 131, no. 46, pp. 16869–16880, 2009.

[62] Petrozza, A., Laquai, F., Howard, I.A., Kim, J.-S. and Friend, R.H.: Dielectric switching of the nature of excited singlet state in a donor-acceptor-type polyfluorene copolymer. *Physical Review B*, vol. 81, no. 20, p. 205421, 2010.

[63] Wang, E., Ma, Z., Zhang, Z., Henriksson, P., Inganäs, O., Zhang, F. and Andersson, M.R.: An isoindigo-based low band gap polymer for efficient polymer solar cells with high photo-voltage. *Chemical Communications*, vol. 47, no. 17, pp. 4908–4910, 2011.

[64] Bundgaard, E. and Krebs, F.C.: Low-band-gap conjugated polymers based on thiophene, benzothiadiazole, and benzobis (thiadiazole). *Macromolecules*, vol. 39, no. 8, pp. 2823–2831, 2006.

[65] Zhang, Z.-G., Min, J., Zhang, S., Zhang, J., Zhang, M. and Li, Y.: Alkyl chain engineering on a dithieno [3, 2-b: 2, 3-d] silole-alt-dithienylthiazolo [5, 4-d] thiazole copolymer toward high performance bulk heterojunction solar cells. *Chemical Communications*, vol. 47, no. 33, pp. 9474–9476, 2011.

[66] Peng, Q., Lim, S.-L., Wong, I.H.-K., Xu, J. and Chen, Z.-K.: Synthesis and photovoltaic properties of two-dimensional low-bandgap copolymers based on new benzothiadiazole derivatives with different conjugated arylvinylene side chains. *Chemistry-A European Jour-*

nal, vol. 18, no. 38, pp. 12140–12151, 2012.